Investigation of Thermal Dynamics of Floor Heating with Solar Gains

Belkacem Chikh

A Thesis

in

The Department

of

Building, Civil & Environmental Engineering

Presented in Partial Fulfillment of the Requirements
for the Degree of Master of Applied Science (Building Engineering)
Concordia University
Montreal, Quebec, Canada

February 2005

ABSTRACT

Investigation of Thermal Dynamics of Floor Heating

with Solar Gains

Belkacem Chikh

An extensive analysis of thermal dynamics of a solar building with floor heating, conducted through an integrated methodology based on frequency domain techniques showed the relative effects of different amounts of thermal mass and of different types of thermal mass. An accurate building heat balance model is developed through a detailed thermal network with distributed parameter elements and lumped elements, accurate representation of interior radiant exchanges and a floor internal heat source with variable depth within the slab.

Frequency domain and finite difference techniques were used to perform analysis of the transient response of the heating system. It is shown that a combined feedback and feedforward controller when used with weather predictions one day ahead can practically provide perfect control. However, the appropriate building transfer functions must be estimated. Various control strategies involving room air temperature and operative temperature control with different thermostat setpoint profiles were investigated and it was demonstrated that control of floor radiant heating based on operative temperature constitutes a preferred approach.

ACKNOWLEDGEMENTS

I would like to express my gratitude to my supervisor, Dr. A.K. Athienitis, for his help, guidance and encouragement during my graduate studies.

Special thanks and appreciation is extended to my wife and my children for their patience and encouragement.

With respect, love and admiration, I would like to dedicate this work to my mother Ounissa Allilouche.

TABLE OF CONTENTS

LIST OF FIGURES

NOMENCLATURE

A	area (m^2)
As	effective sensing area of long wave radiant exchange (m^2)
{D}	vector relating T_{op} to {T}
$[D_{mr}]'$	matrix relating T_{mr} to {T}
E	total error function in the least squares fitting
$F^*_{i,j}$	radiation exchange factor between surface i and j
$F_{i,j}$	view factor between surface i and j
$F_{s,i}$	view factor between a sensor and a surface i
G_c	transfer function representing a proportional integral controller
G_f	transfer function representing a final control element
G_m	transfer function representing a heating system
G_s	transfer function representing a temperature sensor
K_{scr}	magnitude ratio of a final control element
K_p	proportional controller gain factor (kW/°C)
Kp	proportional control constant (W/°C)
K_h	capacity of a heating system (W)
K_u	ultimate gain (W/°C)
$N(\omega)$	numerator polynomial in fitted transfer function model
$D(\omega)$	denominator polynomial in fitted transfer function model
P_u	ultimate period (second)
Q	heat flow (W)

{Q}	vector of room nodal heat sources
Qg	solar irradiation absorbed by window glazing (W/m^2)
$R(\omega)$	real part of a discrete frequency response
Sn	irradiance of solar radiation (W/m^2)
Tair	air temperature (°C)
Tb	basement temperature (°C)
Teq	sol-air temperature (°C)
T_{op}	operative temperature (°C)
To	ambient temperature (°C)
T_{mr}	mean radiant temperature (°C)
{Ts}	vector of room interior nodal temperatures
$U_{i,j}$	conductance between node i and node j (W/°C)
U_{inf}	infiltration conductance (W/°C)
W_{nL}	weighting factor for the iterative least-squares fitting
{X}	vector relating heat sources and operative temperature
Xe	deviation between setpoint and measured temperature (°C)
X(i)	operative temperature transfer function (°C/W)
Xf	fitted operative transfer function (°C/W)
[Y]	matrix of admittance relating nodal temperatures and heat sources
Y(i,j)	component admittance between node i and node j (W/°C)
Ys	Self-admittance transfer function (W/°C)
Yt	transfer admittance transfer function (W/°C)
[Z]	matrix of impedance relating heat sources and nodal temperatures

Z(i,j)	room impedance temperature transfer function (°C/W)
Zf	fitted impedance transfer function (°C/W)
a_i	coefficients of a numerator polynomial
arg	argument of a function
b_j	coefficient of denominator polynomial
c	specific heat capacity (J/kg·°C)
h_c	convective heat transfer coefficient (W/m^2·°C)
hr	time (hour)
h_r	radiative heat transfer coefficient (W/m^2·°C)
h_{rc}	combined convective-radiative heat transfer coefficient (W/m^2·°C)
j	(-1)½
k	thermal conductivity (W/m·°C)
q	heat flow (W)
q+	radiosity (W/m^2)
qr_{aux}	auxiliary heating (W)
s	Laplace transform variable
t	time (second)
t_d	dead time of a component (second)
t_{scr}	time constant of a final control element (second)
u_w	window heat transfer coefficient (W/m^2·°C)
w_i	window inner gazing
w_o	window outer glazing
x	floor thermal mass thickness (m)

SUBSCRIPTS

L	number of iterations
n	number of frequencies
sp	set point
i,j	nodes number

SUPERSCRIPTS

u	order of numerator polynomial in fitted transfer function model
v	order of denominator polynomial in fitted transfer function model

GREEK SYMBOLS

Φ	phase angle (degree)
Ψ	room surface azimuth
α	thermal diffusivity (m^2/s)
$\alpha(\omega)$	real part of a complex
$\beta(\omega)$	imaginary part of a complex
ϵ	longwave emissivity
$\epsilon(\omega)$	error message at discrete frequency
ρ	longwave reflectivity
σ	Stephan-Boltzmann constant ($W/m^2 \cdot K^4$)
ω	frequency (rad/s)
ω_{co}	crossover frequency (rad/s)

CHAPTER 1

INTRODUCTION

1.1 History

Radiant floor heating has been utilized for centuries by many cultures. Around 100 B.C, the Romans used elaborate trenches and underfloor ducting systems to heat the stone floors of bath houses. During this time, the Koreans have used similar system of fire pits filled with stones under their homes for hundreds of years. In this way, the floor slab was also used as a thermal mass storage. It offers an efficient use of space with no cleaning required and a noise free and draft free environment.

While Europeans and far eastern cultures adopted radiant floor heating as a viable heating system, it was not until 1930s that this type of heating was introduced in North America.

In 1940s up to 60s, floor heating installations using circulating water in steel or copper were installed in Europe and in North America. Unfortunately, at this time, lack of insulation in buildings often required floor surface temperature above comfortable levels and produced also wide temperature swings within the space. This issue added to the high cost of materials and labor causing interest to wane in the 60s.

The introduction of higher standards of construction and insulation associated with the use of new materials for piping in the 1970s, such as plastic and rubber compounds contributed to the system to becoming widely used,

particularly in Germany, Switzerland and in the Nordic countries. In North America, floor heating was rediscovered by the solar industry as a perfect match for solar collection systems. The last two decades have seen radiant floor heating applications increase significantly in the residential, commercial and industrial fields.

1.2 Floor heating issues

Efficient design and operation of floor heating systems require several important decisions on a number of design or control variables such as the maximum heating device capacity, the type and thickness of thermal mass integrated in the floor heating system and cover layer and the appropriate control strategies for the system to maintain desired space thermal condition and floor surface within recommended temperature.

Thermal comfort is a critical issue in any building. In most convective heating systems, designers predict satisfaction with the thermal surroundings based on the air temperature alone. In a radiant system, such assumptions are not possible and would neglect one of the operating principles of these systems: heating or cooling the room occupants directly using radiant heat transfer.

Compared to a 100% convective heating system, a floor heating system can reach the same operative temperature at a lower air temperature. This observation has significant influence on the energy consumption particularly in buildings with high ventilation rates. Accordingly, the transmission heat losses depend partly on the convection heat exchange between room air and external

surfaces and partly on the radiant heat transfer between external surfaces and the other surfaces in the space. This involves air and surfaces temperatures and makes the reference temperature for the transmission heat loss closer to the operative temperature than to the air temperature. This implies lower ventilation heat losses with, however, no significant reduction of transmission heat losses.

International standard (ISO Standard 7330, 1994) recommends a 29°C maximum floor surface temperature for optimal comfort in the occupied zones, except for spaces such as bathroom, swimming pools where the floor material is also taken into account. European standard (CEN, EN 1264-1994) accepts 35°C outside occupied zones within 1 m from outside walls/windows. These design elements constitute a limiting factor for the capacity of floor system. However, radiant floor heating can be designed with a higher surface temperature at cold surfaces (wall/window) to compensate for downdraft, other factor of discomfort.

Numerous studies (Olesen, 2002) have shown that radiant heating can contribute to the indoor air quality. The lower air temperature induced by radiant heating system has the advantage to maintain the relative humidity a little higher while the higher surface temperatures reduce the risks of condensation and mold growth. Radiant heating system results in less transportation of dust than conventional heating systems.

Control of the system as well as the potential for thermal lag within the system itself are major preoccupations. The performance of radiant floor heating can be affected by variation more or less important in the room temperature due to internal loads from occupants, lighting, equipment and direct solar radiation,

particularly in buildings with high insulation and /or high thermal mass. In certain low-temperature radiant systems, such as those embedded in concrete slabs, there can be a significant delay in the response of the system due the thermal storage effect of the floor slab. This can leads to overheating with subsequent comfort problem particularly with passive solar building.

Several methods are readily available for radiant heating system design. The main design parameters are pipe distance, water flow rate, piping layout and system capacity. The capacity of a floor system depends on the heat exchange between the floor surface and the space (convective and radiant heat exchange coefficients), the heat exchange between the floor surface and the radiant panel (floor surface material, type of concrete and floor system, slab thickness, pipe spacing between the tubes) and the heat transport by water (water flow rate, temperature difference between supply and return). The maximum heating capacity is independent of the type of floor covering. The required water temperature to obtain the maximum heating capacity is, however, dependant on the thermal resistance of the floor covering and other factors such as system piping characteristics and pipe spacing.

1.3 Building system simulation

Overcoming the enumerated problems is not a simple task and request to be adequately addressed by comprehensive radiant system models taking into account the building envelop, the HVAC system and the control system as well as the interaction between them. There are two general approaches for

simulation analysis for predicting thermal performance of building.

The first approach is through time domain simulation using the finite difference method which is probably the most commonly applied to the problem of building energy modeling because of its ability to deal with linear and non-linear systems.

The second approach, more suitable for system response pattern, involves frequency domain analysis and simulations. The frequency domain method is generally limited to building that can be represented by linear equations and that can be subjected to steady periodic environment conditions.

An important objective of the present study is to make use of a methodology (Athienitis et al., 1990; Athienitis, 1993) based on the frequency domain technique in conjunction with Laplace Transform and associated Fourier series and explore the potential advantages and problems in applying this approach for the investigation of the thermal dynamics of floor heating under steady periodic environmental conditions. Significant building thermal characteristics can be identified and various design option may be compared on a relative basis through frequency domain studies of the magnitude and phase variation of the room transfer functions.

Usually, the analysis is concentrated on wall admittance transfer function with significant thermal mass such as the floor. Wall thermal admittance is particularly useful for analysis of the effect on room temperature of cyclic variations in weather variables such as solar radiation, outside temperature and dynamic heat flows under steady periodic conditions. The floor impedance and

operative transfer functions, which define the effect of auxiliary floor internal heat source on the room air temperature or the room operative temperature, are other interesting parameters useful for thermal control analysis.

The s-domain transfer functions, required for control analysis, are obtained through a modified least-squares polynomial fit to the discrete frequency responses obtained by inversion of the system admittance matrix. The overall system transfer function is then obtained through block diagram algebra and the system thermal response to load and temperature change is performed by means of an efficient numerical Laplace transform inversion.

Simulation of the auxiliary heat source representing the heating panel within the floor slab is carried out with the diakoptic method in conjunction with appropriate use of the Norton and superposition theorems. This method based on an artificial separation of the floor slab in two parts, but still with the same overall characteristics, allows the radiant floor heating system to be handled like any other surface within the heat balance framework.

1.4 Objectives

Despite numerous experimental and simulation studies, radiant heating system still has several obstacles to overcome before it can actually be considered a real and practical alternative to the simpler and more popular forced air system in North America. Most of these obstacles are related to the way in which a radiant system maintains thermal comfort. Understanding the response of the system, its interactions with the building, controlling how the

system responds and developing operative based temperature controller require further investigation.

The focus of this thesis is the investigation of the thermal dynamics of an integrated radiant floor heating-direct gain passive solar system with different floor mass thermal properties (concrete and gypcrete with and without carpet cover) and different heat source depths within the slab using the frequency domain method. The objectives are as follows:

1-Develop an accurate heat balance based model through a detailed thermal network method including a floor internal heat source with variable depth within the slab.

2-Determine the room transfer functions in the frequency domain and in the Laplace domain for thermal dynamic analysis.

3-Perform energy analysis and numerical simulation of transient heat conduction for thermal control purpose and compare the results with finite difference method. Evaluate the performance of different control strategies.

4-Perform numerical simulation to analyze the effect of air and operative temperature control on the system performance.

1.5 Thesis overview

The next chapter presents a literature review on the present status of room modeling, system control and building system simulation.

In chapter 3, a detailed room thermal network is established according to the inputs so as to explicitly and accurately model any combined thermal parameter such as the operative or the mean radiant temperature. This thermal network is based on known information about the building and its HVAC system, including system parameters such as initial desired operation strategies and weather data. The system parameters consist on known numerical values and design variables to be determined. The numerical parameters include the dimension of the room under consideration, the structure of the building envelope, thermal properties of walls and ceiling material, window area, etc... . Convective and accurate radiative heat transfer coefficients calculation is carried out. The design variables are the thermal parameters of the floor material and the depth of the floor internal heat source (floor radiant heating system).

In Chapter 4, the wall admittance transfer functions are determined through appropriate use of Norton theorem and the radiant heat source within the floor slab is modeled using the diakoptic method. The building transfer functions are then obtained by performing an energy balance at all nodes in the Laplace domain (converted in the frequency domain, $s=j\omega$). The admittance matrix derived from the energy balances is then inverted at discrete frequencies and the impedances and operative transfer functions are thus obtained only at these frequencies. Both lumped and distributed elements can be considered with this

approach.

Analytical transfer functions are obtained by fitting a polynomial N(s)/D(s) through a modified least square regression technique. These analytical transfer functions are then used for parametric analysis in order to examine for effect of variables such as thermal mass on the thermal lag (related on phase angle of the relevant transfer function) associated with radiant gains.

In chapter 5, thermal control studies are performed through combination of the building s-domain transfer functions with the HVAC system and control Laplace transfer functions. The resulting overall transfer functions allow analysis of system transient response control to set-point variations, feedback and feedforward control through numerical inversion of Laplace transform. System stability is investigated through frequency response analysis of the open-loop and closed-loop transfer function.

In chapter 6, building heating load and temperature calculations are performed by means of discrete Fourier series through the transfer functions obtained with the building energy balance in the frequency domain. A discrete Fourier transform (DFT) of the weather variables are performed and the time domain load and temperature room variation is obtained through complex algebraic techniques and an inverse discrete transform (IDFT).

Finally conclusions and recommendations for further work are summarized in chapter 7.

CHAPTER 2

LITERATURE REVIEW

2.1 Introduction

Radiant heating systems are receiving considerable attention due to their various advantages such as improved thermal comfort and lower energy consumption but also because of the concerns due to the control of the system and the potential thermal lag inherent in this type of system. Compared to conventional systems, radiant systems has several added complexities such as the delayed transient heat conduction within the system itself, combined surface convection and radiation from/to the system, and a drastically different resulting thermal environment, which make them difficult to model and integrate in a comprehensive simulation. This chapter will review the literature on the subject according to the major themes of floor heating modeling, system control, experimental studies and building system simulation techniques.

2.2 Floor heating modeling

The performance of panel heating and cooling system may be determined by design calculation or testing. Extensive studies have been devoted to laboratory testing of radiant systems with the main aim to quantify the thermal performance and response of radiant systems upon using conventional or newly developed control strategies. Thermal testing and system analysis by experiments being costly and inefficient, several analytical studies for the

prediction of thermal performance of radiant systems have been developed.

Leal and Miller (1972) used an analytical-numerical method to solve the temperature within pavement heating installations. Zhang and Pate (1986 and 1987) developed a two-dimensional finite-difference method for ceiling panels, which then was used to develop a simplified model for radiant slab heating. They predicted the ceiling surface temperature by simulating steady state and transient heat transfer process.

Kilkis et al. (1995) developed a steady state, composite-fin model to predict the heat diffusion in a panel composed of layers with different thermal conductivities. Radiative and convective heat outputs were treated separately and an equivalent thermal conductivity was defined for the lateral heat diffusion along parallel layers of different thermal conductivities. Compared with finite elements solution, the resulting proposed algorithm provided close agreement with respect to the required mean water temperature, thermal efficiency and heat output intensity. Kilkis and Coley (1995) and Kilkis and Sapci (1995) subsequently used the composite-fin model to develop software for the design of floor and sub-floor heating and cooling systems.

Athienitis et al. (1990) applied a methodology based on the frequency domain technique with associated Laplace transform and Fourier series for analysis of the thermal characteristics of a single room subjected to radiative

heat input at the floor surface. The room was modeled with a detailed thermal network model including distributed parameters elements such as the thermal mass and lumped element such as the room-light-weight content for accurate representation of the radiant exchanges. The equivalent first order time constant (time by which the temperature reaches 63% of its steady state) obtained from the transient response for a room with 4 cm concrete floor was found to be 10.8 hours, almost double that of a carpeted floor. This means that the thermal lag for concrete floor is significantly larger than for carpeted floor.

A subsequent analysis (Athienitis, 1993) revealed no clear separation between short- and long-term dynamics for floor heating indicating, as expected, that feedback control of system with high radiant loads or radiant heating system is more complex due to the larger thermal lag times involved. The effect of thermal mass on room temperature with radiative heat input was also found to be higher than with convective heat input and longer time was required to achieve steady state.

Athienitis (1994 and 1997) developed a one-dimensional third–order explicit finite difference network model to study the performance of a floor heating system with thermal storage and high solar gains. The simulations revealed that the maximum floor surface temperature may be reduced through appropriate use of solar gains to reduce heating requirement.

In a companion paper Chen and Athienitis (1998) utilize a 3-dimensional

explicit finite difference model to study heat transfer in floor heating systems with different cover layers and thermal storage materials. Complete and partial (area) carpets were considered as well as hardwood covers layers over concrete or gypcrete thermal storage. Analysis of the results revealed that a thick central carpet cover over a 5 cm concrete thermal storage layer caused an average temperature difference of about 2°C between the carpeted and uncarpeted surface of the floor, and a difference of about 11°C in the corresponding regions of the heating panel. Carpeted floor produced the largest thermal lag time (4.75 hr) between the peaks of heating power supplied and the floor surface temperature and induced also the highest energy consumption (9% than the uncarpeted 5 cm concrete layer). Solar radiation effect was not included.

In a subsequent paper (2000) based on the same approach, they showed, through simulation results validated by experimental data, that solar beam radiation can cause a local floor surface temperature in the illuminated area to be 8°C higher than in the shaded area. Partial carpet cover further increases floor surface temperature difference by up to 15°C when solar radiation is absorbed while solar radiation stored in the floor surface mass was found to reduce by 30% or more the heating energy consumption.

Using finite element method and experimental results involving temperature distribution in the construction, inter-independence between performance and mean carrier fluid temperature, panel surface temperature and room temperature, Bohle (2000) derived a single power function product of all

relevant parameters as a practical algorithm for performance calculation of panel heating and cooling system, adaptable to other systems. These basic equations provided the design standard for German standard DIN 4725 (1992), adopted by European standard EN 1264 (1994). Heat flux results for plaster panel floor heating calculated with the ASHRAE method are about 10% to 30% less than heat flux based on this algorithm, mainly because of lower estimation of heat transfer coefficients.

An important characteristic of radiant heating system which brings additional attention is related to the way in which it maintains thermal comfort, which is based on direct radiant energy transfer from the system to the occupant. The two main parameters for providing acceptable thermal comfort conditions (ANSI/ASHRAE standard 55, 1992) are air temperature and mean radiant temperature and their combined influence is expressed as the operative temperature (ASHRAE, 1989). Despite this fact, control of heating systems in most buildings is still predominantly based on sensors or thermostats that sense primarily air temperature even though the mean radiant temperature may differ significantly from air temperature, often by more than 3°C (Athienitis and Chen, 1993). Space thermal comfort would be enhanced by control of an effective room temperature such as the operative temperature particularly in buildings with high radiant gains due to passive solar systems and radiant heating.

Chapman and Zhang (1995 and 1996) developed a three-dimensional

mathematical model based on the discrete ordinates method to compute heat transfer within a radiantly heated or cooled room, which then calculates steady state mass-averaged room air temperature and wall surface temperature distribution. The model formulation, based on an accurate representation of the radiant heat exchanges, convective and conductive heat flux, allows analysis of the effect of non uniform wall temperatures and properties and accommodates arbitrary placement of the interior surfaces and objects within the room.

By coupling this model with a thermal comfort model such as in the Building Comfort Analysis Program (BCAP) (Jones and Chapman, 1994), the comfort levels throughout the room can be easily and efficiently mapped for a given radiant heater/cooler location. A thermal comfort analysis (Chapman et al., 1997) using the BCAP results confirmed the accuracy of the methodology to evaluate the thermal comfort conditions under various indoor and outdoor conditions. The results validated by experimental data emphasized further the need to design primarily for thermal comfort rather than simply to obtain the desired room air temperature.

The discrete ordinates method, first applied on neutrons transport theory, calculates the radiant intensity I at each point and direction using directions and nodes on surfaces.

A study (Freestone and Worek, 1996), performed through numerical simulation based on energy balance and the Gauss-Seidel method, of radiant perimeter heating systems in conjunction with central-heating systems in multi-

storey buildings concluded that energy use can be lowered by removing the insulation from the top of the panel and placing a partition in the plenum to concentrate the heat in the perimeter area. In addition to the ability of radiant perimeter heating system to directly deliver heat to an occupant in the perimeter area to help compensate for body losses due to a cold surface, this combination of design parameter creates a perimeter area with a higher mean radiant temperature and operative temperature.

2.3 System control

The main thermal comfort problem, which may occur particularly in well-insulated buildings, is large variations in the room temperature due to changes in internal loads from occupants, lighting, equipment or direct solar radiation. The low heat loss in well-insulated buildings means that changes in internal loads have higher impact on the room temperature than in buildings with standard insulation. This influence depends on the thermal mass of the building and on the controllability of the heating system. As floor heating systems often have a higher mass compared to other heating systems, conventional on-off control presents greater risk for overheating. Numerous alternative control strategies have been investigated to tackle this issue, cause of discomfort and loss of energy.

Aldeman (1988) recommended, through steady state analysis, outdoor reset control based on the principle that there is a direct linear relationship between outside temperature and the required water temperature. The supply

water is inversely modulated with outside temperature while maintaining a constant circulation of water. The constant of proportionality relating the rise in water temperature to the drop in outdoor temperature is called the reset slope.

ASHRAE (1987) stated that the supply water temperature should be varied in accordance with outside temperature due to the time lag between the heat demand and the heat delivery to the space. In contrast, MacCluer (1989) proposed the concept of proportional flux-modulation (i.e. simple proportional controller with an anticipatory) and claimed that the rate of heat delivery to the floor slab, in proportion to perceived load, is the parameter to control not the temperature and is not subject to time lag.

Later on MacCluer (1991) also proposed an outdoor reset control with indoor temperature feedback to compensate errors due to interior disturbances such as solar or internal gains. The analytical model based on the frequency domain revealed that only a slight improvement in step or sinusoidal response is projected by inhibiting circulation upon overheating while modulating the reset slope or offset in proportion to zone temperature improves tracking but can induce instability.

In an experimental study (Leigh and MacCluer, 1994) of proportional control of supplied heat and various approaches to temperature modulation including outdoor reset control, proportional flux-modulation was reported to

compare favourably with various types of temperature-modulation approaches by exhibiting consistent performance under dynamic conditions, maintaining a stable indoor temperature around the set point and by demonstrating immediate response to any internal load disturbances. The study deduced also that a simple proportional controller with an anticipator constitutes one of the most economical way of effective and stable room temperature control. With temperature-modulation approach, fine-tuning of the reset ratio was required after installation since an improper reset ratio induces indoor temperature deviation from the set point. Further, they recommend addition of interior temperature feedback control to help compensate for these potential errors due to interior disturbances such as solar or internal gains.

Athienitis and Chen (1991) recommended a feedback proportional control based on operative temperature. Numerical simulations, based on detailed room transfer function for the operative temperature and simple Laplace transfer function for the heating and control system components, of a radiant ceiling heating system response to operative set point changes indicated significant potential for faster control compared with air based temperature control. Preliminary experimental results also indicated better overall performance for control with a globe temperature sensor emulating the operative temperature sensor. Solar gains were, however, not included in that study. The globe temperature, as measured by a 15-cm diameter globe thermometer, is expected to be close to the operative temperature.

Athienitis (1997) and Athienitis & Chen (2002) used an explicit nonlinear one-dimensional finite difference network model to conduct a numerical simulation study of efficient control strategies for a floor heating system with high passive solar gains. The simulations were performed for sunny or cloudy cold winter conditions, with two different quantities of floor thermal (5cm and 10 cm thick slab). The control strategies considered constant or half-sinusoid set point profile for proportional control of room air temperature or operative temperature, simple on/off control based on a 29°C maximum floor surface temperature and feedback-outdoor reset control.

The simulation revealed that control of radiant heating based on the operative temperature reduces the maximum floor surface temperature and the maximum operative temperature, subsequently improving thermal comfort. Further, it increases utilization of passive solar gains and reduces auxiliary energy consumption. However floor thermal mass thicker than necessary may contribute to large room temperature swings when high solar gains are present.

Combined feedback-outdoor reset control resulted in generally higher room temperature and increased energy consumption. Utilization of auxiliary heating shut off based on maximum floor surface temperature is necessary with reset control.

Gibbs (1994) simulated three different control strategies of multizone radiant floor heating system: Pulse-width modulated zone valves with constant-supply water temperature, outdoor reset with indoor feedback and outdoor reset

plus pulse-width-modulated zone valves. The project used a lumped capacity model of the plant and control system. Outside temperature was modeled as a sinusoidal function with a 24 hour period and a step function.

Pulse-width modulated zone valves with constant-supply water temperature: This control strategy assumes constant supply water temperature while the individual zone temperature relied on room thermostat with a 3°C proportional band that pulse width modulates the zone valve four times per hour for a variable time period in relation to the air temperature set point. This approach based on flow inhibition maintains room air and floor surface temperature within acceptable limits for most application but suffers from numerous disadvantages such a large variation in water flow rates, unsteady floor surface temperature, large thermal expansion-contraction cycles inducing heating system failure and zone thermal discomfort.

Outdoor reset with indoor feedback: This second approach is based on supply water temperature modulation via mixing valve and outdoor reset control with limited interior temperature feedback effect. There is only one zone and the heat delivery to the different area of the zone is balanced through adjustment of the water flow in the tubing loops. This strategy offsets most of the problems encountered with the first approach but temperature control is limited to one zone and heating system needs re-balancing to compensate for changes in building parameters.

Outdoor reset plus pulse-width-modulated zone valves: This last approach, combining the previous two systems, is based on system supply water

temperature modulation through mixing valve and outside temperature while individual zone control is performed through pulse-width modulating valves according to room air set point. The zone requiring the hottest supply water temperature provides indoor feedback to the outdoor reset control. This approach provides the best control of the room air and floor temperature and offers the greatest flexibility in application.

Experimental and theoretical studies (Athienitis and Chen, 1993; Athienitis, 1994) indicated that proportional control of room temperature with a constant setpoint resulted in improved thermal performance. It was reported, however, that implementation of energy saving strategies, such as storage of passive solar gains in the floor and a lower setpoint at night, renders effective control difficult. Results showed that on-off control with night set-back (square wave set-profile) contributes to energy conservation but often leads to a very high increase (over 100%) in the peak heating load on cold days particularly for building with thermal storage. A smoother setpoint profile with a ramp change in the set point is required to obtain the desired temperature and limit the maximum heating load. Storage of solar gains can be effectively achieved by lower night time set point, to keep cool the floor mass in anticipation of the upcoming solar gains, followed by a gradual increase in the morning to the desired comfort range.

Cho and Zaheer-uddin (1997) conducted an experimental study to asses

performance of on-off, proportional integral (PI) and two-parameter (air and floor slab temperature) controls under similar conditions. Air temperature based on-off control resulted in a 3°C variation in air temperature and 9°C in the floor slab temperature. On the other hand, on-off control using slab temperature as a control signal resulted in a good room temperature regulation (within +/- 0.75°C of the set point). The PI control mode, relying on a modulating mass flow rate in response to a feedback signal from the room air temperature sensor while maintaining the hot water temperature constant, was by far the better of the strategies tested. However, the two-parameter on-off strategy with the performance that came close to that of PI control was rated a good candidate for radiant heat control because of its simplicity and cost-effectiveness.

Thermal mass integrated with a floor heating system in a passive solar house is known for its capacity to reduce peak heating loads by loads shifting and decrease temperature swings while using the solar gain to reduce energy consumption. However the inherent large thermal lag encountered, particularly with heavy floor thermal mass, may present control difficulties using conventional techniques. Conventional system weakness such as their inability to compensate for thermal lag, varying set-points and changing dynamics requires innovative technique such as the Generalised Predictive Control (GPC). Predictive control algorithm can compensate not only for a process thermal lag but also for the pre-programmed set point. The thermal lag compensation provided by a predictive controller can greatly improve closed-loop stability, while its prediction property

enables control action to start earlier so as to closely track the varying set point.

An evaluation (Chen, 2002) performed through computer simulation revealed that performance of floor heating system controlled by GPC is superior to that on-off and P.I. controllers in terms of response speed to changes in set point, minimum offset and on-off cycling. This simulation required the development of a set of supervision rules for robust system identification and a recursive least squares algorithm. Experimental results with an indoor globe simulating operative temperature agreed well with the predicated data.

Following this trend, a recent study (Cho and Zaheer-uddin, 2003) involving both computer simulation and experiments was conducted to asses and compare the energy performance of predictive control strategy with an existing conventional control strategy of intermittently operated radiant floor heating system. Intermittent control strategy is known to utilize effectively the thermal storage characteristics of the floor slab. This mode of control is based on heat flux delivery a certain number of times of certain (and possibly different) period durations, at some prescribed hours and the whole depending on outside conditions. The current practice for the evaluation of theses parameters is based on past operating experience. Under this control mode, Radiant floor heating system practically runs in an open loop mode, eliminating thermostat and associated hardware

In order to implement this predictive control strategy, a forecasting model based on the Fourier series method was adapted to predict the hour-by-hour

magnitude of outdoor air temperature. The required input to the model, expected maximum and minimum temperature and their time–of-day occurrence, were obtained from the meteorology services. Heat distribution pattern, heat supply on time and heating loads determination are based on the forecasting model, building geometry and thermal design data. A dynamic simulation program (TRNSYS) with an incorporated radiant floor heating model was used to perform the simulations.

Results showed that the predictive control strategy was 10% to 20% more energy efficient. The room fluctuation remained within comfort range in spite of the fact that no zone temperature control was used.

This approach is reinforced by a recent article (Tse, 2003) describing an innovative algorithm to predict the daily thermal loading of a building. This new algorithm utilizes updated weather forecast information from the internet and analyzes it by a knowledge-based system to simulate the overall weather condition in terms of air temperature profile, air relative humidity profile and solar radiation profile. Daily thermal load profile of a building is then predicted through computer simulation using the simulated weather condition. The algorithm was proven to have a good thermal load prediction capability with prediction error well within acceptable region.

2.4 Experimental investigations

Dale (1993) conducted in the early 90's a three years study on the thermal

performance of a radiant floor panel in a test house at a research facility in Alberta. The evaluation involved two commonly installed radiant floor systems: the first system utilized hot water tubes placed below the subfloor between the floor joists on the main floor while the second had tubes laid over the subfloor and embedded in gypsum-based cement. Both systems were compared to a conventional duct distribution forced air-heating system. The control strategy relied on simple air thermostat.

They observed contrarily to their expectation, no significant energy saving with radiant floor panel heating. This surprising result was attributed to the increased losses due to the higher ceiling and basement floor temperature in the test house resulting from the use of the radiant heating system. Further, the radiant floor panel system was found to produce very uniform floor-to-ceiling temperature profiles with 0.5°C to 1.0°C typical variation from very near to the floor to near the ceiling.

The temperatures inside two black 150mm diameter globe thermometers, located at different distances from a cold south-facing window, were also measured to asses the use of panel heating in counteracting the asymmetric radiant filed produced by a south-facing window (Asymmetric radiant filed may lead to discomfort due to heat exchange between a person and a cold surface such as a window). The radiant panel systems were found to produce higher globe temperature, up to 0.5°C above air temperature, indicating a higher mean radiant temperature and thus the possibility of reducing the interior air temperature while maintaining the same comfort level, with subsequent potential

energy savings.

In an experimental study (Olesen, 1994), the controllability of a standard floor heating systems with tubes embedded in concrete was compared to a low temperature radiator system. The study was conducted in a low thermal mass test room and simulated dynamic conditions to variation in outdoor temperature, occupant load and sunlight and night set back operation, with a hydronic floor heating system. The test room was equipped with 50 permanent sensors for measuring air and surface temperatures, temperature difference across the floor insulation and across wall and across insulation, heating system water supply and return temperature and energy consumption.

The thermal comfort conditions in the room were evaluated with the Predictive Mean Vote (PMV) index (ISO Standard 7730, 1994) and equivalent temperature (Madsen et al. 1984) are measured 0.6 m above the floor at three locations in the room with an integrated sensor simulating a sedentary person. The equivalent temperature integrates the combined influence of air temperature, mean radiant temperature and air velocity. The equivalent temperature is equal to the operative temperature for low air velocity less than 0.1 m/s. Tests were carried out with control flux-modulation with and without outdoor reset.

The results showed that, for both heating systems, energy consumption was similar and the control easily kept the room temperature within acceptable limits. It was also observed that night set back operation induced greater decrease room temperature for the radiator system and for the low-mass radiant

floor heating system.

De Carli (2002) conducted field measurement of operative temperature in four buildings heated or cooled by embedded water-based radiant systems. The analysis of the data showed that, for the major part of the time of occupancy, the operative temperature was inside the comfort range. The data showed an increase in space temperature during the day, which is counterbalanced by a corresponding decrease during the night. This study concluded that hydronic radiant systems constituted a viable alternative to full-air conditioning systems for obtaining acceptable indoor thermal environments.

A project (Scheatzle, 2003), initiated by ASHRAE with objective to provide documented performance of a hybrid HVAC system, successfully demonstrated the use of radiant panels for both heating and cooling in conjunction with ventilation/ dehumidification units to achieve thermal comfort in a residence. The scene of this project is a single-storey adobe house, with high mass walls insulated on the exterior, radiant heating panels over the entire concrete floor area and 60 % of the ceiling. The control is divided into central control based on the water supply temperature according to the outside temperature and individual zone control based on the operative temperature. The control strategy included the use of passive components such as the high thermal mass of the house for use of off-peak energy rates and active component such as the high mass floor panels to keep the temperature within the zones spaces within comfortable limit

while using the low mass ceiling panels to provide quick warm-up response, especially during the early cold morning hours. The convective system was used for additional peak-load capabilities and indoor air quality.

2.5 Building performance evaluation techniques

Traditionally, building thermal dynamics and control studies are performed separately from HVAC system design and building thermal energy analysis without sufficient considerations of the system loads, their variability and the interaction between the building envelope, the HVAC system and the control system. This approach combined with static control does not take full advantage of the existing potentiality. This evidence reinforced by the accelerated trend towards energy efficient building and environmental issues confirms the requirement for a unified approach involving the building subnetworks in order to analysis the overall system performance. In broad terms, there are two main approaches: time domain versus frequency domain.

Time domain technique

Time domain simulation approach includes finite difference and finite element, state space and response factor techniques. Finite difference is the technique most commonly applied to the problem of building energy modeling. Finite-difference methods usually fall into two categories: explicit and implicit, depending on whether one can predict the temperature at a node independent of the predictions made at other nodes, or whether all node predictions must be

made simultaneously. This method generally provides a more accurate estimation of temperature and heat flows due to its capability to model both linear and non-linear system. The explicit finite difference method is particularly suitable for analysis of non-linear heat diffusion problems such as heat transfer through the floor (Athienitis, 1997).

These techniques use discretization in space and time and may require a large number of nodes and sometimes small time step to avoid error in the simulation of thermal mass behavior. However, too many nodes and very small time step increase the model complexity and may lead to computation inefficiency. The response factor requires time discretization only and can be used if non linear element in building system can be linearzed so that the whole or subsystem becomes linear. It uses fewer nodes avoiding therefore the error from discretization. One major disadvantage of these techniques is that initial conditions are usually unknown. This implies repeated simulation until a steady periodic response is obtained.

HVACSIM$^+$ (1985) is a time domain simulation program developed for comprehensive building approach, primarily for research purposes. Some of the required parameters, however, such as time constant of various system components lack accuracy.

Another more recent comprehensive building approach tool, still under evaluation at this date, is the EnergyPlus software (Strand and Pederson, 1997and 2002) which in addition to its ability to model configurable forced air system, also included models for low-temperature radiant heating, cooling systems (electric

and hydronic) and high-temperature radiant heating systems. Accurate temperature and comfort prediction is reached through an integrated simultaneous simulation. Loads calculated at a user-specified time step are passed to the building systems simulation module at the same time step. The building systems simulation module calculates, with a variable time step down to seconds, heating and cooling system and plant and electrical system response, with space temperature feedback. The ability of this program to model radiant heating system and thermal comfort evaluations gives designers the possibility to make comparison with forced air system. It allows also selection of multiple systems for a single zone, that is hybrid-system such as multiple active radiant surfaces /systems and/or combination of convective/radiant systems.

Frequency domain method

The frequency domain technique is an alternative approach to linear and time invariant system simulation. This method is based on the development of a mathematical model describing the heat transfer process. The methodology presented by Athienitis et al. (1990) for system thermal analysis utilizes frequency domain technique with associated Laplace transform and Fourier series. This frequency domain approach allows accurate representation of the actual system and identification of building significant thermal characteristics such as transient response, state variables and system parameters. The detail with which the model describes the building thermal characteristics has a significant impact on the degree of accuracy of the analysis. This technique is

particularly suitable for passive solar analysis and load calculations (Kimura, 1977).

The frequency method has proven several advantages over time domain technique. It provides ease and flexibility in simulation and energy analysis with variables numbers of harmonics although this number must be kept within reasonable limit to avoid computation inefficiency. The resulting solutions are rapid and can be made exact, which is useful for validation of other more approximate solution methodologies. The main disadvantage of frequency domain technique compared to time domain technique is its application mostly limited to linear and time invariant system. This technique, on the other hand, does not require discretization and is particularly useful in building modeling with significant thermal mass amount (Balcomb, 1992).

Both techniques have their specific application and have been showed to be sufficiently accurate (Haghighat and Athienitis, 1988), time domain method is more appropriate and widely used for non linear system analysis whereas frequency domain methods find its application where the final objective is the determination of the building response pattern through a linearization of system, a compromise generally accepted in engineering practice.

2.6 Conclusion and motivation for proposed work

Radiant heating systems can be complex to design and control, particularly when they utilize much thermal storage which is intended also to

store passive solar gains. There is a need for development of accurate and practical techniques for design and control analysis of such systems. This thesis uses a frequency domain approach for analysis of radiant heating with solar gains to investigate its thermal dynamics and implications for design and control. Results are also compared with finite difference simulations.

CHAPTER 3

ROOM THERMAL NETWORK

3.1 Introduction

In order to perform room thermal analysis using the frequency method, an accurate heat balance describing the thermal processes involving conduction, convection and radiation inside and outside the space is required. To write heat balance equations, a space in the building under analysis is considered as an enclosure bounded by a number of discrete surfaces (walls, floors, windows, and ceiling), subjected to internal conditions such as floor heating system and external weather conditions. To help in describing and understanding the different heat transfer occurring within the space, a schematic representation of the room with radiant floor along with a detailed thermal network model of 9 nodes with interconnecting paths in shown in Figure 3.1.

Borrowing a terminology from electrical circuit elements, the thermally massive walls are modeled by a two-port distributed element while the room air and light-weight content are modeled by a lumped capacitance. Outdoor temperature and solar radiation are represented respectively by temperature source and heat source. Node 0 denotes the indoor air temperature, node 1 and 2 represent the interior surfaces of the 02 windows, nodes 3 to 7 are the interior surfaces of the surrounding walls plus the ceiling, node 8 denotes the upper surface of the radiant floor with the most significant thermal mass.

In order to accurately assess the impact of conductive, convective, and

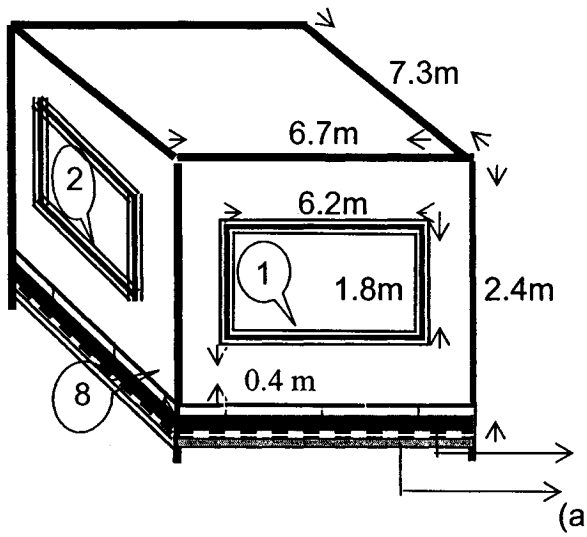

Material properties

R-values

Walls	: 2.6 m².°C/W
Ceiling	: 7 m².°C/W
Windows	: 0.32 m².°C/W
Floor	: 1 m².°C/W

		Concrete	Gypcrete
Thickness (m)	x	0.09	0.09
Density (kg/m³)	ρ	2242	1600
Conduct.(W/m°C)	k	1.8	0.68
Spec. heat (J/Kg°C)	c	840	943

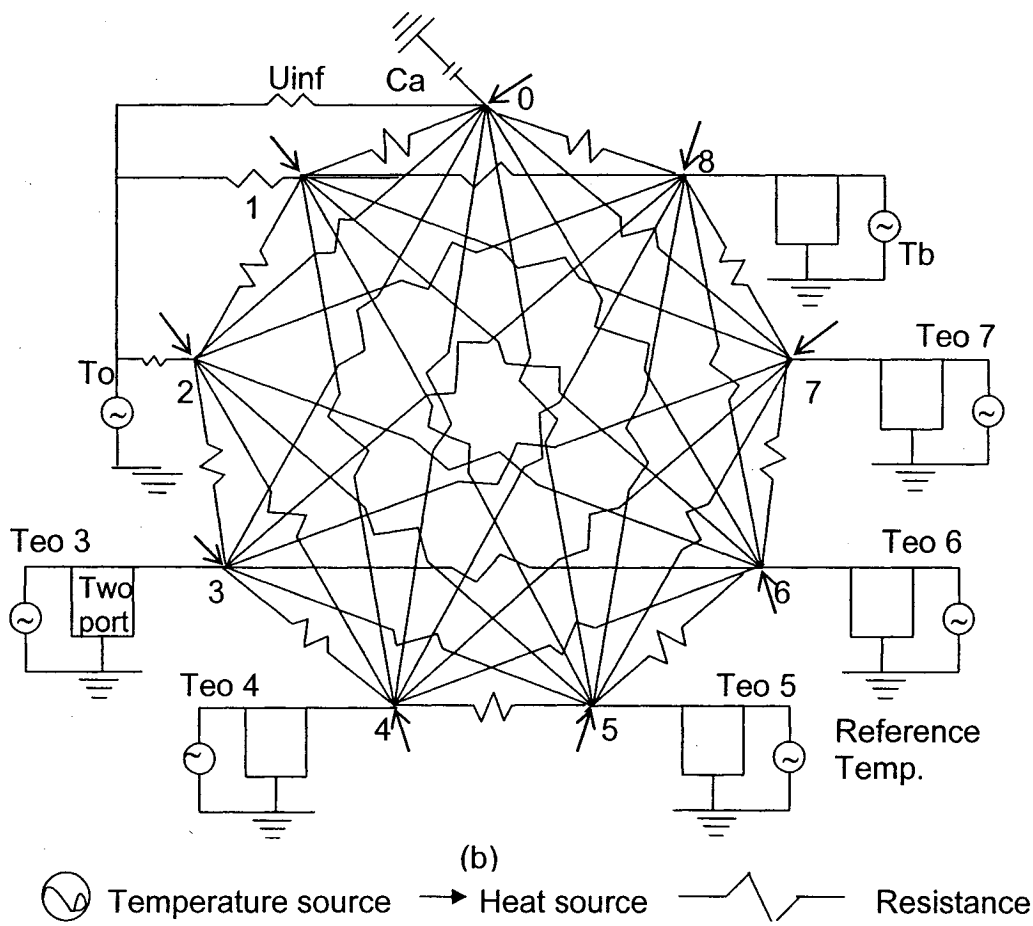

Figure 3.1: (a) Room schematic, (b) Detailed room thermal network: nodes: 0 = room air, 1–8 interior surfaces, 1 = south window, 2 = west window, 3 = south wall, 4 = ceiling, 5 = east wall, 6 = north wall, 7 = west wall, 8 = floor; Teo = sol-air temperature, To = outside temperature

radiative effects within the room, it is necessary to evaluate as accurately as possible the corresponding different heat transfer coefficients.

Conduction, covered in detail in the next chapter, is a transient process and thus cannot be modeled with steady-state equation due to the presence of thermal mass within the room, whose multilayered walls are modeled by transfer admittance and self-admittance using the frequency domain technique. Convection coefficients can vary with time both at the inside and the outside surface due to changing temperatures and flow conditions. Radiation is a complex process involving mainly long-wave radiant radiation due to interior surfaces exchanges and short-wave radiations to the sun.

The accuracy of the heat balance solution depends obviously on the accuracy of the solution components. However, the goal of this research work not being to study in depth all the different parameters and in order to find a reasonably accurate solution in an acceptable period of time, the following common assumptions are made to simplify the calculations:

-All the building interior surfaces and the room air are at uniform temperature (At any given point in time, each building element is characterized by a single temperature at the interior side and a single temperature at the exterior side; larger surfaces may be broken up into multiple surfaces for better temperature differentiation such as a wall incorporating a window).

-Thermal properties of the material are time and temperature independent.

-Heat transfer through the building envelope is one-dimensional.

-Convective heat transfer coefficients are time invariant and valid over the

entire surface.

-Infiltration is constant.

-The radiative conductances are linearized

3.2 Thermal convection

Thermal convection is the process by which heat transfer takes place between a solid surface (i.e. wall) and the fluid surrounding it (air). The motion of the fluid due solely to the action of buoyancy forces arising from the density variation of the fluid as the result of heating is called free convection while the motion of the fluid caused by forces independent of the temperature differences in the fluid arising from external imposed pressure differences is referred as forced convection. The rate of heat transfer by natural convection between the fluid and the boundary surface is evaluated by the following expression:

$$q = A h_c (T_s - T_{ai}) \tag{3.1}$$

where A, h_c, T_s and T_{ai} are respectively the area, the heat transfer coefficient, wall surface and air temperature.

The convective conductances represented by the resistances connecting node 0 (room air) to node J (interior surfaces 1 to 8) in Figure 3.1 is given:

$$U_{0,j} = A_j h_{c(j)} \tag{3.11}$$

3.21 Convective heat transfer coefficients

Calculation of the coefficient h_c is a very complicated function of the air flow and its geometrical arrangement. Heat transfer coefficients are evaluated

from empirical equations, often linearized, obtained from experimental results with the method of dimensional analysis (Athienitis, 2000)

Horizontal Surfaces: Heat flow downward or upward occurs mainly with horizontal surfaces such floor and ceiling. Downward flow is applicable generally for cold surface such as the floor and the recommended correlation is:

$$h_c = 0.59((T_s - T_{ai})/x)^{0.25} \quad (3.2)$$

x is the characteristic dimension and laminar flow is assumed with Rayleigh number in the range of $3x\ 10^5$ to $3x\ 10^{10}$

Heat flow upward, applicable in the present case, occurs with heated floor or/and ceiling. The following turbulent flow correlation with Rayleigh number in the range of $2x\ 10^7$ to $3x\ 10^{10}$ is recommended:

$$h_c = 1.52(T_s - T_{ai})^{1/3} \quad (3.3)$$

A 10°C constant temperature differential between design air temperature (20°C) and the 29°C maximum allowed surface temperature (ANSI/ASHRAE standard 55, 1992) is assumed for the heated floor and the ceiling. The numerical value for the case under consideration is h_c=3.275 watt/(m^2·°C) (for Figure 3.1).

Vertical Surfaces: Heat flow follows a horizontal path with vertical surfaces and is independent of direction. The convective heat transfer is commonly assumed to occur under turbulent flow conditions because flow is well developed after a short distance from the bottom or top of a wall. The following correlation is often used with an assumed Rayleigh number in the range of 10^4 to 10^9.

$$h_c = 1.31(T_s - T_{ai})^{1/3} \quad (3.4)$$

There is considerable disagreement on recommended convective heat transfer coefficient values for h_c to be used in building analysis. Holman (1976) argued that ASHRAE convective heat transfer coefficients can significantly over predict convective heat transfer. ASHRAE (1981) recommended coefficient (h_c=3.08 watt/($m^2 \cdot °C$)), is based on approximately a 13°C temperature differential, which may be considered as a typical value for window surfaces during cold days. However, simulations carried out with the suggested ASHRAE coefficient resulted in the present case in smaller temperature differential (10°C and 4°C for window and walls respectively). This may be due to passive solar radiation and clear day assumptions. In view of this fact and in order to be consistent, iterative calculation is conducted to determine the up flow heat transfer coefficients corresponding to the assumed temperature differential. The results confirmed Holman statement (windows: $h_1=h_2$=2.822 watt/($m^2 \cdot °C$) and walls: $h_3=h_5=h_6=h_7=h_c$=2watt/($m^2 \cdot °C$)

3.3 Radiation heat transfer

Thermal radiation (Athienitis and Santamouris, 2002) is electromagnetic radiation emitted by a body as a function of its temperature. Thermal radiation is in the wavelength range from about 0.1 to 100 μm. The visible portion lies in the range of about 0.35 μm - 0.75 μm. In building thermal analysis we generally separate thermal radiation into two regions: the short-wave region with less than or equal to 3 micrometers and the long-wave region with wave-length greater than 3 micrometers. More than 99% of the radiation emitted by the sun is

shortwave, while more than 99% of the radiation emitted by bodies at earth temperatures (40°C to 45° C) is long-wave.

Long-wave radiation is an important mode of heat transfer between surfaces on the inside of buildings (particularly with radiant floor system). The walls transfer heat directly to each other by radiation, and some heat is radiantly exchanged with the air. The radiant heat exchanges within the room can be calculated more accurately than the convective exchanges.

3.31 Radiation proprieties

The absorptance of a surface is the fraction of total irradiation (incident radiation) absorbed by the body. The reflectance of the surface represents the fraction of the irradiation reflected from the surface. The transmittance represents the fraction of the irradiation transmitted by the surface (equal to 0 for opaque surfaces such as walls and approximated to 0.035 to double glazed window). Applying the first law of thermodynamics, an energy balance at the surfaces shows that:

$$\alpha + \tau + \rho = 1 \qquad (3.5)$$

where ρ = reflectivity, τ = transmittance and α = absorptance

Emissivity, absorptance, transmittance and reflectance generally vary with wavelength. It can be shown that the monochromatic emissivity and the absorptance of a surface are equal. Consequently, the reflectivity of a surface is: $\rho = 1 - \varepsilon - \tau$. Walls and windows long-wave emissivities ϵj can usually be approximated as ϵ =0.9, therefore their reflectivity are equal to 0.1 and 0.065.

3.32 Radiative conductances

The radiative conductances interconnecting room interior surfaces nodes 1 to 8 (Figure 3.1) are given by:

$$U_{i,j} = A_i \sigma 4 Tm^3 F^*_{i,j} \qquad (3.6)$$

$4Tm^3$ is a linearization factor which is based on an estimated average room temperature Tm=294°K (may be reevaluated for each pair of surfaces). The Stephan-Boltzmann constant σ is equal to $5.669 \cdot 10^{-8}$ $W/m^2 \cdot K^4$ and temperature is in Kelvin. The radiation exchange factor $F^*_{i,j}$ between the pair of surfaces under consideration (i and j) are determined from the radiation view factors $F_{i,j}$ and the radiative properties of the room surfaces as follows:

$$F^*_{i,j} = (m_i \varepsilon_i \varepsilon_j)/\rho_i \qquad (3.61)$$

Where $[m] = [M]^{-1}$ (3.61a)

and the elements of matrix [M] are:

$$M_{i,j} = I_{i,j} - \rho_i F_{i,j} \qquad (3.61b)$$

with $I_{i,j} = 1$ if $i = j$; otherwise $I_{i,j} = 0$ (identity matrix).

The radiation exchange factor $F^*_{i,j}$ of a surface to itself is equal to 0 and the resulting convective and radiative heat loss conductances U of the surfaces room under consideration is under matrix format as shown by equation (3.62).

3.4 Carpeted floor heat transfer coefficient

Precise investigation of the floor concrete with carpet requires complexes calculations and involves cascades matrix. The carpet thermal capacity being

negligible in the overall room response, simulations are carried out assuming the carpet as a simple resistance in series with the inside air film, and the radiative heat loss coefficients as material independent which is an acceptable assumption for the purpose undertaken by this research paper.

Assuming carpet thermal conductivity k_c=0.06 watt/m·°C and a thickness of x_c=0.02m, the carpet heat loss coefficient would be equal to $u_c=k_c/x_c$. In accordance with the assumption made above, the overall convective heat loss coefficient carpet in parallel with the air film is would be: $h_{cc}=(h_c \cdot u_c)/(h_c+u_c)$, (1.566 watt/m^2·°C in the present case). This constitutes the only modification to be made to the convective and radiative conductances matrix $U_{(i,,j)}$ within the room with floor carpet cover. The convective conductance interconnecting the carpeted floor surface node 8 and the room air node 0 (that is entries $U_{0,8}$ and $U_{8,0}$ of equation (3.62)) is subsequently lower and equal to 76.58·watt/m·°C.

$$U_{i,j}=\begin{bmatrix} 0 & U_{0,1} & U_{0,2} & U_{0,3} & U_{0,4} & U_{0,5} & U_{0,6} & U_{0,7} & U_{0,8} \\ U_{1,0} & 0 & U_{1,2} & U_{1,3} & U_{1,4} & U_{1,5} & U_{1,6} & U_{1,7} & U_{1,8} \\ U_{2,0} & U_{2,1} & 0 & U_{2,3} & U_{2,4} & U_{2,5} & U_{2,6} & U_{2,7} & U_{2,8} \\ U_{3,0} & U_{3,1} & U_{3,2} & 0 & U_{3,4} & U_{3,5} & U_{3,6} & U_{3,7} & U_{3,8} \\ U_{4,0} & U_{4,1} & U_{4,2} & U_{4,3} & 0 & U_{4,5} & U_{4,6} & U_{4,7} & U_{4,8} \\ U_{5,0} & U_{5,1} & U_{5,2} & U_{5,3} & U_{5,4} & 0 & U_{5,6} & U_{5,7} & U_{5,8} \\ U_{6,0} & U_{6,1} & U_{6,2} & U_{6,3} & U_{6,4} & U_{6,5} & 0 & U_{6,7} & U_{6,8} \\ U_{7,0} & U_{7,1} & U_{7,2} & U_{7,3} & U_{7,4} & U_{7,5} & U_{7,6} & 0 & U_{7,8} \\ U_{8,0} & U_{8,1} & U_{8,2} & U_{8,3} & U_{8,4} & U_{8,5} & U_{8,6} & U_{8,7} & 0 \end{bmatrix} \quad (3.62)$$

The effective results for thermal network Figure 3.1 with floor concrete are as shown in Table (6.62a)

3.5 Calculation of view factors

The view factor $F_{i,j}$ represents the radiant interchange factor of surface i with respect to surface j and is equal to the ratio of the diffuse radiant energy emitted by surface i and ultimately absorbed by surface j (both directly and after reflections off other surfaces) to the total radiant energy emitted by surface i as if it were a blackbody. It can be noted that the concept of blackbody is introduced for the purpose of studying the characteristics of thermal radiation while for the convenience of calculations, real surfaces are often assumed diffuse and grey. The view factor between two surfaces as depicted by Figure 3.2 is given by:

$$A_i F_{i,j} = \iint \frac{\cos\varphi_i \cos\varphi_j}{\pi r^2} dA_i dA_j \qquad (3.7)$$

Where dA_i and dA_j are elementary areas of the surfaces and r is the distance between the two areas and ϕ_1 and ϕ_2 are the angle between the respective normal to the surfaces and the line r connecting the two surfaces

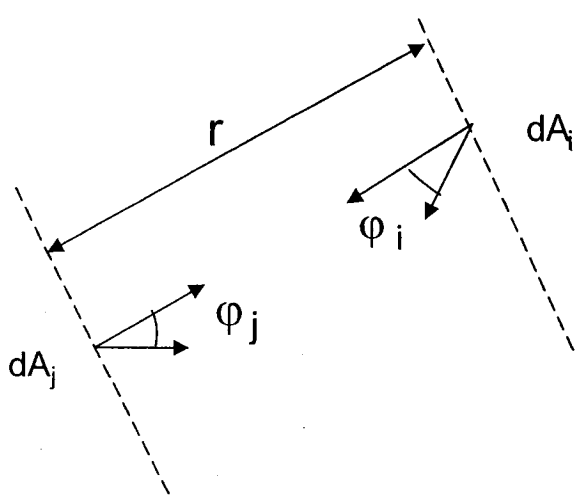

Figure 3.2: View factor $F_{i,j}$ geometry

When the equation can not be integrated analytically, numerical integration techniques may be applied, replacing the integrals with summations avec the discretized surfaces. There are three main types of view factors between room surfaces:

1-between surfaces at right angle

2-between parallel surfaces

3-between the window and another surface

The angle factor from j to i is similarly defined, simply by interchanging the role of i and j. However this does imply that the second angle factor is numerically equal to the first one. The determination of the view factors for the room under consideration are carried out in two steps (Athienitis, 1998). The first step consists in calculating the view factors between the rectangular finite surfaces inclined at 90 degrees to each other with one common surface as follows:

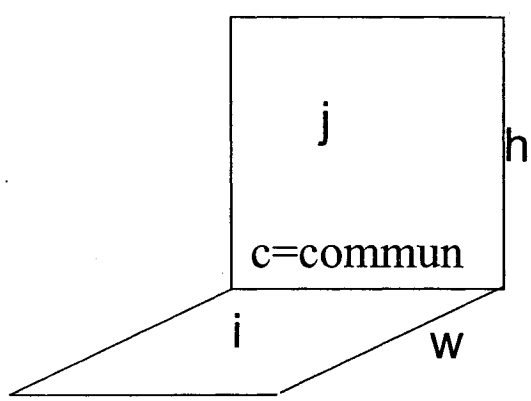

$$X = \left(\frac{w}{c}\right) \qquad Y = \left(\frac{h}{c}\right)$$

Figure 3.3: View factor from i to j

The View factor $F_{i,j}$ from i to j is defined by the following relationship:

$$F_{i,j} = \frac{1}{\pi X}\left(\begin{array}{l} X\tan^{-1}\left(\frac{1}{X}\right) + Y\tan^{-1}\left(\frac{1}{Y}\right) - \sqrt{X^2+Y^2}\tan^{-1}\left(\frac{1}{\sqrt{X^2+Y^2}}\right) \\ +\frac{1}{4}\ln\left(\left(\frac{X^2\left(1+X^2+Y^2\right)}{\left(X^2+Y^2\right)\left(1+X^2\right)}\right)^{X^2}\left(\frac{Y^2(1+X^2+Y^2)}{\left(X^2+Y^2\right)\left(1+X^2\right)}\right)^{Y^2}\left(\frac{\left(1+X^2\right)\left(1+Y^2\right)}{1+X^2+Y^2}\right)\right) \end{array}\right) \quad (3.8)$$

The second step consists in calculating the other view factors between the room surfaces by applying the following principles:

1. Reciprocity: $A_iF_{i,j} = A_jF_{j,i}$

2. Symmetry e.g.: $F_{7,5} = F_{5,7}$

3. Energy conservation: $\sum_j F_{i,j} = 1$

<u>Example of calculation of view factors between windows and related surfaces</u>

The same principles, by means of view factor algebra method, can be applied to other geometries. Surfaces with a non uniform temperature such a wall with a window are subdivided into smaller isothermal zones and a configuration factor algebra method is applied based on the same principles .The window view factors are then calculated by adding and subtracting already calculated views factors of related configuration. Because of geometrical complexities, view factors values are difficult to determine and require a tedious three-dimensional description of the spaces. An example of room schematic representation of thermal network under consideration (Figure 3.1) with view factors calculations between window 1 and window 2 is given below.

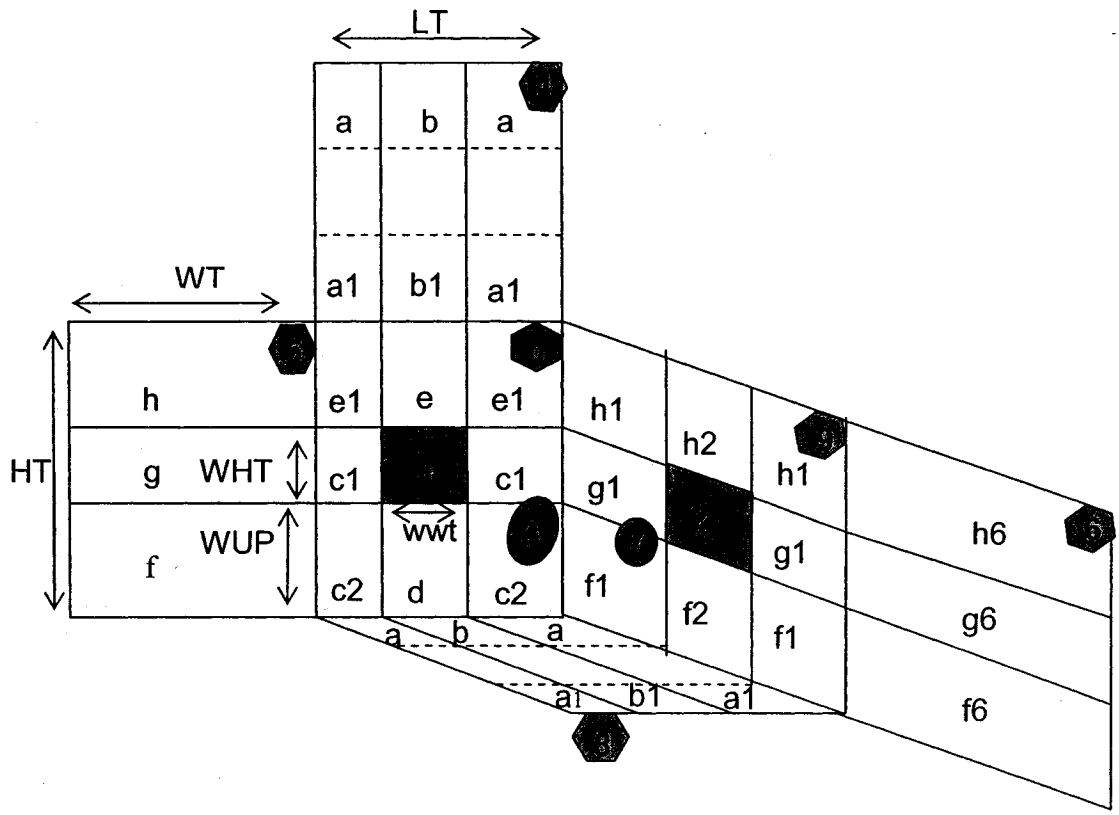

Figure 3.4: Partitioned room schematic

$$DIS = \frac{LT - WWT}{2} \qquad Ag1 = \frac{WT - WWT}{2}$$

$$Ab = WWT \times WT \qquad Ad = WWT \times WUP$$

$$Ac1 = WHT \times DIS \qquad Ac2 = WUT \times DIS$$

Calculation of the windows different view factors requires determining related view factors as follows:

View factor $F_{g1,1c1}$ from surface A_{g1} to surface A_{1+c1} is obtained through application of equation with the following modification:

$$w = \frac{WT - WWT}{2} \qquad h = \frac{LT + WWT}{2} \qquad comm = WHT$$

View factor $F_{g1,c1}$ from surface A_{g1} to surface A_{c1} is obtained through application

of equation with the following modification:

$$w = \frac{WT - WWT}{2} \qquad h = DIS \qquad comm = WHT$$

View factor $F_{c1,2g1}$ from surface A_{c1} to surface A_{2+g1} is obtained through application of equation with the following modification:

$$w = DIS \qquad h = \frac{WT + WWT}{2} \qquad comm = WHT$$

View factor $F_{1c1,2g1}$ from surface A_{1+c1} to surface A_{2+g1} is obtained through application of equation with the following modification:

$$w = \frac{LT + WWT}{2} \qquad h = \frac{WT + WWT}{2} \qquad comm = WHT$$

View factor $F_{1,2}$ is obtained by subtraction and additions of the related view factors calculated previously.

$$F_{1,2} = \frac{(A_1 + A_{c1})F_{1c1,2g1} - A_{g1}F_{g1,1c1} + A_{g1}F_{g1,c1} - A_{c1}F_{c1,2g1}}{A_1}$$

Application of the reciprocity principle yields:

$$F_{2,1} = \frac{A_1}{A_2} F_{1,2}$$

In the same way:

$$F_{1,7} = F_{1,9} - F_{1,2} \qquad F_{7,1} = \frac{A_1}{A_7} F_{1,7}$$

$$F_{2,3} = F_{2,0} - F_{2,1} \qquad F_{3,2} = \frac{A_2}{A_3} F_{2,3}$$

Based on the fact that the radiant interchange factor of a surface is the summation of the view factors of its different zones ($A_0F_{0,9}=A_{(1+3)}F_{(1+3),(2+7)}$):

$$F_{3,7} = \frac{A_0 F_{0,9} - (A_1 F_{1,2} + A_1 F_{1,7} - A_3 F_{3,2})}{A_3} \qquad F_{7,3} = \frac{A_3}{A_7} F_{3,7}$$

Surfaces facing the same direction cannot see each other, consequently cannot exchange radiation, and therefore are assigned a view factor of zero. The energy conservation principle can be used to derive view factors for parallel opposite surfaces and for conducting preliminary verification of the results. The sum of view factors of any surface with respect to all the others surfaces for thermal network Figure 3.1 is equal to 1.

$$\sum_{i=1}^{8} F_{i,j} = \sum_{j=1}^{8} F_{i,j} = 1$$

<u>Effective results for thermal network Figure 3.1 (uncarpeted floor)</u>

$$U_{i,j} = \begin{bmatrix} 0 & 31.49 & 31.49 & 12.72 & 160.18 & 32.16 & 35.04 & 9.84 & 160.18 \\ 31.49 & 0 & 4.49 & 0 & 20.30 & 5.97 & 5.53 & 1.49 & 19.24 \\ 31.49 & 4.49 & 0 & 1.91 & 19.78 & 5.80 & 6.39 & 0 & 18.72 \\ 1.72 & 0 & 1.91 & 0 & 9.85 & 4.42 & 2.90 & 2.52 & 10.92 \\ 160.18 & 20.30 & 19.78 & 9.85 & 0 & 27.42 & 30.09 & 7.7 & 126.78 \\ 32.16 & 5.97 & 5.80 & 4.42 & 27.42 & 0 & 10.37 & 0.69 & 27.42 \\ 35.04 & 5.53 & 6.39 & 2.90 & 30.09 & 10.37 & 0 & 4.00 & 30.1 \\ 9.84 & 1.49 & 0 & 2.52 & 7.7 & 0.69 & 4.00 & 0 & 8.77 \\ 160.18 & 19.24 & 18.72 & 10.92 & 126.78 & 27.42 & 30.1 & 8.77 & 0 \end{bmatrix}$$

Table (3.62a): Convective and radiative heat loss conductances

CHAPTER 4

ROOM THERMAL RESPONSE

4.1 Introduction

As pointed out in the literature review, several approaches are available for the analysis of the behaviour of system through time. The frequency response method is a powerful mean for the analysis of linear dynamic systems and constitutes the transfer function formulation privileged in this thesis to investigate the thermal dynamics of a floor radiant heating system under different design option and weather conditions and to evaluate heating loads and room temperature response for any specified time history of inputs.

Fisk (1981) explains the implication of this choice with the Fourier's theorem which shows that any time varying quantity, say the heat input, can be represented by the sum of a number of sinusoidally time varying components at specified frequencies. Fourier's theorem states how to calculate the different components (frequency ω, amplitude of sinusoidal variation $q(\omega)$, its phase lag or lead $\Phi(\omega)$) from a time varying quantity q(t). A frequency response transfer function basically relates the values of the input amplitude to the output amplitude along with any change in phase angle for any specified frequency. The frequency response transfer function provide a convenient mean to determine the final temperature response from any input and is particularly useful in the context of building thermal response because two of the continuum of possible frequencies have special significance to the inputs.

The first frequency, called the fundamental frequency, is that associated with diurnal changes (24 hours period). Knowledge of the value of thermal response transfer functions during this period has been successfully adapted to an approximate theory of building thermal response theory called the admittance procedures (Milbank and Harrington-Lynn, 1974).

The second frequency of importance is zero since this frequency component gives the mean values of the input which represents the steady state thermal conditions whose only non-zero frequency component is that of the zero frequency itself. The zero frequency transfer function is basically the normal steady-state heat transfer coefficient.

4.2 Determination of room transfer functions

Heat transfer out of a building envelope can essentially occur by infiltration of external air displacing internal air, the ventilation loss and by conduction through the building fabric itself. Dynamic state, with time varying temperature, of wall thermal property is modeled by replacing its steady state conductance by a thermal admittance describing the effect of its thermal capacity.

The thermal admittance of a wall is a transfer function parameter useful for the analysis of the effects on room temperature of cyclic variations in the weather variables such as solar radiation, outside temperature and dynamic heat flows under steady periodic conditions. There are two transfer functions of primary interest, the self-admittance Ys relating the effect of a heat source at one surface to the temperature of that surface and the transfer admittance Yt relating the

effect of an outside temperature variation to the resulting heat flow at the inside surface. Two passive components are being identified in the frequency domain modeling of building heat transfer (Athienitis 1986):

-Non-massive layer identified as a two-terminal components and representing the thermal coupling between two nodes such as convective heating between a surface (walls nodes) and a fluid (air node 0) or radiative coupling between two surfaces exchanging energy. This includes conductive coupling if the relevant wall layer has negligible thermal capacitance.

-Massive layer identified as a three-terminal component (two-port) because of the third nodes required as a reference to quantify the thermal state of the slab, the two other terminals being the interior and exterior surfaces.

The two-port terminals equation can be expressed in many forms; the most widely used being the cascade form. The cascade form is derived by first taking the Laplace transform of the one-dimensional heat diffusion to obtain an ordinary differential equation which can be solved to relate heat flux and temperature at one surface to those at the other surface, without discretizing (Kimura 1977). The heat diffusion equation is as follows:

$$\frac{\partial T}{\partial t} = \alpha \frac{\partial^2 T}{\partial x^2} \tag{4.0}$$

The cascade equation for a massive single layer element is:

$$\begin{pmatrix} T_1 \\ q_1 \end{pmatrix} = \begin{pmatrix} D & B \\ C & D \end{pmatrix} \begin{pmatrix} T_2 \\ -q_2 \end{pmatrix} \tag{4.1}$$

The elements of the storage mass cascade matrix are given by:

$$D = \cosh(\gamma x) \tag{4.1a}$$

$$B = \sinh(\gamma x)/(\gamma x) \tag{4.1b}$$

$$C = (k\gamma)/\sinh(\gamma x) \tag{4.1c}$$

with the quantity k defining the storage mass thermal conductivity, x the mass thickness and γ equal to $(s/\alpha)^{1/2}$ with s being the Laplace transform variable and $\alpha=(k/c\cdot\rho)$ the storage mass thermal diffusivity. For frequency domain analysis, s is set equal to $j\omega$ where j=(-1)½ and ω is the frequency (equal to $(2\pi n)/P$, P represents a period of 86 400 seconds for diurnal analysis).

The cascade equation for a non-massive element (two-terminal components) is as follows:

$$\begin{bmatrix} T_1 \\ q_1 \end{bmatrix} = \begin{bmatrix} 1 & 1/u \\ 0 & 1 \end{bmatrix} \begin{bmatrix} T_2 \\ -q_2 \end{bmatrix} \tag{4.2}$$

The cascade matrix for multilayered wall, is obtained by multiplying the cascade matrices for consecutive layers represented by a two-terminal components (mass less insulation layer in series with an external air film) and a three-terminal components (inner layer of storage), both of uniform thermal properties. The resulting wall cascade matrix relates the temperature and heat flow at the inside and outside surface of that wall. In this way, the wall interior temperatures of no immediate interest are eliminated and the inside or the outside temperature is obtained. Each of the two-port elements in the thermal network Figure 3.1 represents the resulting equivalent two-port for each wall and the parameter of interest is the inside temperature.

$$\begin{bmatrix} T_1 \\ q_1 \end{bmatrix} = \begin{bmatrix} D & (D/u)+B \\ C & (C/u)+D \end{bmatrix} \begin{bmatrix} T_2 \\ -q_2 \end{bmatrix} \tag{4.3}$$

T_1 and q_1 are the temperature and heat source at node 1, T_2 and $-q_2$ are temperature and heat source at node 2 and heat conductance u is per unit area. Figures 4.1 and 4.1a show a two–port analogues and a multilayered representation for a slab and a multilayered wall, as well as the sign convention used for heat flows.

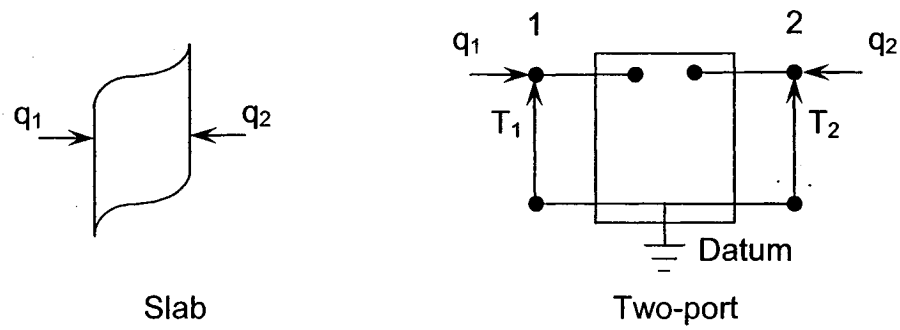

Figure 4.1: Representation of a single layered wall

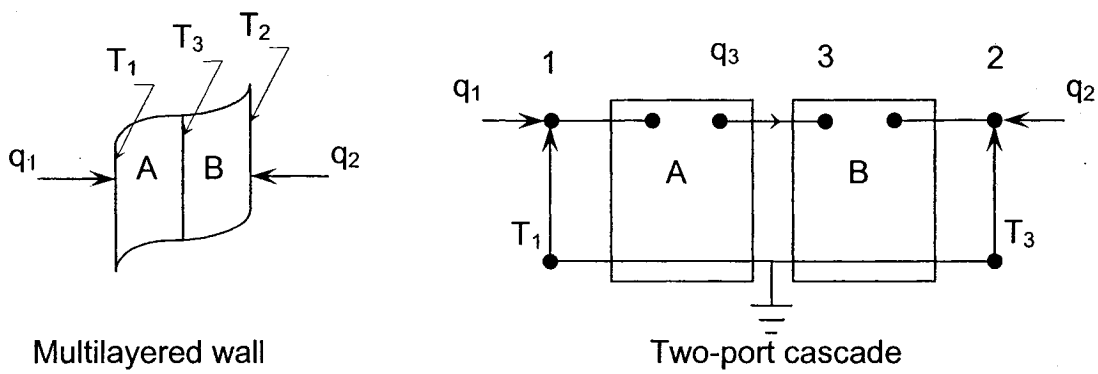

Figure 4.1a: Representation of a multilayered wall

4.21 Transformation from cascade to admittance form

The admittance form is necessary in modeling buildings with massive interior walls. It relates heat fluxes to temperatures as follows:

$$\begin{pmatrix} q_1 \\ q_2 \end{pmatrix} = \begin{pmatrix} Y(1,1) & Y(1,2) \\ Y(2,1) & Y(2,2) \end{pmatrix} \begin{pmatrix} T_1 \\ T_2 \end{pmatrix} \tag{4.4}$$

Application of conversion equations given in circuit theory books (Athienitis, 2002) translates to for a single layer wall:

$$Y(1,1) = D/B = (k\gamma)/\tanh(\gamma x) \quad (4.4a)$$

$$Y(1,2) = (BC - AD) = (-k\gamma)/\sinh(\gamma x) \quad (4.4b)$$

The matrix is symmetric because the two-port is reciprocal (heat flow does not depend on the direction of flow) hence Y(1,2)=Y(2,1). The diagonal elements in the cascade equation are equal, thus Y(2,2)=Y(1,1). These equations are per unit wall area. These results can be directly derived by application of the Norton theorem with the temperature sources and heat flows calculation at the proper ports as follows in the case of a multilayered wall.

4.22 Norton equivalent network for multilayered wall

A linear subnetwork connected to a network at only two terminals can be represented by its Norton equivalent (Athienitis et al, 1986), consisting of a heat source and an admittance connected in parallel between the terminals (Figure 4.2). The heat source is the short circuit heat flow at the node and the admittance is the subnetwork equivalent admittance as seen from the connection nodes.

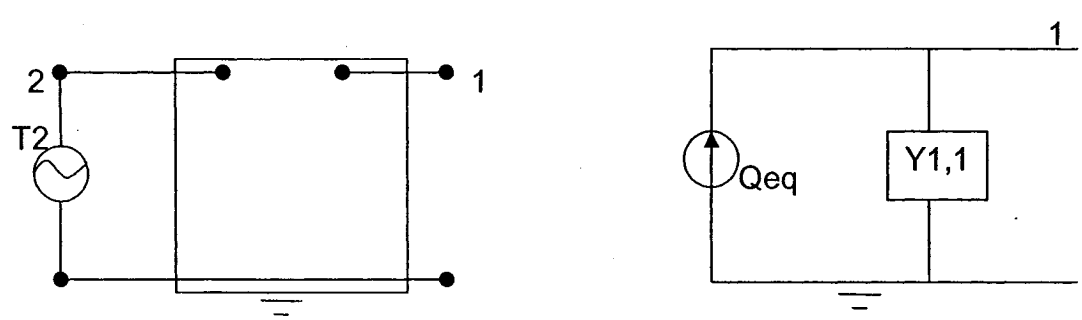

Figure 4.2: Wall Norton equivalent

Considering a multilayered wall (Figure 4.1a) represented by equation (4.3), the Norton equivalent source $Qsc = -Yt\,T_2$ is obtained after temporarily setting T_1 to 0 (short circuit) where the transfer admittance Yt is given by:

$$Yt = \frac{A}{\frac{\cosh(\gamma x)}{u} + \frac{\sinh(\gamma x)}{k\gamma}} = Y(1,2) \tag{4.5}$$

The self-admittance Ys is obtained by temporarily setting T_2 to 0 and as seen from the interior surface

$$Ys = A\frac{u + k\gamma\tanh(\gamma x)}{\frac{u}{k\gamma}\tanh(\gamma x) + 1} = Y(1,1) \tag{4.6}$$

The self-admittance mean term is basically equal to wall U-value excluding interior film. The admittances have been multiplied by the related area A to obtain the total value.

The transformation leaves only two-terminals with only the room interior nodes remaining. Therefore for a room with n walls, the number of simultaneous nodal heat balance equations is reduced by n after the transformation is carried out for each wall. When there is no mass, the simple equality is obtained Ys=Yt=U. Similar results are obtained for windows as well as for the infiltration conductance.

Wall self-admittance for infinitely thick wall with no heat loss at the back (high amount of insulation or adiabatic surface) can be approximated for design purpose by $Ys = A\,k\,\lambda\tanh(\lambda x)$

When the penetration depth defined as $d = \sqrt{2k/c\rho\omega}$ at a particular

frequency greatly exceeds the width of the slab; the slab behaves at that frequency as if it had no thermal mass at all. When the penetration depth is much smaller than the slab width, then the slab behaves like a semi-infinite solid equal to: $Ys = Ak\lambda$ and the phase lead is simply 45°. The transfer admittance, in theses cases, is negligible for all frequencies apart from the mean.

The frequency domain transfer function of the wall admittance (self admittance Ys and the transfer admittance Yt) are studied in terms of magnitude and phase lag and are then used together with Fourier series models for the weather variable, such solar radiation and ambient temperature, to determine the steady periodic thermal response of the walls.

4.3 Modeling of radiant floor internal heat source

The thermal mass integrated with the floor heating system has a considerable influence on the room response and thus make its thermal admittance the most useful parameters to analyze. Simulation of the internal heat source depth within the floor slab is achieved by the use of the Y-diakoptic techniques in conjunction with Norton theorem (Athienitis et al., 1986). The diakoptic method, based on the development for a thermal network analogous to that described by Brameller et al for electrical networks (1969), takes advantage of the topology and physical characteristics of a network by dividing it into a number of subnetworks by removal of edges (ties-network). The resulting equivalent source and equivalent self-admittance allow the floor heating system to be handled like any other surface within the heat balance framework. Heat

balances at the inside and outside surfaces take on the same form as other surfaces and the participation of the radiant system in the radiation balance within the space and thermal comfort is automatically included. Thus, the radiant system model is fully integrated into the heat balance and any improvement that are made in area such as convections coefficient are immediately available to the radiant system as part of the overall heat balance solution.

4.31 Diakoptic method

Considering a slab divided into two smaller slabs separated by the floor heating system, the upper slab would be the two-port components (edges 3 and 4, Figure 4.3) representing the thermal coupling between two zones, the lower slab and the floor surface. This separation allows the depth of installation of the floor radiant heating system to be defined by the thickness of the upper slab with respect to the surface floor. By inter-relating this upper slab thickness with that of the lower slab, the overall slab thickness remains the same.

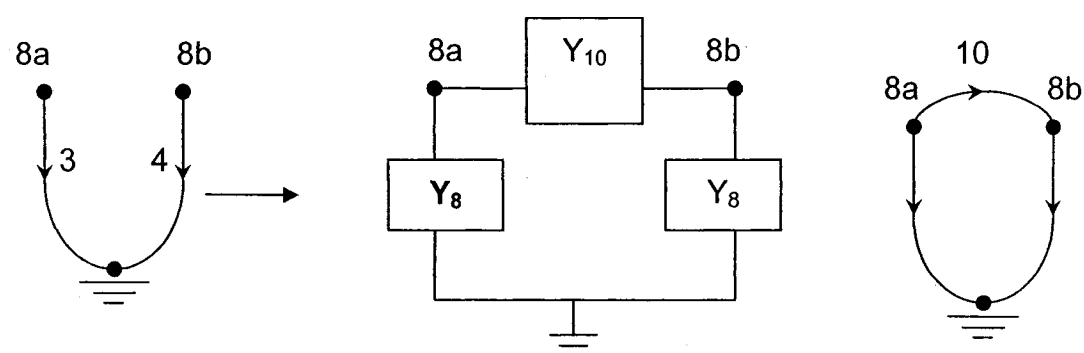

Figure 4.3: Slab diakoptic representation

The diakoptic method will be now applied to derive admittances of the upper slab of the floor. It is convenient to transform this three-terminal component into an equivalent delta section made up of three two-terminal components, such that no extra node is introduced (Figure 4.3). Considering the upper slab as a single massive layer, the delta section equivalent is derived as follows:

Let Y(i,j) be the two-port admittance matrix elements of the floor slab before the transformation and Y"(i,j) be the elements after the transformation. The two matrices must be equal for the transformation to be valid.

Thus $$\begin{bmatrix} Y''_{1,1} & Y''_{1,2} \\ Y''_{2,1} & Y''_{2,2} \end{bmatrix} = \begin{bmatrix} Y_{1,1} & Y_{1,2} \\ Y_{2,1} & {}_{2,2} \end{bmatrix} \tag{4.7}$$

$$Y(1,1) = Y(2,2) = \frac{Ak\gamma}{\tanh(\gamma x)} \tag{4.7a}$$

$$Y(1,2) = Y(2,1) = \frac{Ak\gamma}{\sinh(\gamma x)} \tag{4.7b}$$

The element Y"(i,j) for the transformed subnetwork are obtained by inspection (nodal formulation) as:

$$Y''(1,1) = Y''(2,2) = Y8 + Y10 \tag{4.7c}$$

which is the sum of admittances connected to node 1, or node 2.

$$Y''(1,2) = Y''(2,1) = -Y10 \tag{4.7d}$$

Setting Y"(i,j)=Y(i,j) and solving for Y_8 and Y_{10}

$$Y8 = \frac{Ak\gamma(\cosh(\gamma x) - 1)}{\sinh(\gamma x)} \tag{4.8}$$

$$Y10 = \frac{Ak\gamma}{\sinh(\gamma x)} \tag{4.9}$$

The above transformation is only applicable to frequencies n=1,2....k and is invalid for ω=0 which represents the mean term in the frequency domain or a non massive layer. In both of these cases, Y8=0 and Y10 is equal to the wall conductance and the transformation is therefore not necessary.

Therefore for n=0

$$Y8_0 = 0\frac{watt}{degC} \tag{4.8a}$$

$$Y10_0 = \frac{Ak}{x} \tag{4.9a}$$

This transformation allows the representation of the slab in two subnetworks separated artificially by the internal heat source, but still with the same overall thermal characteristics. The upper slab is represented by the diakoptic transformation and the lower floor slab part, considered as multilayered (thermal mass and insulation with bottom air film), is represented by the normal admittances (equations (4.5) and (4.6)).

After the transformation, the slab thermal network (Figure 4.4) requires the determination of an equivalent heat source and an equivalent admittance in order to keep the same heat flow. The auxiliary floor internal heat source is defined as qr_{aux} while qb and Ybs represent respectively the basement equivalent heat source and the self-admittance of the slab lower part. Simplification of this network to one equivalent source in parallel with one self-admittance is carried out using the Norton and the superposition theorems.

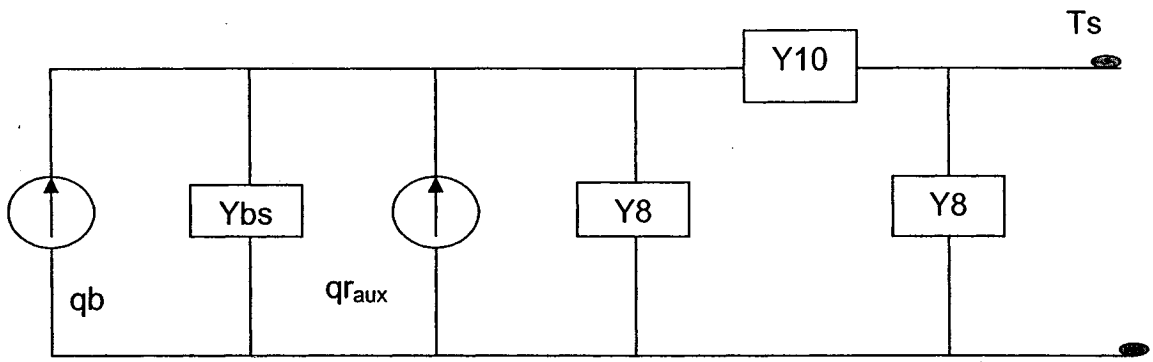

Figure .4.4 Floor network diagram

4.32 Equivalent source using the superposition theorem

This theorem states that the equivalent source of a circuit is the algebraic summation of the effects generated by each source acting separately. Consequently, the effect of each source acting alone on a specified port is to be evaluated with all the others remaining sources set to 0 (open-circuited). This process is to be repeated for each source and the overall effect is obtained by addition of all these effects

Figure 4.4a shows that with Ts short-circuited with the ground, the 02 admittances Y10 and (Ybs+Y8) become parallel and thus are added together (The short circuit at Ts makes the heat to flow directly to the ground, by-passing Y8). The heat source at the bottom floor surface (basement) qb=Ybt Tb and the floor internal heat source qr_{aux} are in parallel and therefore added together.

With qb temporarily set to 0, the equivalent source Qeq1 at port Ts is:

$$Qeq1 = \frac{qr_{aux} Y10}{Ybs + Y8 + Y10} \qquad (4.10a)$$

With qr_{aux} temporarily set to 0, the equivalent source Qeq2 at port Ts is:

$$Qeq2 = \frac{qb\,Y10}{Ybs + Y8 + Y10} \tag{4.10b}$$

The resulting equivalent source Qeq is:

$$Qeq = Qeq1 + Qeq2 = (qb + qr_{ux})\frac{Y10}{Ybs + Y8 + Y10} \tag{4.10}$$

This transfer function represents the effect of the temperature variation due to the combined effect sources qr_{aux} and qb on the resulting heat flow at the floor surface and simplifies the calculation by integrating the node representing the floor heat source.

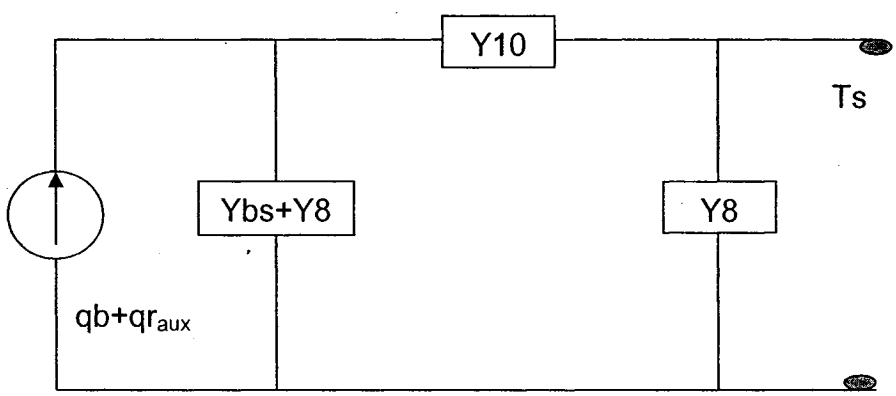

Figure 4.4a: Equivalent heat source

4.33 Equivalent self admittance using the Norton theorem

Figure 4.4b shows that, with (qr_{aux}+qb) open circuited as seen from port Ts; the resulting circuit is a representation of Y10 and (Ybs+Y8) in series, both in parallel with Y8. The resulting heat balance (Ys_8=Qs/Ts) yields the following equivalent self-admittance:

$$Ys_8 = \frac{(Ybs + Y8)Y10}{Ybs + Y8 + Y10} + Y8 \tag{4.11}$$

Equations (4.10 and 4.11) are valid over the frequency range n=1, 2...k and their mean term is the result of the individual mean term of all the components.

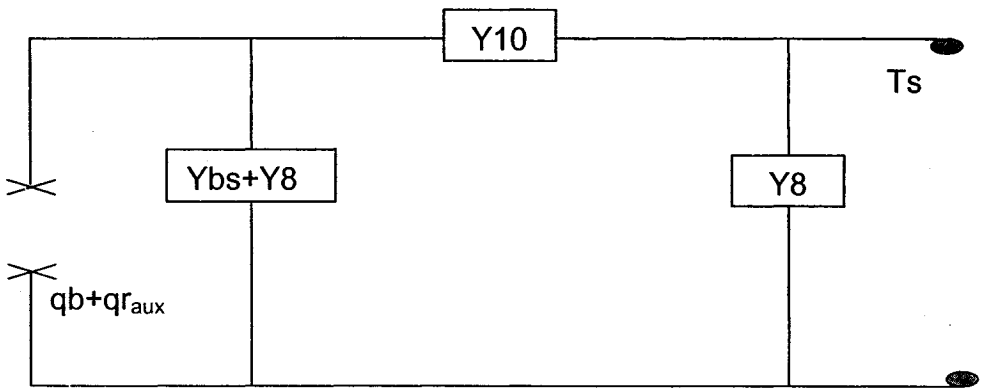

Figure 4.4b: Equivalent self-admittance Ys

The resulting final equivalent network Figure 4.4c is identical to the network before the transformation and consists of a heat source and admittance connected in parallel between the terminals (Norton equivalent).

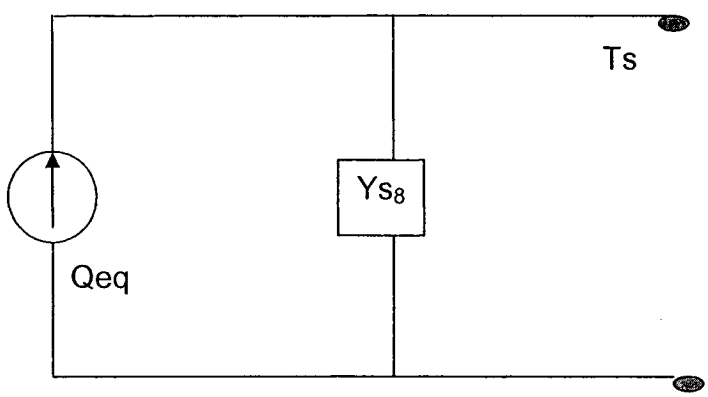

Figure .4.4c: Floor network Norton equivalent

4.4 Analysis of room admittances

Significant insight into wall dynamic thermal behaviour may be obtained by studying admittance transfer functions magnitude and phase angle as a function of frequency, and thermal properties (mass thickness). All the admittance derived from the thermal network Figure 3.1 have an impact more or less important, related to their thermal mass, on the room thermal behaviour. Consequently, the analysis is concentrated on wall admittance with most significant thermal mass (such as the floor mass). The time lead of the self admittance is the time difference between the peak of a sinusoidal input function, such as solar radiation in the case of the room interior surface, and the resulting peak of the interior surface temperature. Diurnal frequency (n=1) is important in the analysis of variables with a dominant diurnal harmonic such as solar radiation. High frequencies are important in analyzing the effect of varying inputs such as those due to on/off cycling of a furnace.

Figure 4.5 shows that the optimum wall thermal thickness, corresponding to the maximum admittance Ys and which will reduce room temperature fluctuation most, is 0.21 m and 0.15 m respectively for concrete and gypcrete. This very important result in steady-periodic analysis of building thermal response revealed by Athienitis et al. (1986) is of particular interest for passive solar design.

Figure 4.6 shows that for n=48 (period equal to half an hour), the wall behaves like a semi-infinite solid for thicknesses greater than 0.06 m. The magnitude of self-admittance Ys is constant for L>0.06 m for both material

concrete and gypcrete and the corresponding time delay ((argument(Ys))/ω_n) varies little with wall thickness.

Figure 4.7 indicates that for the zero frequency, the magnitude of the self-admittance (for mass thickness of 6 cm) is equal to the wall steady state U-value while on the other hand it increases with frequency. The floor behaves like an infinitely thick wall (constant temperature heat sink) starting from harmonic numbers higher than about 15 (periods of 96 minutes) and 11 (periods of 131 minutes) respectively for concrete and gypcrete. The corresponding phase angle (argument(Yt)) in the same order is 47 and 44.6 degrees. Consequently, the inside room temperature fluctuations are smaller for high frequency fluctuations in internal heat gains.

The wall concrete self admittance Ys is higher than that of the gypcrete confirming the fact that admittance increases for choices of material with larger values of thermal conductivity. On the other hand it is established that the admittance decreases for choice of larger specific heat per unit mass and density of the material in question.

Figure 4.8 shows that for fundamental frequency (n=1), the magnitude of the transfer admittance Yt decreases while the corresponding time delay increases with mass thickness, consequently the fluctuations of the sol-air temperature are significantly modulated as they are transmitted to the room interior. This phenomenon has been efficiently used in traditional architecture in adobe (clay) buildings. The time lag ((argument(Yt))/ω_n) of the heat gains can reach up to 7 hour and 10 hours respectively for concrete and gypcrete for a

mass thickness of 30 cm. In addition to the attenuation of the room temperature swings, the time delay, provided in transmission of heat wave through the wall, allows interior resulting peak heat gains to coincide with cooler outside temperature so that natural ventilation can be employed to reduce total instantaneous cooling loads.

Figure 4.9 shows the magnitude of the transfer admittance decreasing fast with increasing harmonic number n (and decreasing period). Thus the heat gains fluctuations transmitted into the room as a result sol-air temperature are significantly reduced at high frequency with very limited effect on short term dynamic control. A 2°C temperature swing over a 1 hour period for a surface wall with thermal characteristics identical to the floor induces heat gains swings of about 0.49 and 0.25 watt per square meter respectively for concrete and gypcrete.

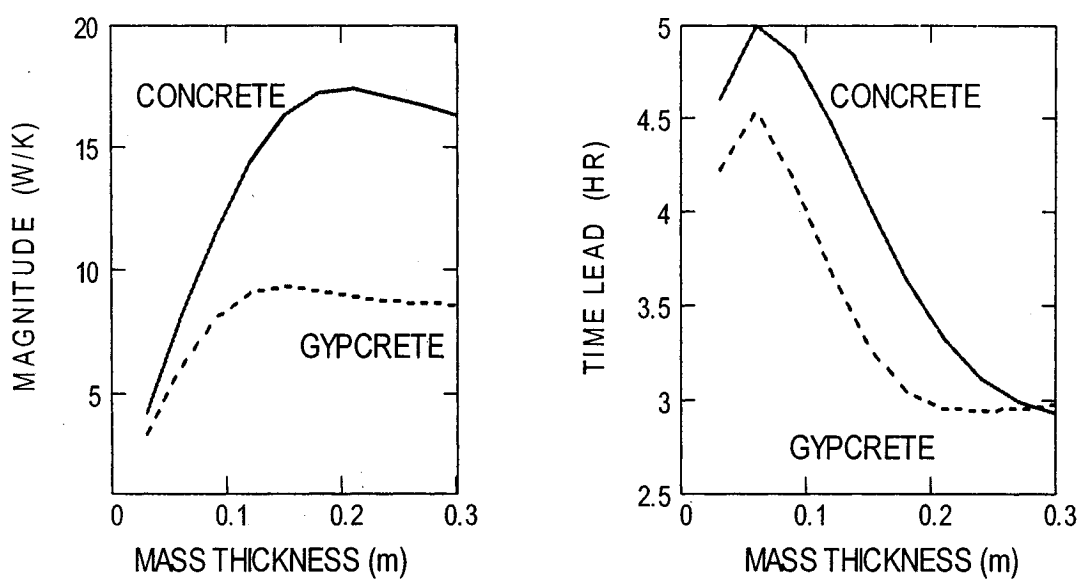

Figure 4.5: Variation of self-admittance Ys and corresponding time delay with mass thickness for the first frequency.

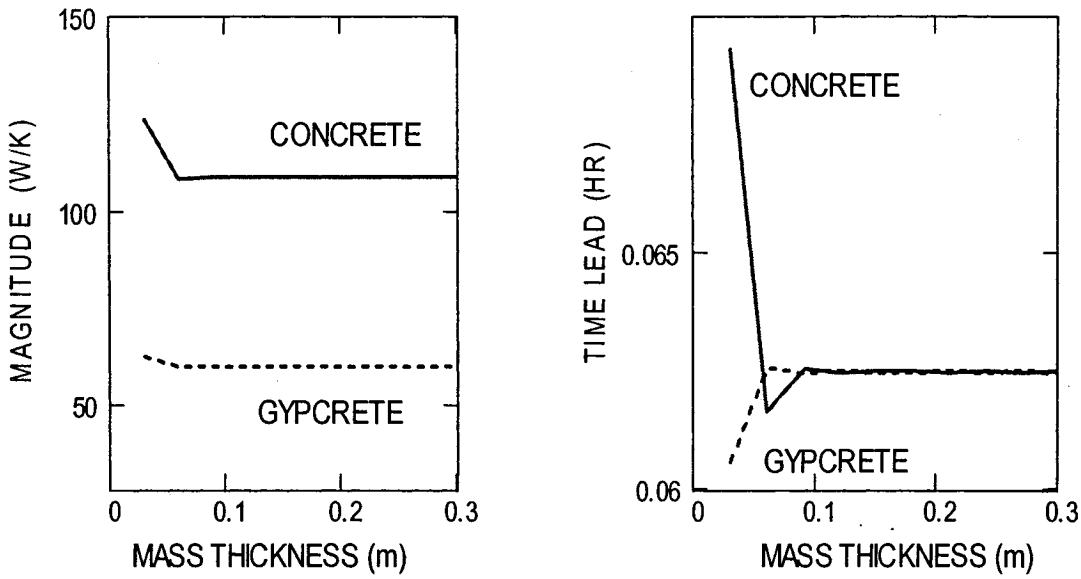

Figure.4.6 Variation of self-admittance Ys and corresponding time delay with mass thickness for frequency n=48 (30 minutes).

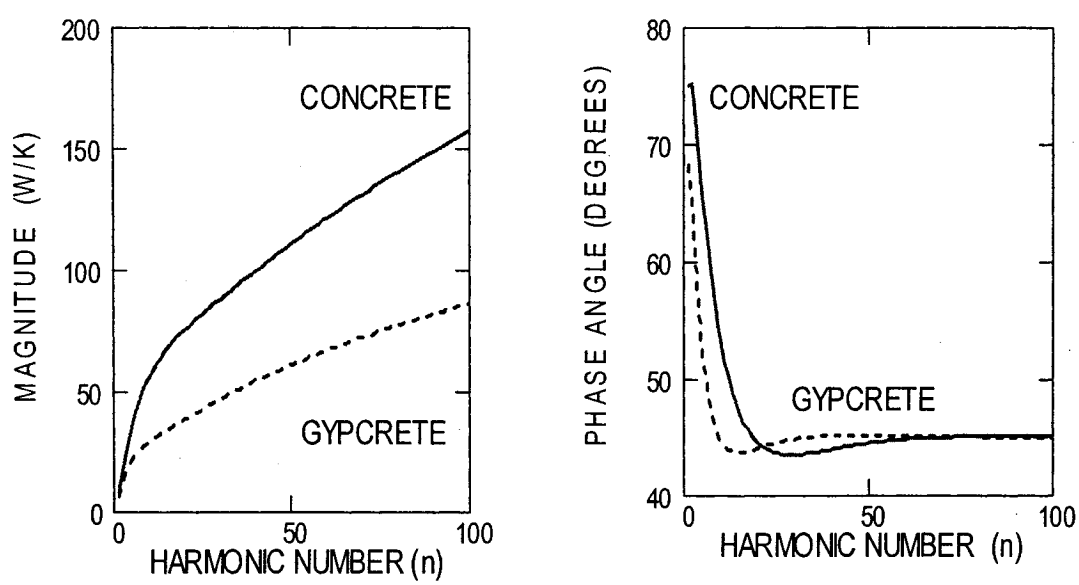

Figure.4.7: Variation of self-admittance Ys and corresponding phase angle with harmonic number n for mass thickness equal to 0.06 m.

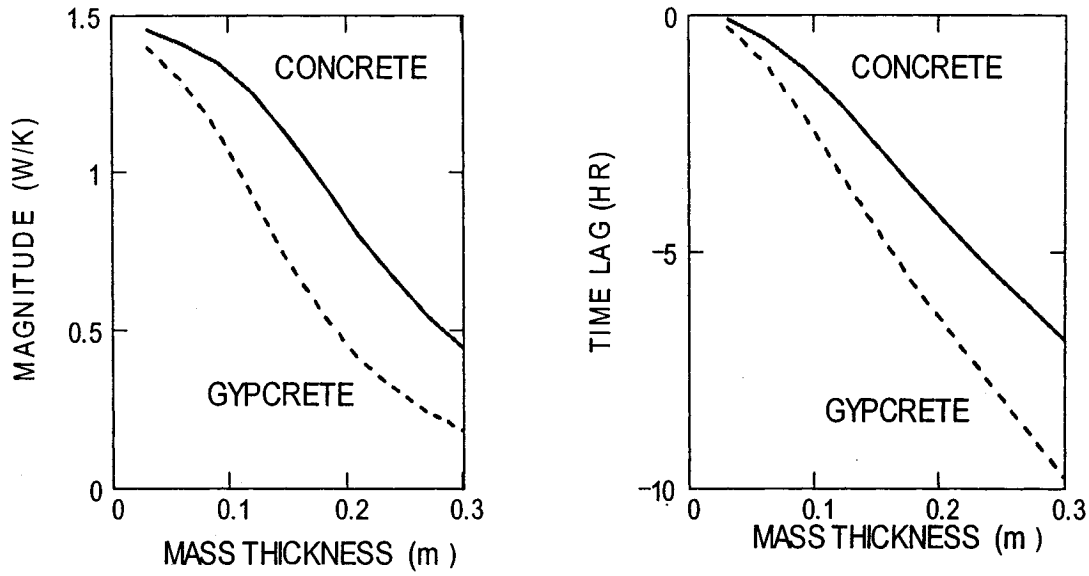

Figure.4.8: Variation of transfer admittance Yt and corresponding time delay with mass thickness for the first frequency.

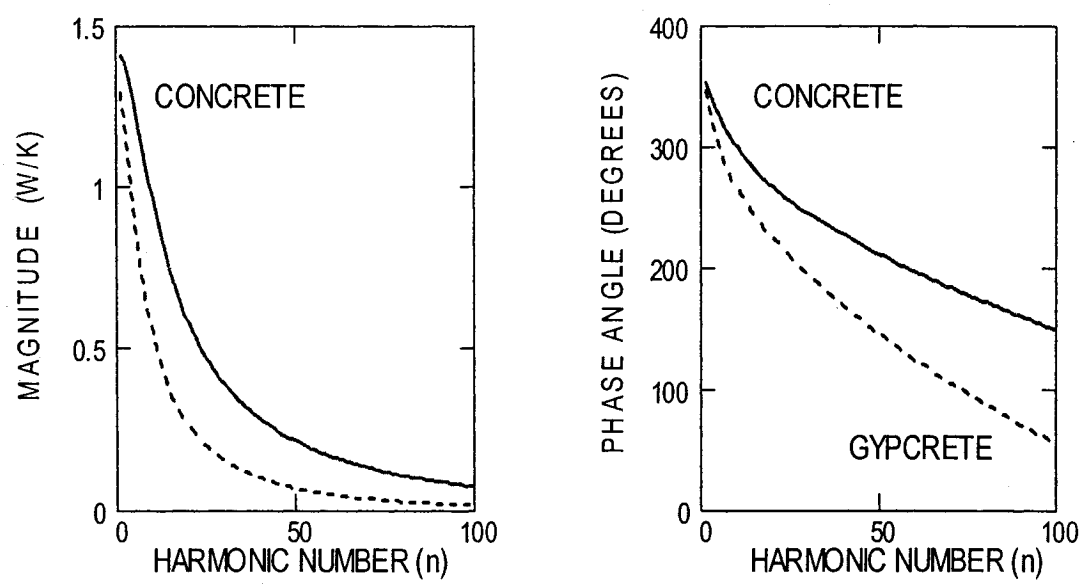

Figure 4.9: Variation of transfer admittance Yt and corresponding phase angle with harmonic number n for mass thickness equal to 0.06 m.

4.5 Energy balance

The energy balance is written for each enclosing surface, plus one for the air. The resulting set of equations is then solved simultaneously for the unknown surfaces and air temperature. The heat balances at the room interior nodes used for thermal network Figure 3.1 are obtained after replacing each of the 8 walls by their respective Norton equivalent subnetwork, which consists of an equivalent heat source Q and a self-admittance Ys as defined previously, thereby eliminating all exterior nodes without discretizing the massive elements. The equivalent heat source Q is equal to the wall transfer admittance Yt times the outside (Ton), ground temperature (Tbn) or other equivalent specified temperature (Teq) plus any internal heat source such as auxiliary heating system (qr_{aux}) and/or solar radiation. Internal and external heat sources are modeled with discrete Fourier series.

Solar radiation absorbed by exterior surfaces can be combined with outside temperature (Ton) to form an equivalent temperature known as the sol-air temperature (Teq). Teq is defined by writing an energy balance at the wall exterior surface (ignoring long wave radiant exchange with the sky).

Sn represents the instantaneous solar radiation transmitted through windows and absorbed by room surfaces and Qg the solar radiation absorbed by widows glazing and released to room air. Sn can be modeled as absorbed 70% at the floor surface, and the remainder by the other surfaces in proportion to their areas. Hourly and daily solar radiation incident on exterior walls surfaces and transmitted to room through the windows may be estimated using the clear sky

Hotel's method or the average clearness index (Athienitis and Santamouris, 2002).

The room air and its lightweight contents are modeled by a lumped thermal capacitance which, although with no effect on load calculations at low frequencies, is an important parameter to include for high frequency, short-term control analysis. Windows and infiltration transfer admittance are equal to their thermal conductance U.

The energy balance $[Y]_N \cdot [T]_N = [Q]_N$ in the frequency domain is as shown in matrix form in Figure (4.12). The elements of the admittance matrix $[Y]_N$ may be obtained by inspection from the topology of the network (Vlach and Singal 1983). The diagonal entry Y(i,j) is equal to the sum of the component admittances connected to node I while off-diagonal entry Y(i,j) is the sum of component admittances/conductances connected between nodes i and j multiplied by -1. The heat source vector element Q(i) is the sum of the heat sources connected to node I, positive if directed to the node as in the present case. As can be seen for thermal network Figure 3.1, the admittance matrix is a square matrix of order 9×9 and has two noticeable characteristics: it is symmetric with all off-diagonal elements Y(i,j) being real and equal to conductances $U_{i,j}$ multiplied by -1 and all self-admittances and capacitances appear in the diagonal entries which are consequently complex. For the energy balance with material (concrete or gypcrete) incorporating carpet cover, the only modification to the matrix is the off-diagonal elements $U_{8,0}$ and $U_{0,8}$ and the off-diagonal elements $\sum U_{0,,j} + U_{inf}$ and $Ys_8 + \sum U_{8,,j}$ which now incorporates the carpeted floor convective conductance

$$
\begin{pmatrix} Ts_0 \\ Ts_1 \\ Ts_2 \\ Ts_3 \\ Ts_4 \\ Ts_5 \\ Ts_6 \\ Ts_7 \\ Ts_8 \end{pmatrix}
\times
\begin{bmatrix}
\sum_j U_{0,j} + U_{inf} + C & -U_{1,0} & -U_{2,0} & -U_{3,0} & -U_{4,0} & -U_{5,0} & -U_{6,0} & -U_{7,0} & -U_{8,0} \\
-U_{0,1} & A_1.u_W + \sum_j U_{1,j} & -U_{2,1} & -U_{3,1} & -U_{4,1} & -U_{5,1} & -U_{6,1} & -U_{7,1} & -U_{8,1} \\
-U_{0,2} & -U_{1,2} & A_2.u_W + \sum_j U_{2,j} & -U_{3,2} & -U_{4,2} & -U_{5,2} & -U_{6,2} & -U_{7,2} & -U_{8,2} \\
-U_{0,3} & -U_{1,3} & -U_{2,3} & Ys_3 + \sum_j U_{3,j} & -U_{4,3} & -U_{5,3} & -U_{6,3} & -U_{7,3} & -U_{8,3} \\
-U_{0,4} & -U_{1,4} & -U_{2,4} & -U_{3,4} & Ys_4 + \sum_j U_{4,j} & -U_{5,4} & -U_{6,4} & -U_{7,4} & -U_{8,4} \\
-U_{0,5} & -U_{1,5} & -U_{2,5} & -U_{3,5} & -U_{4,5} & Ys_5 + \sum_j U_{5,j} & -U_{6,5} & -U_{7,5} & -U_{8,5} \\
-U_{0,6} & -U_{1,6} & -U_{2,6} & -U_{3,6} & -U_{4,6} & -U_{5,6} & Ys_6 + \sum_j U_{6,j} & -U_{7,6} & -U_{8,6} \\
-U_{0,7} & -U_{1,7} & -U_{2,7} & -U_{3,7} & -U_{4,7} & -U_{5,7} & -U_{6,7} & Ys_7 + \sum_j U_{7,j} & -U_{8,8} \\
-U_{0,8} & -U_{1,8} & -U_{2,8} & -U_{3,8} & -U_{4,8} & -U_{5,8} & -U_{6,8} & -U_{7,8} & Ys_8 + \sum_j U_{8,j}
\end{bmatrix}
=
\begin{pmatrix} Ton\, U_{inf} + Qg \\ Ton\, A_1\, u_W \\ Ton\, A_2\, u_W \\ Teq_3\, Yt_3 + Sn_3 \\ Teq_4\, Yt_4 + Sn_4 \\ Teq_5\, Yt_5 + Sn_5 \\ Teq_6\, Yt_6 + Sn_6 \\ Teq_7\, Yt_7 + Sn_7 \\ Qeq + Sn_8 \end{pmatrix}
$$

Figure: 4.12

(chapter 2) instead.

An alternative form for this energy balance is the impedance transfer function Z(I,J) determined at specific frequencies by inversion of the admittance matrix [Y] as follows:

$$[T_s] = [Z][Q] \tag{4.12a}$$

where

$$[Z] = [Y]^{-1} \tag{4.12b}$$

The floor internal heat source integrated in the heat balance with the use of the diakoptic method is not represented by a specific node in the admittance matrix. It is implicitly included in the transfer functions $Z_{0,8}$ which represents the effect of equivalent heat source Qeq (equation (4.10)) at node 8 (floor surface) on the air temperature of node 0; however a supplementary transfer function $Z_{0,9}$ defining only the effect of the auxiliary floor internal heat source qr_{aux} on the air room temperature is useful for thermal control analysis. With qr_{aux} represented by node 9 and all the other sources set to zero, $Z_{0,9}$ is derived as follows:

$$Z_{0,8} = \frac{Ts_0}{Qeq} = \frac{Ts_0}{qr_{aux}\left(\frac{Y10}{Y8 + Ybs + Y10}\right)} \tag{4.13}$$

$$Z_{0,9} = \frac{Ts_0}{qr_{aux}} \tag{4.13a}$$

Hence

$$Z_{09} = Z_{0,8}\left(\frac{Y10}{Y8 + Ybs + Y10}\right) \tag{4.13b}$$

The temperature equation at each node i for each frequency is given by:

$$\begin{pmatrix} Ts_0 \\ Ts_1 \\ Ts_2 \\ Ts_3 \\ Ts_4 \\ Ts_5 \\ Ts_6 \\ Ts_7 \\ Ts_8 \end{pmatrix} = [Z] \begin{pmatrix} Ton U_{inf} + Qg \\ Ton A_1 u_W \\ Ton A_2 u_W \\ Teq_3 Yt_3 + Sn_3 \\ Teq_4 Yt_4 + Sn_4 \\ Teq_5 Yt_5 + Sn_5 \\ Teq_6 Yt_6 + Sn_6 \\ Teq_7 Yt_7 + Sn_7 \\ Qeq + Sn_8 \end{pmatrix} \tag{4.14}$$

It is useful to determine the effective room temperature such as the operative temperature and by the same way the operative transfer function X. The operative temperature is defined as the uniform temperature of an enclosure in which an occupant would exchange the same amount of heat by radiation and convection as in the actual non-uniform environment (ASHRAE 1981) and has proven to achieve better thermal control with radiant heating (Athienitis and Dale 1987). It is given by:

$$T_{op} = \frac{h_r T_{mr} + h_c Ts_0}{h_r + h_c} \tag{4.15}$$

Where Ts_0 is the air temperature, T_{mr} the mean radiant temperature and h_r and h_c are radiative and convective coefficients respectively for a person or object (sensor) The operative temperature T_{op} is a scalar functions of nodals temperatures {(Ts_0) ..... (Ts_8)} as determined with equation (4.14) and the weighting factors for the individual surface temperatures are obtained with a detailed model for radiant heat exchanges and T_{mr}.

4.51 Mean radiant temperature

The MRT describes the uniform surface temperature of a radiantly black enclosure in which an occupant would exchange the same amount of radiant heat as in the actual non-uniform space (ASHRAE 1981). Assuming the sensor to sense the same operative temperature as a person, the long wave radiant heat gain as sensed at a location in the room is given by:

$$q_s = A_s \varepsilon_s \left(\left(q_i^+ F_{s,i} + \ldots + q_j^+ F_{s,L} \right) - \sigma T_s^4 \right) \tag{4.16}$$

Where A_s is the effective sensing area with emissivity ϵ_s, q^+ represents radiosity, i=1...L (surface number, 8 in the present case) and T_s is the temperature of the sensor (or object/person). The mean radiant temperature T_{mr} is defined by the equivalent energy balance:

$$q_s = A_s \varepsilon_s \sigma \left(T_{mr}^4 - T_s^4 \right) \tag{4.17}$$

To simplify the calculations, the sensor or person is assumed to be located in the center of the room and the view factors $F_{s,i}$ between the sensor and surface areas A_i are approximated To:

$$F_{s,i} = A_i / A_t \quad \text{, where the total room area is} \tag{4.18}$$

$$A_t = \sum_i A_i \tag{4.18a}$$

If the effect of location within the room is to be studied, the view factors $F_{s,i}$ must be calculated accurately. The surface radiosities q_i^+ are given by the following matrix equation:

$$\{q_i^+\} = [M]^{-1} \{q_e\} \quad \text{, where} \tag{4.19}$$

$$q_e(i) = \varepsilon_i T_i^4 \tag{4.19a}$$

The inverse $[M]^{-1}$ has been already obtained when evaluating the exchange factors $F^{*}_{I,j}$ (equation (3.61a)) in chapter 3, so a new matrix is not required. The long wave emissivities, ϵ_i, of the surfaces can usually be approximated to ϵ=0.9. After substituting in equation (4.16) for q^{+}, then for $F_{S,I}$ and linearizing the T^4 terms, q_s may be expressed with the following matrix equation:

$$q_s = A_s h_r \left[(\varepsilon/A_t)\{A\}^T [M]^{-1}\{T\} - T_S\right] \quad \text{, where} \tag{4.20}$$

$$h_r = \varepsilon_s 4\sigma T_{mr}^3 \quad \text{and} \tag{4.20a}$$

$$\{A\}^T = [A_1, A_2, \ldots, A_L] \tag{4.20b}$$

$\{A\}^T$ being the transpose of area vector A_i. After linearising equation (4.17) and comparing it with equation (4.20), we may deduce T_{mr} as:

$$T_{mr} = \{D_{mr}\}\{T_s\} \quad \text{, with row vector} \tag{4.21}$$

$$\{D_{mr}\} = \{\varepsilon/A_t\}\{A\}^T [M]^{-1} \tag{4.21a}$$

$\{D_{mr}\}$ represents the weighting factors[(D_{mr1}) , (D_{mr2}) .....(D_{mr8})] related to the nodal temperature T_s of wall surfaces 1 to 8 for thermal network figure 3.1. Node air (0) mathematical weighting factor is equal to 0.

4.52 Operative temperature

The operative temperature T_{op} can be rewritten as a function of the room interior temperature in the matrix form (equation (4.14)):

$$T_{op} = \{D\}\{T_s\} \tag{4.22}$$

$\{T_s\}$ is the room interior temperature vector (Ts_0....Ts_8) and $\{D\}=[D_0, D_1, \ldots, D_8]$ where D_0 represents the weighting factor for the room air temperature Ts_0 and

the entries [(D_1), (D_2),...(D_8)] are the relative weighting factors D_{mr} of the surfaces temperatures calculated above in the mean radiant temperature times the ratio $h_c/(h_r+h_c)$. The coefficients h_r and h_c are generally assumed to be equal respectively to 5 W/(m^2.°C) and 2 W/(m^2.°C).

$$D_0 = \frac{h_c}{h_r + h_c} \tag{4.22a}$$

$$D_1, D_2, \ldots, D_8 = D_{mr} \frac{h_r}{h_r + h_c} \tag{4.22b}$$

4.53 Operative transfer functions

The transfer function X(i) denotes the effect of source elements Q(i) on the operative temperature and is derived as follows:

The first step is to substitute {Ts_n} from equation (4.12a) in equation (4.22)

$$T_{op} = \{D\}[Y]^{-1}\{Q\} \tag{4.23}$$

Defining the adjoint vector {X} by:

$$\{X\}^T = \{D\}[Y]^{-1} \tag{4.24a}$$

Multiplying both sides of equation (4.24) by [Y] yields:

$$\{X\}^T [Y] = \{D\} \tag{4.24b}$$

Taking the transpose of both side of equation (4.24)

$$[Y]^T \{X\} = \{D\}^T \quad \text{, however} \tag{4.24c}$$

$$[Y] = [Y]^T \quad \text{, therefore}$$

$$[Y]\{X\} = \{D\}^T \tag{4.24d}$$

and the operative transfer function is:

$$\{X\} = [Y]^{-1}\{D\}^T \tag{4.24e}$$

Since D^T is a function of room geometry and surface properties only, it is evaluated only once for the room and since [Y] is a function of room construction and frequency only, it has to be determined only once for each frequency. Consequently, equation (4.24e) needs to be solved only once for each frequency to obtain the operative temperature transfer function.

4.56 Radiant floor operative transfer function

Following the same procedure as for the impedance transfer function Z_{09}, an operative transfer function X_{09} relating the effect of the auxiliary floor internal heat source qr_{aux} at node 9 on the operative room temperature of node 0 is required for thermal analysis involving operative control. With all other sources set to zero, it is derived as follows:

$$X_{8,0} = \frac{T_{op}}{Qeq} = \frac{T_{op}}{qr_{aux}\left(\dfrac{Y10}{Y8 + Ybs + Y10}\right)} \tag{4.25}$$

$$Z_{9,0} = \frac{T_{op}}{qr_{aux}} \tag{4.25a}$$

Thus

$$X_{09} = X_{8,0}\left(\frac{Y10}{Y8 + Ybs + Y10}\right) \tag{4.25b}$$

4.6 Transfer function identification method

The Impedance and operative transfer function obtained at discrete

frequencies through inversion of the admittances matrix [Y] can not be employed directly for transient thermal control studies and frequency domain studies, such as stability analysis. A continuous form of the Laplace transfer function is required for the dynamic analysis of the building thermal systems and constitutes the first step for obtaining an overall system response. A simple and efficient method based on the least square method is used to obtain the appropriate transfer function in the s-domain defining those functions in terms of the variable s. The least squares method is commonly used to estimate the parameters of a dynamic constant parameter system of linear generalized form.

The transfer function $Z_f(s)$ may be represented as a ratio of complex polynomials N(s)/D(s) from the discrete frequency response data. The polynomials N(s) and D(s) are then determined as a continuous function of s by performing a least squares complex interpolation on the discrete values by means of a technique developed by Levy appropriately modified for the present application (Athienitis et al., 1990). The weighted least square error between the frequency response of the room and the fitted model is the criterion for optimization. The actual discrete frequency responses for the impedance transfer function $Z(j\omega)$ equation calculated previously can be represented by the sum of its real and imaginary part:

$$Z(j\omega) = R(\omega) + jI(\omega) \tag{4.26}$$

For a linear model, the fitted polynomial transfer function can be expressed in the frequency domain as follows:

$$Z_f(j\omega)=\frac{\sum_u a_u(j\omega)^u}{\sum_v b_v(j\omega)^v}=\frac{\left(a_0-a_2\,\omega^2+a_4\,\omega^4-\ldots\right)+j\omega\left(a_1-a_3\,\omega^2+a_5\,\omega^4+\ldots\right)}{\left(b_0-b_2\,\omega^2+b_4\,\omega^4-\ldots\right)+j\omega\left(b_1-b_3\,\omega^2+b_5\,\omega^4+\ldots\right)} \quad (4.27)$$

where u or v (the highest of them) is the order of the fitted transfer function Z_f.

Stated otherwise:

$$Z_f(j\omega)=\frac{\alpha+j\omega\beta}{\sigma+j\omega\upsilon}=\frac{N(j\omega)}{D(j\omega)} \quad \text{, where} \quad (4.27a)$$

$$\alpha=a_0-a_2\,\omega^2+a_4\,\omega^4-\ldots \qquad \beta=a_1-a_3\,\omega^2+a_5\,\omega^4-\ldots$$

$$\sigma=1-b_2\,\omega^2+b_4\,\omega^4-\ldots \qquad \upsilon=b_1-b_3\,\omega^2+b_5\,\omega^4-\ldots$$

The objective is to find the different coefficients a_m and b_m that will give the best representation of the transfer function $Z(j\omega)$ with $Z_f(j\omega)$ in terms of the least square error. The error ϵ in the fitting is defined by the numerical difference between the two functions $Z(j\omega)$ and $Z_f(j\omega)$:

$$\varepsilon(j\omega)=Z(j\omega)-Z_f(j\omega)=Z(j\omega)-\frac{N(j\omega)}{D(j\omega))} \quad (4.28)$$

Multiplying equation (4.28) by D(jw), we obtain:

$$\varepsilon(j\omega)D(j\omega)=Z(j\omega)D(j\omega)-N(j\omega) \quad (4.28a)$$

The magnitude of the deviation can be expressed by the following weighted square error to be minimized.

$$\left|\varepsilon(j\omega)D(j\omega)\right|^2=\left|Z(j\omega)D(j\omega)-N(j\omega)\right|^2 \quad (4.28b)$$

After substituting equations (4.26) and (4.27a) in the equation (4.28b), the total square error function summed over the range of the discrete frequencies n is given by:

$$E(\omega)=\sum_n \left|(R_n+jI_n)(\sigma_n+j\omega_n\upsilon_n)-(\alpha_n+j\omega_n\beta_n)\right|^2 \tag{4.29}$$

$$E(\omega)=\sum_n \left|(R_n\sigma_n-\omega_n I_n\upsilon_n-\alpha_n)^2+(\omega_n R_n\upsilon_n+I_n\sigma_n-\omega_n\beta_n)^2\right| \tag{4.29b}$$

Examination of equation (4.26) reveals that $a_0=Z(\omega=0)$ and $b_0=1$. The coefficient a_0 does not need to be evaluated because the steady state of Z (at $\omega=0$) is known. Equation (4.29a) is differentiated with respect to each unknown coefficient a_u and b_v and the results set equal to zero to find the minimum. Partial differentiation with respect to any one specific unknown coefficients (one each time) will simply ignore the fact that the rest of the coefficients are also unknown, treating them as constants. A set of linear simultaneous algebraic equations is required to derive the considered coefficients as follows:

Numerator coefficients a_m

$$\frac{dE}{da_1}=\sum_n -2\omega_n(\omega_n R_n\upsilon_n+I_n\sigma_n-\omega_n\beta_n)=0$$

$$\frac{dE}{da_2}=\sum_n 2\omega_n^2(R_n\upsilon_n-\omega_n I_n\sigma_n-\alpha_n)=0$$

$$\frac{dE}{da_3}=\sum_n -2\omega_n^3(\omega_n R_n\upsilon_n+I_n\sigma_n-\omega_n\beta_n)=0$$

.....

$$\frac{dE}{da_u}=\text{.....} \tag{4.30}$$

Denominator coefficients b_m

$$\frac{dE}{db_1}=\sum_n -2\omega_n\left[(R_n\sigma_n-\omega_n I_n\upsilon_n-\alpha_n)I_n+(\omega_n R_n\upsilon_n+I_n\sigma_n-\omega_n\beta_n)R_n\right]=0$$

$$\frac{dE}{db_2} = \sum_n -2\omega_n^2 \left[(R_n \sigma_n - \omega_n I_n \upsilon_n - \alpha_n) R_n + (\omega_n R_n \upsilon_n + I_n \sigma_n - \omega_n \beta_n) I_n \right] = 0$$

$$\frac{dE}{db3} = \sum_n -2\omega_n^3 \left[(R_n \sigma_n - \omega_n I_n \upsilon_n - \alpha_n) I_n + (\omega_n R_n \upsilon_n + I_n \sigma_n - \omega_n \beta_n) R_n \right] = 0$$

.....

$$\frac{dE}{db_v} = \ldots\ldots\ldots \qquad (4.30a)$$

A matrix form is required for the resolution of the above set of simultaneous equations with the different parameters expressed in a non-dimensionalized form as follows:

$$\begin{bmatrix} \lambda_2 & 0 & -\lambda_4 & .. & -Y_2 & T_3 & Y_4 & .. \\ 0 & -\lambda_4 & 0 & .. & T_3 & Y_4 & -T_5 & .. \\ \lambda_4 & 0 & -\lambda_6 & .. & -Y_4 & T_5 & Y_6 & .. \\ : & : & : & : & : & : & : & : \\ -Y_2 & -T_3 & Y_4 & .. & M_2 & 0 & -M_4 & .. \\ T_3 & -Y_4 & -T_5 & .. & 0 & M_4 & 0 & .. \\ -Y_4 & -T_5 & Y_6 & .. & M_4 & 0 & -M_6 & .. \\ : & : & : & : & : & : & : & : \end{bmatrix} \begin{bmatrix} a_2 \\ a_3 \\ a_4 \\ .. \\ a_u \\ b_1 \\ b_2 \\ b_3 \\ .. \\ b_v \end{bmatrix} = \begin{bmatrix} T_1 \\ Y_2 - \lambda_2 a_0 \\ T_3 \\ .. \\ .. \\ -T_1 a_0 \\ M_2 - Y_2 a_0 \\ -T_3 a_0 \\ .. \\ .. \end{bmatrix}$$

(4.31)

The elements of the matrix are as follows:

$$\lambda_h = \sum_n (\omega_n)^h \qquad T_h = \sum_n (\omega_n)^h \, Im(Z_n)$$

$$Y_h = \sum_n (\omega_n)^h \, Re(Z_n) \qquad M_h = \sum_n (\omega_n)^h \left(Re(Z_n)^2 + Im(Z_n)^2 \right)$$

The coefficients Re(Z) and Im(Z) are the real and the imaginary part of the

impedance transfer function [Z] (equation (4.12a)) obtained at discrete frequencies through inversion of the admittances matrix [Y], the prefix h= 0,1...p, with p equal to the order numerator u plus that of the denominator v for a matrix u x v. The two orders number may be equal. The numerical values of the unknown coefficients a and b can thus be obtained through inversion of the above matrix.

Since an arithmetic error is always possible, verification of the results can be carried out by substituting the values for a and b into the original equations (equation (4.30,... , 4.30a)). All the equations should check perfectly with results nearing zero. It should be noted also that the accuracy of a and b depends upon the number of decimal places carried in the calculations. The more decimal places carried, the more accurate the results.

However, this approach as established up to now may lead to significant error if the discrete frequency response spans over several decades. Optimum fitting may not be obtained at lower frequency because data at this frequency have little influence on the fitting. The denominator $D(j\omega_n)$ may also vary significantly over the range of frequency range fitted, consequently introducing large error. These shortcomings are overcome by an iterative approach developed by Sanathanan and Koerner (Athienitis, 1993) in which the error function as expressed in equation (4.28a) is weighted by the ratio of the denominator polynomial calculated in the current iteration to the denominator calculated in the previous iteration:

$$\varepsilon^* = \frac{\varepsilon(j\omega_n)D(j\omega_n)}{D(j\omega_n)_{L-1}} = \frac{Z(j\omega_n)D(j\omega_n) - N(j\omega_n)}{D(j\omega_n)_{L-1}} \qquad (4.32)$$

The modified square function E_L is defined as:

$$E_L = \left|\varepsilon^*(j\omega_n)\right|^2 = \sum_n \left|Z(j\omega_n)D(j\omega_n)_L - N(j\omega_n)_L\right|^2 W_{nL} \tag{4.33}$$

Where L is the number of iterations and the weighting factor defined as:

$$W_{nL} = \frac{1}{\left|D(j\omega_n)_{L-1}\right|^2} \tag{4.33a}$$

W_{nL} has been derived in the previous iteration assumed initially to be 1. The error function equation (4.33) is solved again following the same procedure as described above. Basically the only parameters of the above procedure to be modified are as follows:

$$\lambda_h = \sum_n (\omega_n)^h W_{nL}$$

$$T_h = \sum_n (\omega_n)^h W_{nL} \, Im(Z_n)$$

$$Y_h = \sum_n (\omega_n)^h W_{nL} \, Re(Z_n)$$

$$M_h = \sum_n (\omega_n)^h W_{nL} \left(Re(Z_n)^2 + Im(Z_n)^2\right)$$

The squared error is weighted more evenly at all frequencies with this modified iteration approach. The same procedure as described before is used to solve the error function and optimum fitting is obtained by iteration with regard to the accuracy required. The fitted function defines the input signal in terms of the variable s and represents the appropriate transfer function that is required for obtaining the time domain solution (of linear network) by means of Laplace transform. The same procedure applies for defining the appropriate operative transfer function X(i) in the s-domain .

4.7 Discussion

4.71 Analysis of impedance and operative transfer functions

Again, substantial insight into the room thermal behavior can be obtained by studying the magnitude and phase angle of the impedance and operative transfer functions. The transfer functions of interest in the present case are $(Z)_{0,8}$ and $(X)_{8,0}$ which represent the effect of solar radiation at node 8 (floor surface) respectively on the air temperature and the operative temperature of node 0:

$$(Z_n)_{0,8} = \frac{Ts_{0,n}}{Sn_{n,8}} \qquad \text{All other sources set to zero} \qquad (4.34)$$

$$(X_n)_{8,0} = \frac{T_{op_n}}{Sn_{n,8}} \qquad \text{All other sources set to zero} \qquad (4.35)$$

The magnitude of $(Z_n)_{0,8}$ and $(X_n)_{8,0}$ can be used to determine the approximate room temperature swings (in degree Celsius) due to solar radiation absorbed at the floor surface, both parameters at fundamental frequency and respectively equal to:

$$|(Z_1)_{0,8}||Sn_{1,8}| \qquad (4.36)$$

$$|(X_1)_{8,0}||Sn_{1,8}| \qquad (4.37)$$

The time delay (hours) between the peak of solar radiation (noon for south-facing window) and the resulting peak of the room temperature is respectively equal to:

$$\Phi_z = \frac{\arg((Z_1)_{0,8})}{w_1} \qquad (4.38)$$

$$\Phi_x = \frac{\arg((X_1)_{8,0})}{w_1} \tag{4.39}$$

With phase angle equal respectively to:

$$\arg((Z_n)_{0,8}) = \tan^{-1}\left(\frac{\mathrm{Im}((Z_n)_{0,8})}{\mathrm{Re}((Z_n)_{0,8})}\right) \tag{4.38a}$$

$$\arg((X_n)_{8,0}) = \tan^{-1}\left(\frac{\mathrm{Im}((X_n)_{8,0})}{\mathrm{Re}((X_n)_{8,0})}\right)$$

(4.39a)

The analysis of Figures 4.10a&b indicates that the temperature amplitude decreases with floor thickness and that depending on thermal mass properties, there is an optimum floor thickness that reduces most the temperature fluctuations, hence confirming the result obtained in paragraph 4.4 and the usefulness of this parameter in passive solar design. On the other hand, the time lag increases until saturation of the thermal mass is obtained. Gypcrete having lower thermal capacity reaches this point faster than concrete and thus provides lower thermal lag (3 hours for a floor thickness of about 0.25 m) and higher temperature fluctuation. We also observe that the amplitude and time lag difference between the two considered material gypcrete and concrete increase with floor thickness respectively up 0.15 m and 0.21 m, which correspond to their passive solar optimum floor thickness.

The same figures reveal that the introduction of a carpet cover reduces room air temperature amplitude and increases the corresponding time lag. This effect tends to decrease with floor thickness. With floor thickness from 0.03m to 0.24 m, temperature amplitude and corresponding time lag decrease from 0.26 to

0.15 degree and 8.2 to 6.8 minutes respectively with gypcrete material while with concrete, the amplitude varies from 0.24 to 0.09 degree and time lag from 8.4 to 6.6 minutes. This added thermal resistance basically reduces heat transfer while simultaneously delaying its transmission. Further more its effect is inversely proportional to floor thickness.

Figures 4.11a&b is a representation of the effect of solar radiation on the operative temperature. It follows a general pattern identical to Figure 4.10a&b. However we note that the difference in amplitude and phase lag between a carpeted floor and a non carpeted floor is less pronounced. This suggests that introduction of a carpet has lesser effect on the operative temperature.

Figures 4.12a&b show the effect of solar radiation on both operative and air temperature. We observe that for non carpeted floor, operative temperature has slightly higher amplitude and higher constant thermal lag (approximately 1.2 minute more). For carpeted floor, the same observation is made for the amplitude but the thermal lag is lower (approximately by 2.4 minutes). The amplitude interval between the two operating modes decreases with floor thickness and is higher for carpeted floor.

The temperature swings and the time delays are consistent. Gypcrete being a lightweight concrete-gypsum mixture has less thermal capacity, the temperature swing is more important and the time delay is lower. Introduction of a carpet cover has a more significant effect on the temperature swings than on the time lag. It behaves like a resistance with minimal effect on the time delay because of its very low thermal capacity.

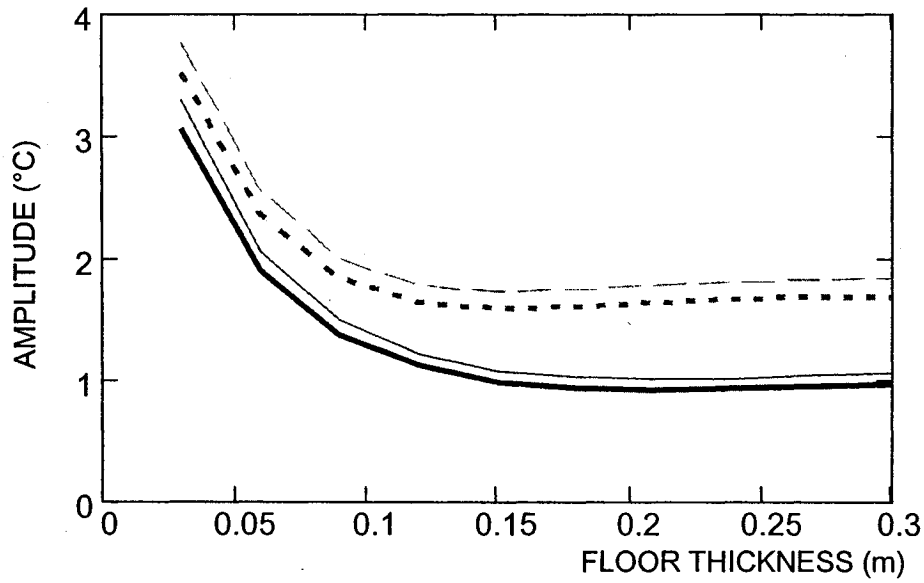

(a)

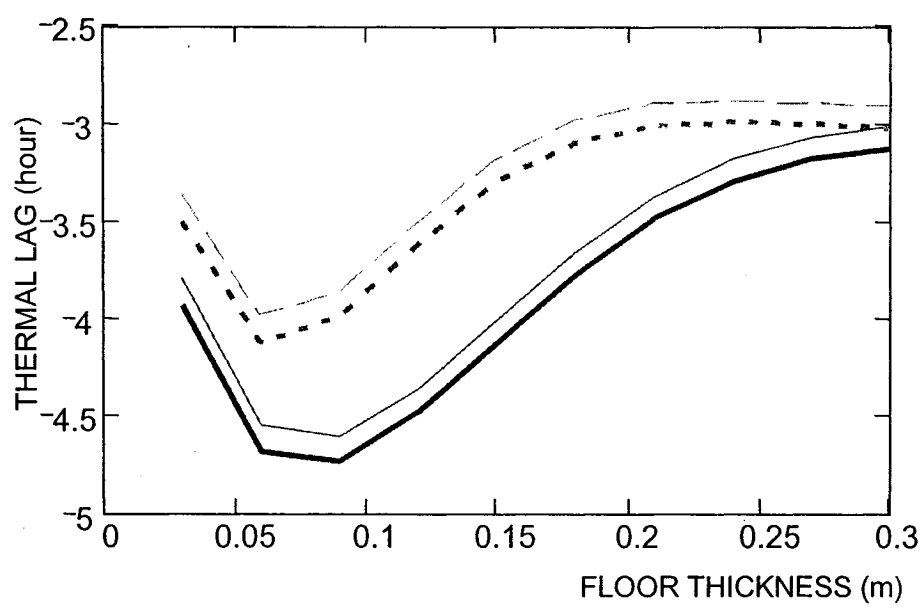

(b)

--- Gypcrete
—— Concrete
- - - Gypcrete with carpet cover
—— Concrete with carpet cover

Figures 4.10a&b: Variation of approximate air temperature swing amplitude ($Z_{0,8}$) and corresponding time lag due to solar radiation

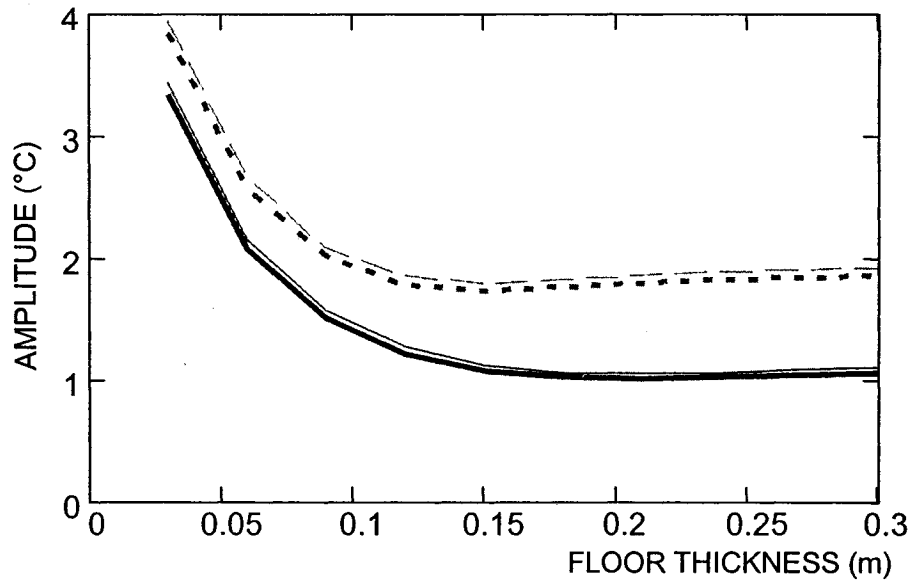

(a)

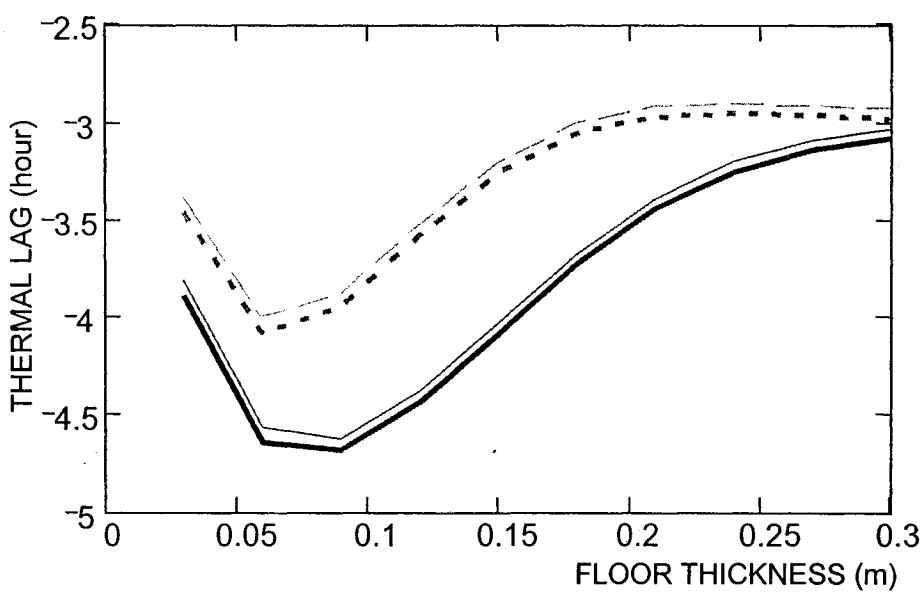

(b)

--- Gypcrete
—— Concrete
- - - Gypcrete with carpet cover
—— Concrete with carpet cover

Figures 4.11a&b: Variation of approximate operative temperature swing amplitude ($X_{8,0}$) and corresponding time lag due to solar radiation

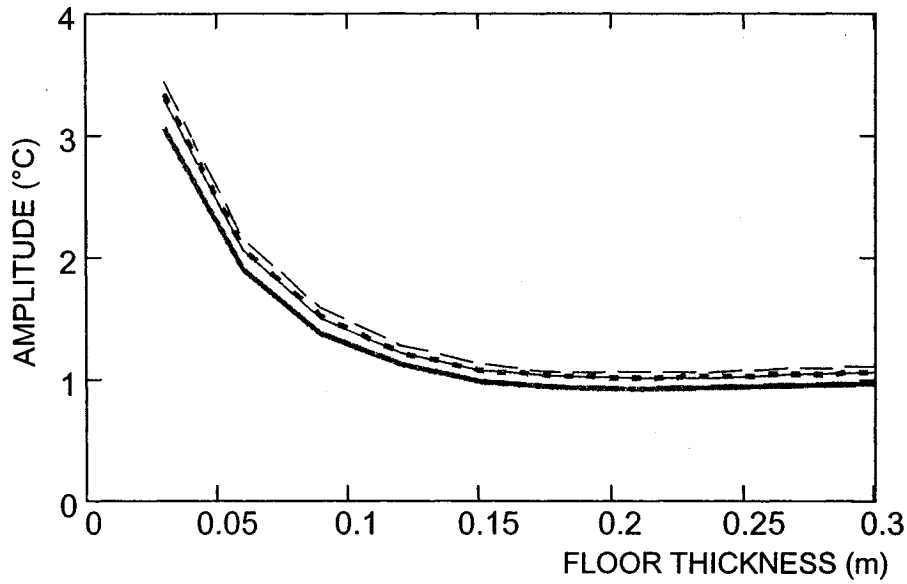

(a)

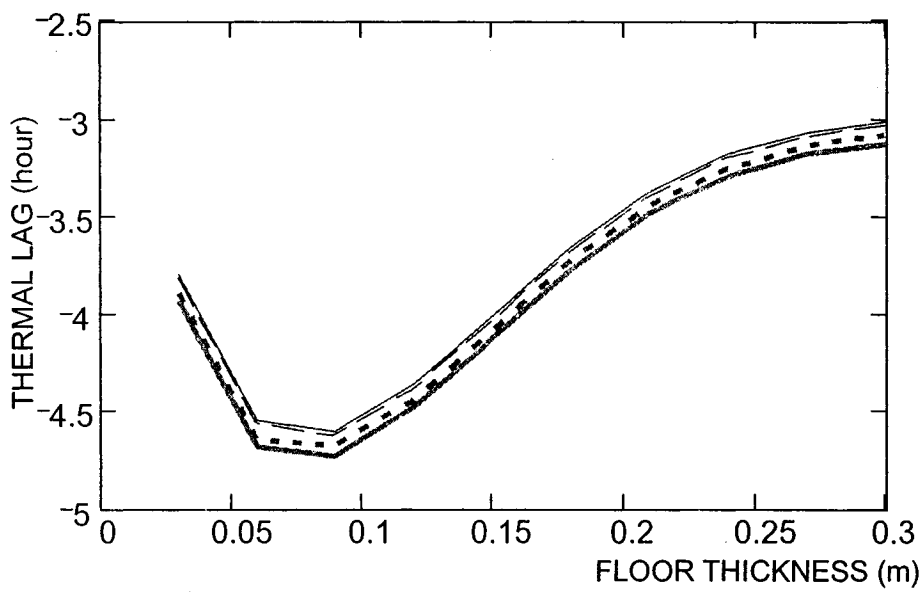

(b)

—— Concrete X_{08} —— Concrete with carpet cover X_{08}
– – – Concrete Z_{08} - - - Concrete with carpet cover Z_{08}

Figures 4.12a&b: Variation of approximate operative ($X_{0,8}$) and air temperature ($Z_{0,8}$) swing amplitude and corresponding time lag due to solar radiation

4.72 Analysis of Bode plot transfer function Z_{09} and X_{09}

Figures 4.13 to 4.17 depict the magnitude ratio and phase variation (Bode plots) for Z_{09} and X_{09} with respect to different internal heat source depth. These transfer functions relate the effect of the floor internal heat source at node 9 on the room temperature at node 0. The magnitude are non-dimensionalized by dividing with the steady state (ω=0). Z_{09} and X_{09} are evaluated at discrete frequencies with four different floor inner (room-side) layers: concrete floor, concrete floor with carpet cover, gypcrete and gypcrete with carpet cover. All four materials at three different internal floor heat source depths 0.01 m, 0.03 m and 0.08 m with an overall floor thermal mass thickness of 0.09 m. The 02 first depths represent typical radiant floor heating system installation recommendations.

Carpeted versus uncarpeted floor

Examination of Figures 4.13, 4.14 and 4.17 indicates that the room response can be approximately separated into short-term dynamics high frequency range and long term dynamics low frequency range. We observe in general that carpeted floor temperature amplitude and its corresponding phase lag are lower throughout the frequency range, with higher phase lag interval difference in the frequency range of 5 to 30 cycles a day between the two considered options. There is however no noticeable difference in the low frequency range less than 5 cycles a day.

In the high frequency short-term dynamics region (about 35 cycles a day and more), the room air thermal capacitance is significant and the difference between the two options is small in both magnitude and phase angle. The phase

lag difference decreases while the amplitude ratio increases with frequency. This shows the influence of carpet cover on the room temperature response and its possible impact of the thermal control particularly in the medium to high frequency short-term dynamics. We observe also that the effect of thermal mass with or without carpet cover is minimal in the low frequency long term dynamics.

Concrete floor versus gypcrete floor

Examination of Figures 4.13 and 4.14 indicates that the impedance magnitude ratio and phase lag for gypcrete floor is higher that that of the concrete floor. The magnitude ratio difference remains approximately constant throughout the frequency range whereas the phase lag difference tends to decrease at high frequency. Clear difference in the phase angle is observed in the frequency range less than 10 cycles a day. This suggests that the thermal mass characteristics have an effect on the low frequency long-term dynamics and a limited effect in the high frequency short term dynamics (less than a minute). The operative transfer functions for both alternatives follow the same pattern as shown by Figure 4.16.

Effect of internal heat source depth

Examination of Figures 4.15a&b shows that the room response at high frequency short term dynamics is clearly related to floor internal heat source. Both magnitude ratio and phase lag decrease with increasing frequency and the rate of decrease is function of heat source depth. No significant discrepancies are observed in the low frequency up to 5.

Operative transfer function versus impedance transfer function

Examination of Figures 4.16 and 4.17 reveals that the operative magnitude ratio is slightly lower compared to that of the air temperature. The magnitude ratio interval difference is minimal and tends to increase with frequency (from 0.0001 for 1 cycle to 0.0008 for 100 cycles a day). On the other hand, the time lag interval tends to increase in the low frequency but decreases in the high frequency. Separation starts occurring between the operative and impedance phase lag around 5 cycles, increases up to about 40 cycles then decreases in the high frequency. As a result for room short term dynamics, operative and air temperature have similar phase angle but different magnitudes

Thermal mass has lower effect of the operative temperature as compared with air temperature. This effect, though limited and higher for thermal mass with carpet cover, intervenes in the low frequency range and decreases in the high frequency. For lower frequencies such as one to four cycles per day, the magnitude and phase angle of Z_{09} and X_{09} is a strong function of room construction. Carpet cover may require increasing the floor temperature in order to reach desired room temperature which may lead to floor surface overheating with resulting possible comfort problem and stress on the floor material.

All these parameters taken alone or together have significant impact on the short terms dynamics and are thus important for control strategy, particularly with passive solar design. This shows also the benefits of predictive control associated with a heated source imbedded in a thermal mass and the importance to be given to the depth of installation.

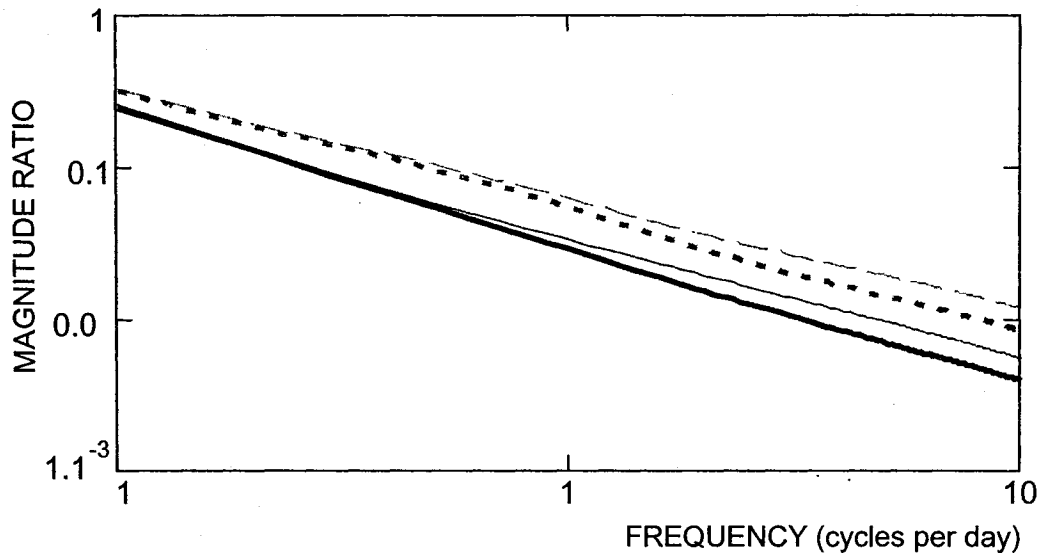

(a)

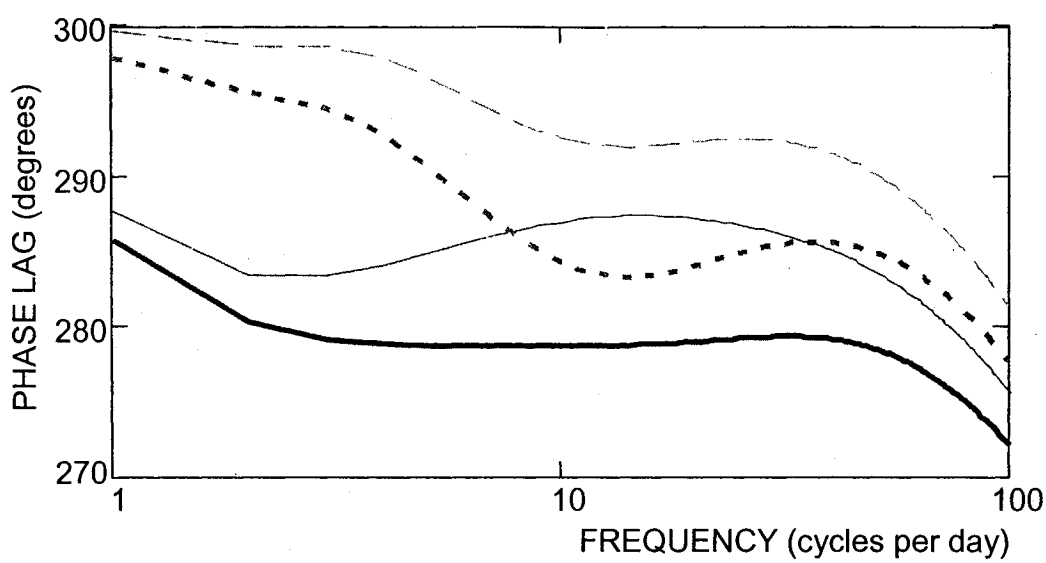

(b)

– – – Gypcrete
——— Concrete
- - - Gypcrete with carpet cover
▬ ▬ Concrete with carpet cover

Figures 4.13a&b: Magnitude ratio and phase angle for impedance transfer function Z_{09} with floor internal heat source depth of 0.01 m

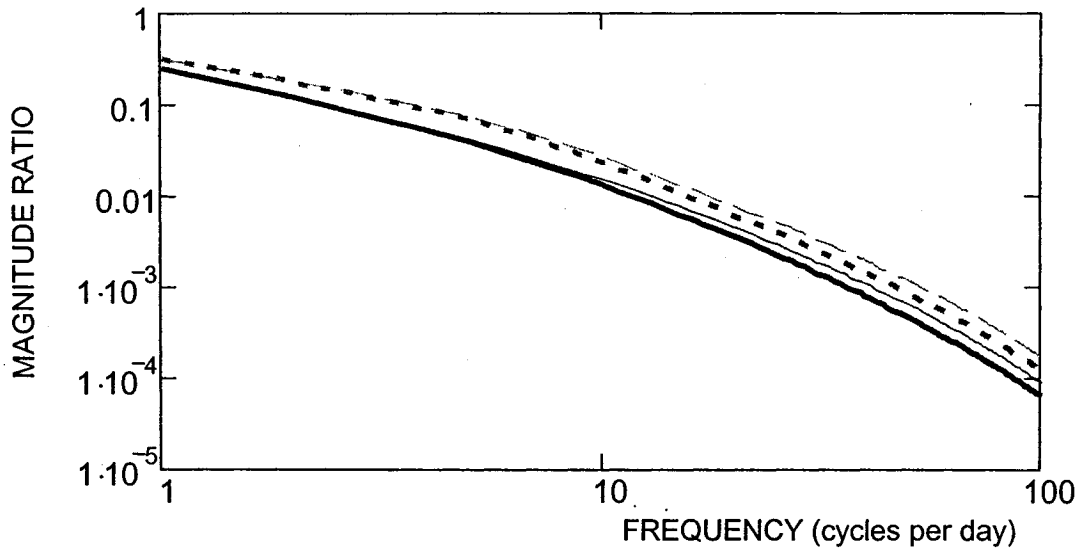

(a)

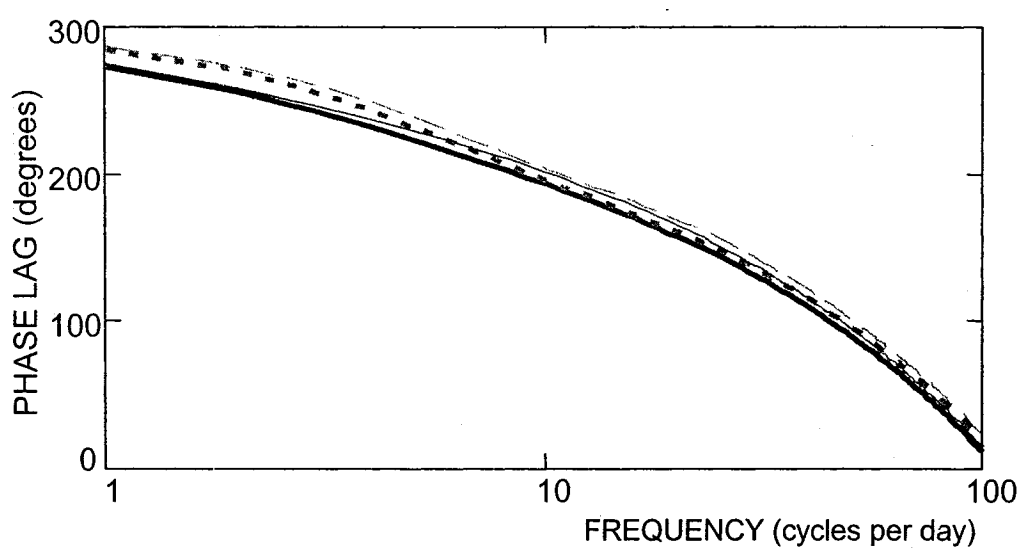

(b)

--- Gypcrete
—— Concrete
- - - Gypcrete with carpet cover
— — Concrete with carpet cover

Figures 4.14a&b: Magnitude ratio and phase angle for impedance transfer function Z_{09} with floor internal heat source depth of 0.08m

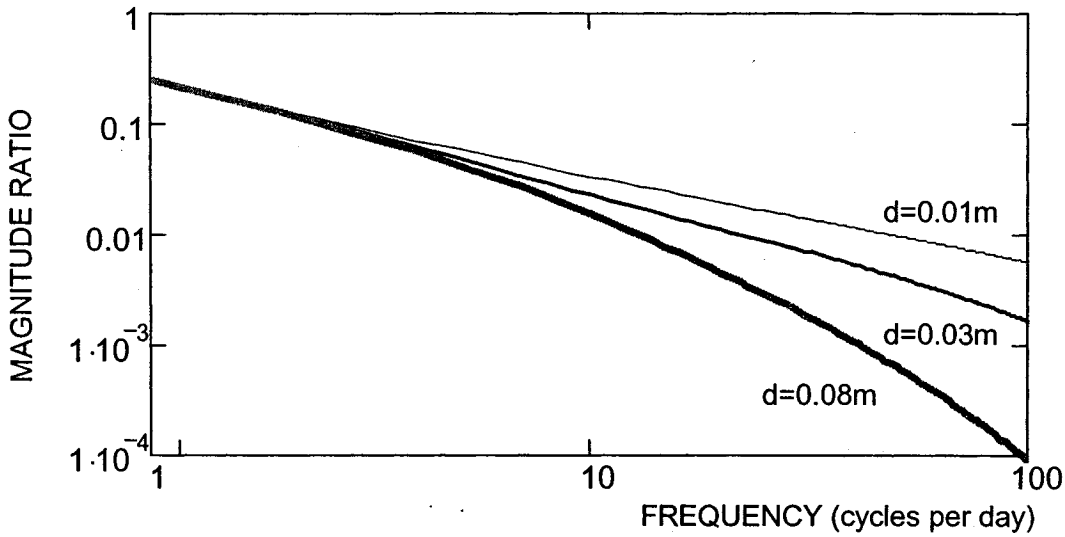

(a)

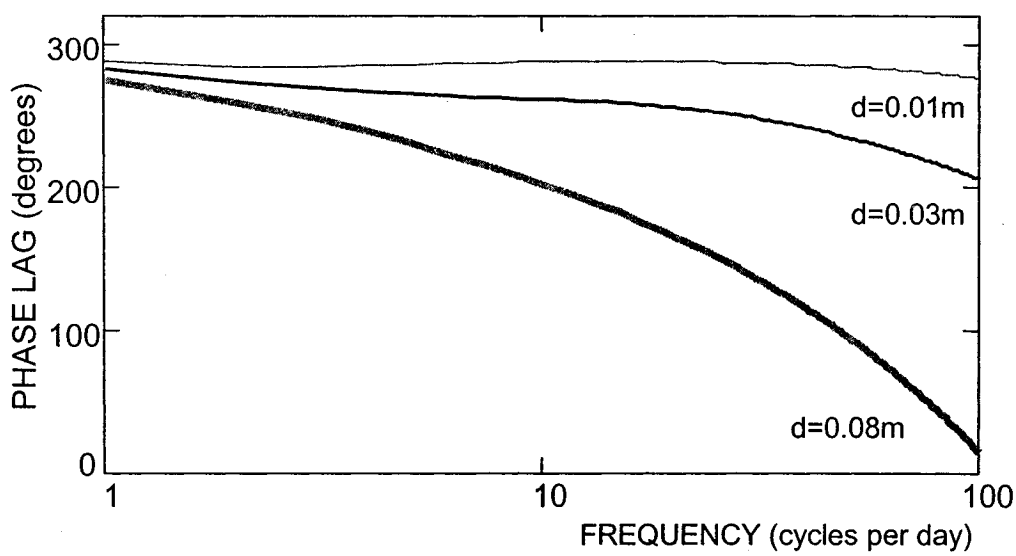

(b)

Figures 4.15a&b: Magnitude ratio and phase angle for impedance transfer function Z_{09} with concrete floor and different internal heat source depths d

Concrete versus gypcrete

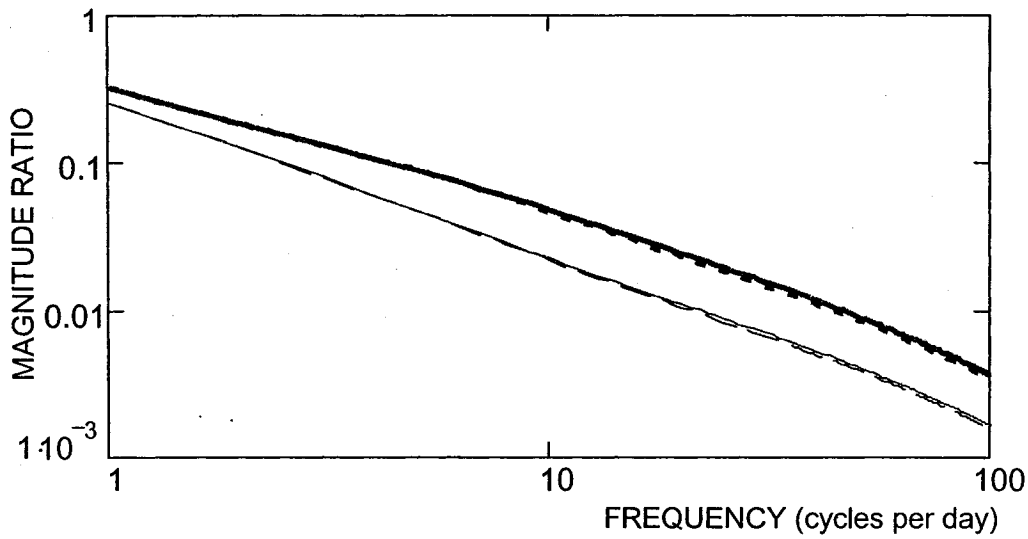

(a)

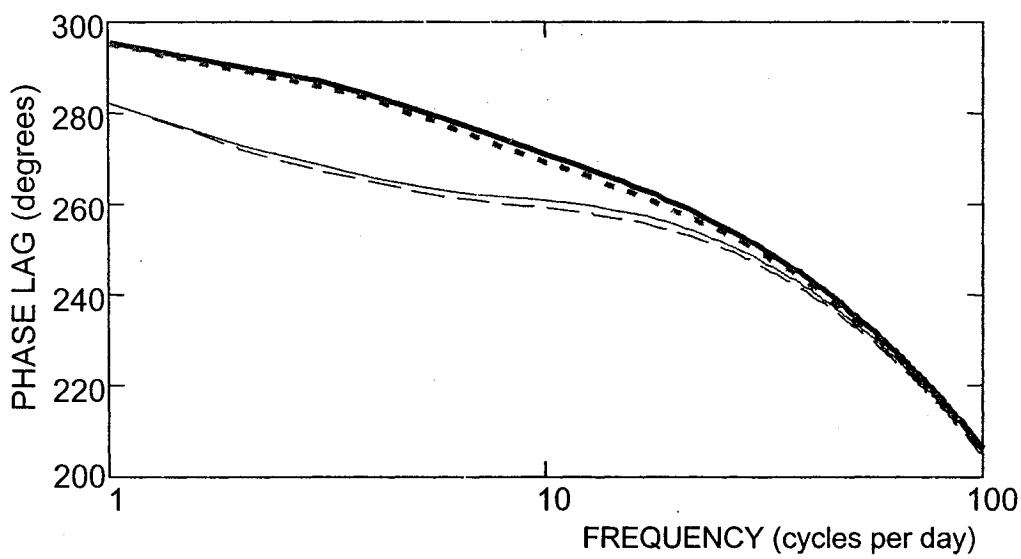

(b)

Gypcrete — Zg_{09} — Xg_{09}
Concrete — Z_{09} — X_{09}

Figures 4.16a&b: Magnitude ratio and phase angle for impedance Z_{09} and operative X_{09} transfer functions with floor internal heat source depth of 0.03 m

Carpeted concrete versus uncarpeted concrete floor

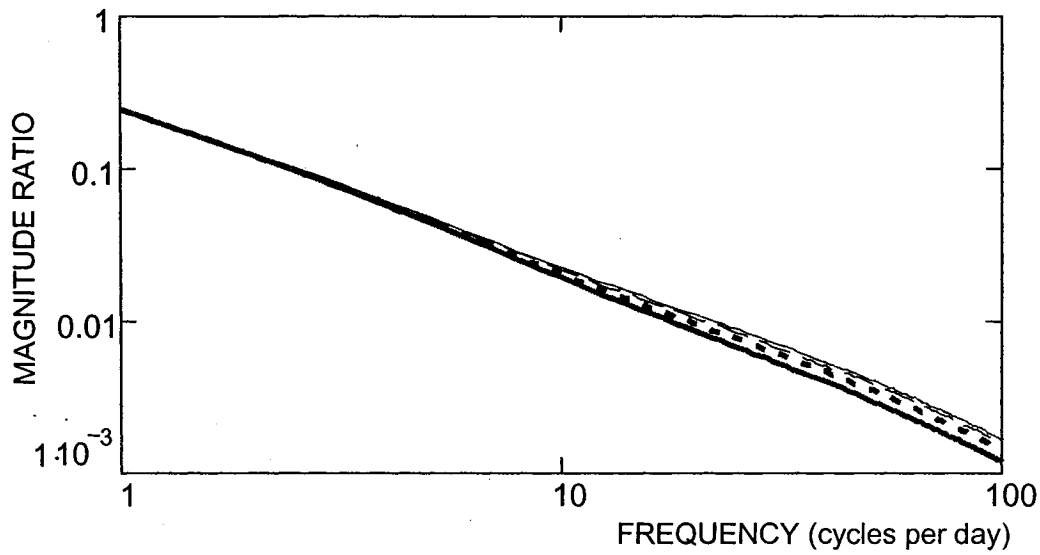

(a)

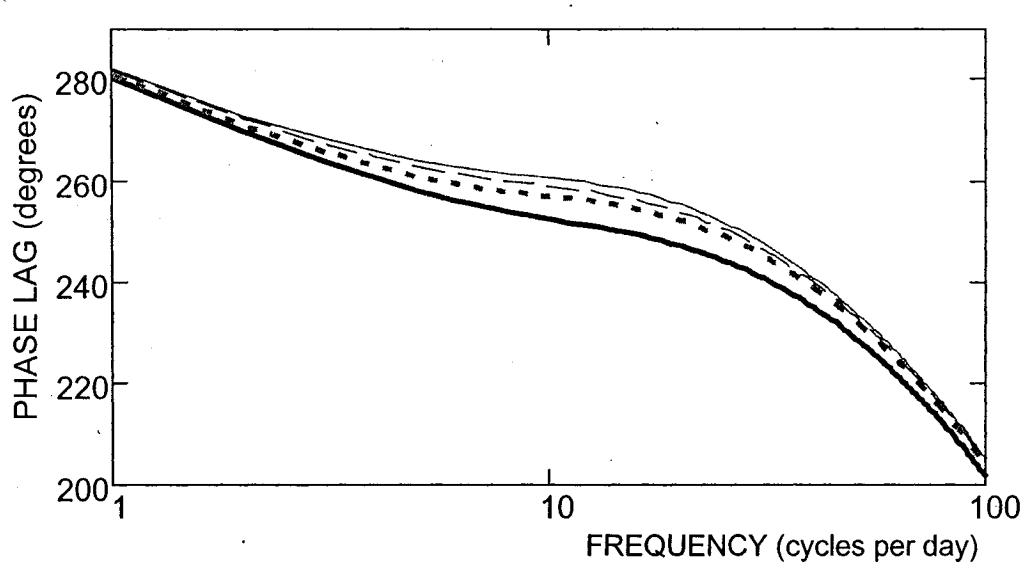

(b)

Uncarpeted —— Z_{09} - - - X_{09}
Carpeted — — Zc_{09} - - - Xc_{09}

Figures 4.17a&b: Magnitude ratio and phase angle for impedance Z_{09} and operative X_{09} transfer functions with floor internal heat source depth of 0.03 m

4.73 Analyze of transfer function identification method

Figures 4.18 to 4.21 show the magnitude and phase variation of the exact impedance and operative transfer function Z_{09} and X_{09} representing the effect of the floor internal heat source along with their respective fitted functions Zf_{09} and Xf_{09} obtained with the Least square method. The heat source depth is 0.0225 m with a concrete floor thickness of 0.09 m. The magnitude is non-dimensionalized by dividing with the steady state values of the respective transfer functions. The fitted functions obtained with polynomial of order 5 (M=N=5 and with no iteration), corresponding to Figures 4.18 to 4.19 are as follows:

Impedance transfer function

$$Zf_{09} = \frac{4.713\times10^{-3} + 10.9s + 1.47\times10^{-5}s^2 - 6.212\times10^{6}s^3 + 1.729\times10^{8}s^4 - 1.845\times10^{9}s^5}{1 + 5.571\times10^{4}s + 1.302\times10^{8}s^2 - 3.477\times10^{9}s^3 - 6.184\times10^{13}s^4 - 4.62\times10^{15}s^5}$$

Operative transfer function

$$Xf_{09} = \frac{4.92\times10^{-3} + 11.013s + 1.2\times10^{-5}s^2 - 5.635\times10^{6}s^3 + 1.576\times10^{8}s^4 - 1.71\times10^{9}s^5}{1 + 5.571\times10^{4}s + 1.301\times10^{8}s^2 + 7.859\times10^{8}s^3 - 5.686\times10^{13}s^4 - 4.288\times10^{15}s^5}$$

These figures obtained with no iteration show perfect agreement up to a frequency of 100 cycles a day for both magnitude and phase variation. The error of the fit is 3.71×10^{-8} and 9.42×10^{-6} respectively for impedance and operative transfer functions. However we observed that discrepancies start occurring after 100 cycles a day and 2 to 3 iteration are required to keep the error within reasonable values particularly for the phase lag. No precise calculations were carried out at these high frequencies range for lack of computer capacity and software.

Figures 4.20 to 4.21 show the same transfer functions with polynomial of order 3 (M=3, N=2) obtained after 03 iterations. Additional iterations did not improve the accuracy of the fitted function. The corresponding s-Laplace transfer functions are as follows:

$$Zf = \frac{4.713\times10^{-3} + 1.539s - 20.144s^2}{1 + 5.409\times10^4 s + 1.938\times10^7 s^2 + 1.623\times10^9 s^3}$$

$$Xf = \frac{4.92\times10^{-3} + 512\times10^{-3} s - 3.136s^2}{1 + 5.405\times10^4 s + 9.684\times10^6 s^2 + 7.172\times10^8 s^3}$$

The figures still show excellent agreement with an error of the fit equal to$1.1\text{x}10^{-5}$ and $1.\text{x}10^{-6}$ respectively for impedance and operative transfer function. The degree of accuracy is sufficient to carry out analysis of thermal control for frequency up to 100 cycles.

We observe that accuracy is function of the polynomial order but that order higher than 5 was not needed in the present case. The least square method gives good results but still requires further investigation in order to establish simple and reliable criterions for determining the required polynomial order that will allow reaching acceptable accuracy level for both magnitude and phase lag at any frequency range.

Bode plot of impedance transfer function Z_{09}

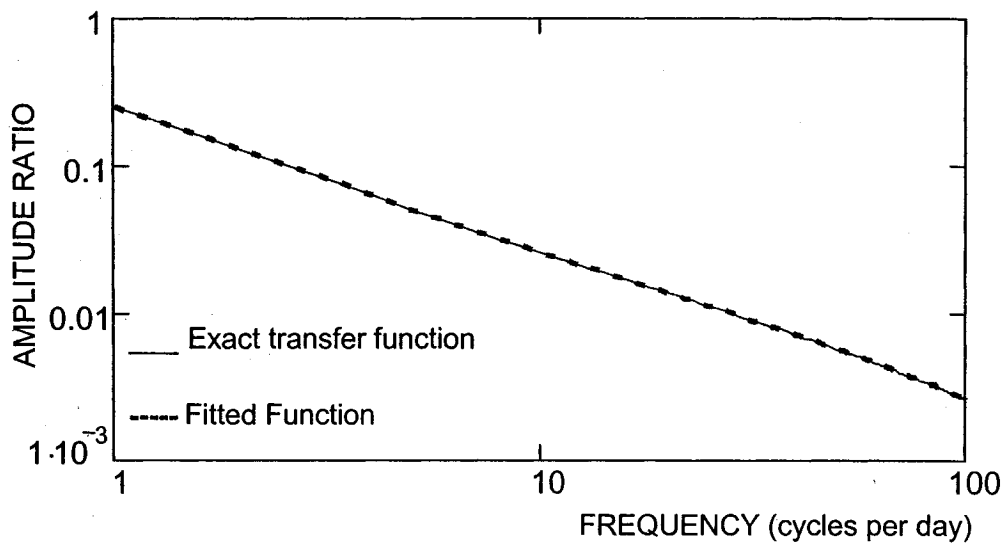

(a)

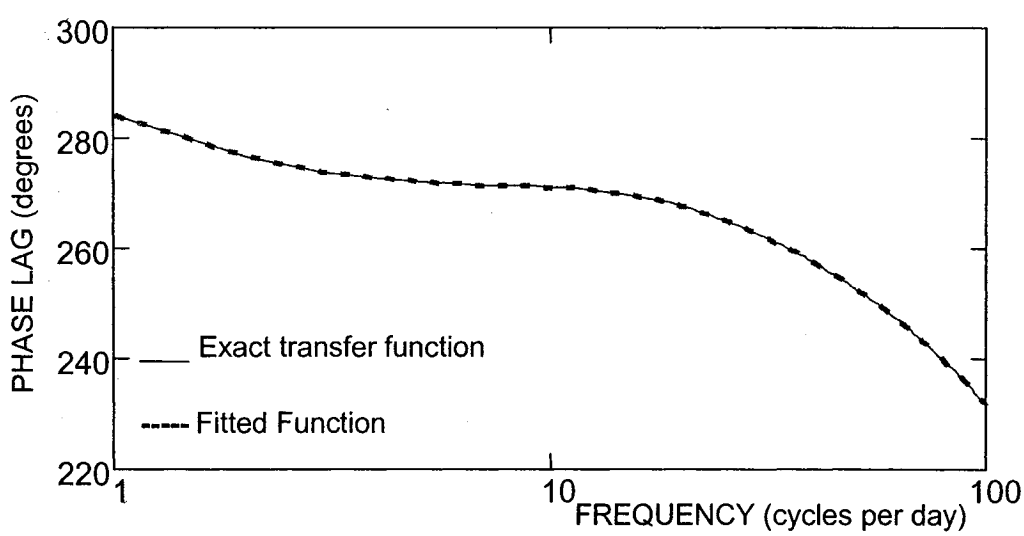

(b)

Figures 4.18a&b: Exact discrete frequency responses Z_{09} and fitted fifth order transfer function Zf_{09} (M=N=5) with internal floor heat source depth of 0.0225m

Bode plot of operative transfer function X_{09}

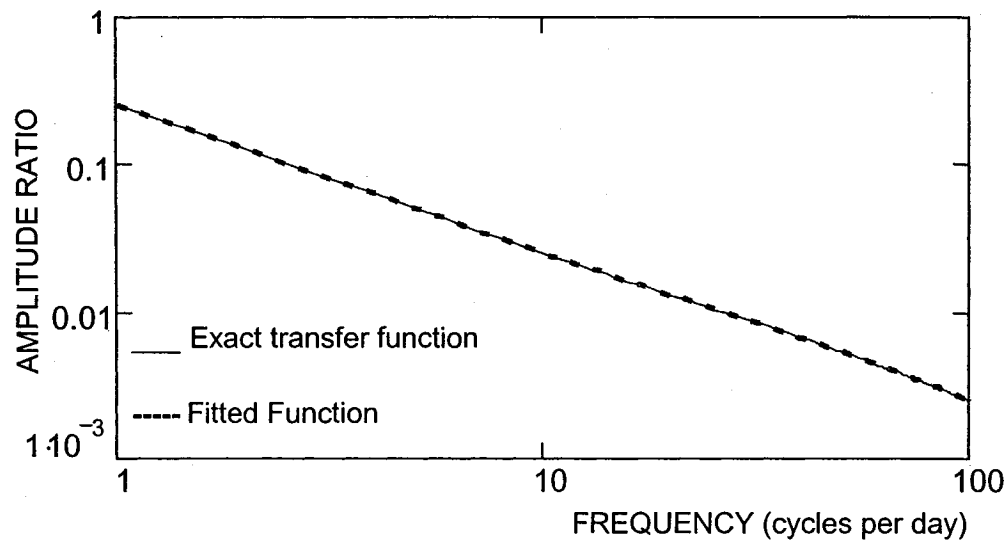

(a)

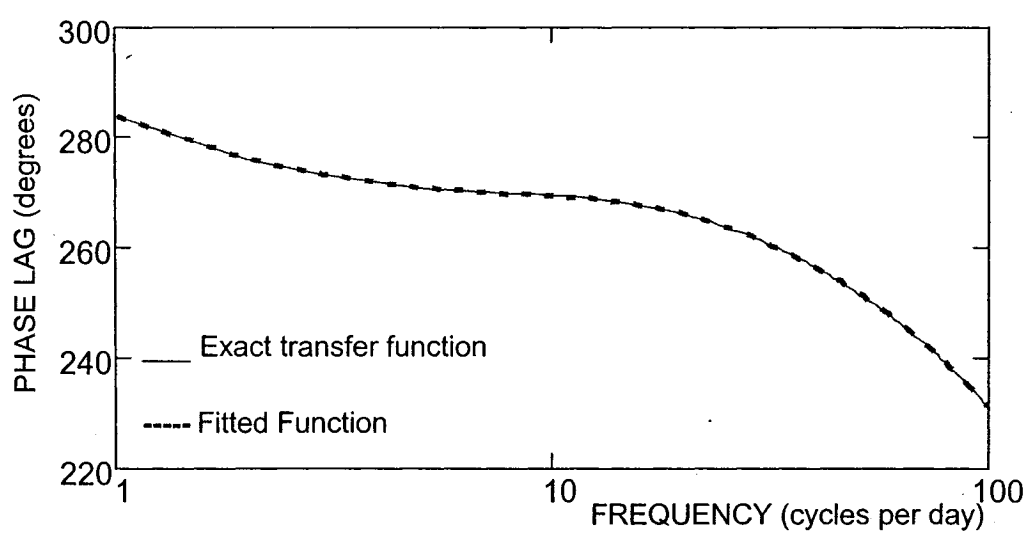

(b)

Figures 4.19a&b: Exact discrete frequency responses X_{09} and fitted fifth order transfer function Xf_{09} (M=N=5) with internal floor heat source depth of 0.0225m

Bode plot of operative transfer function Z_{09}

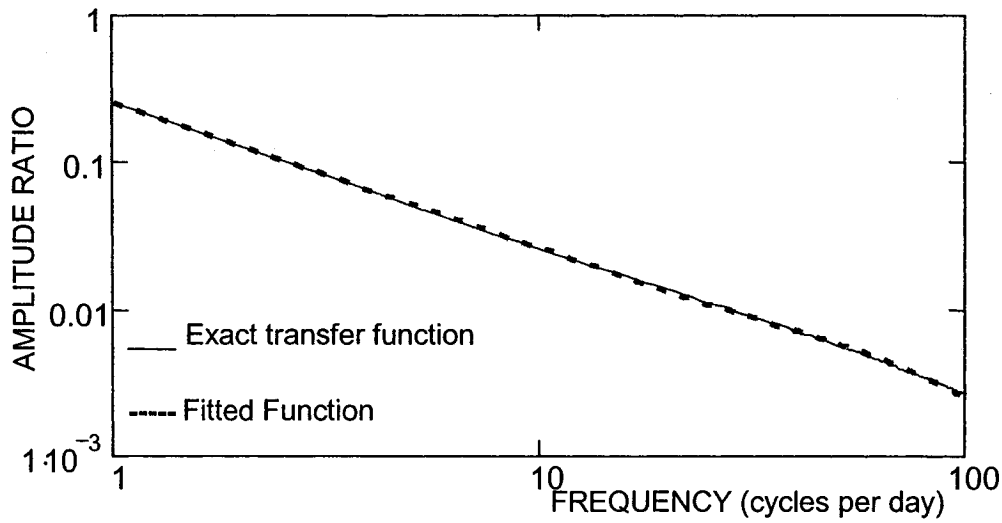

(a)

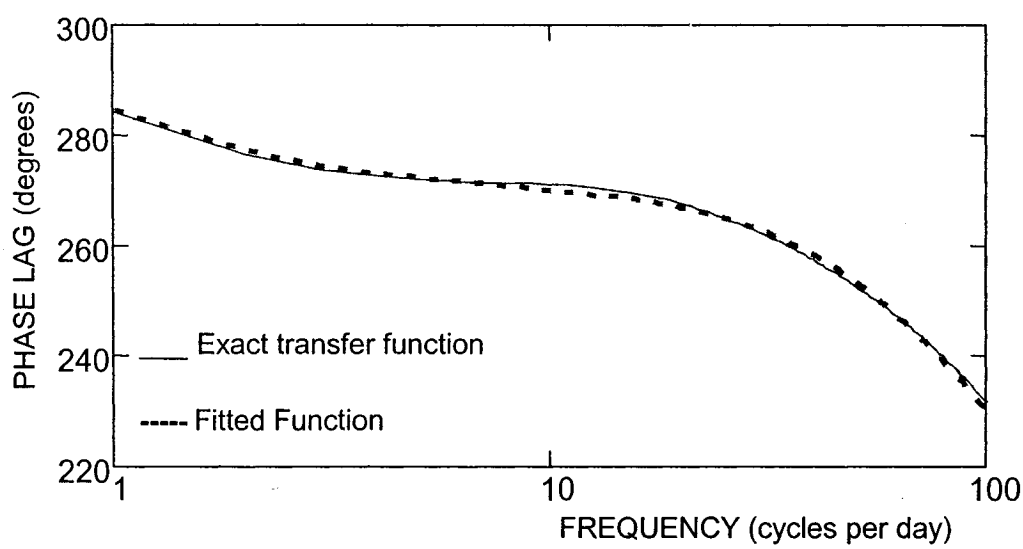

(b)

Figures 4.20a&b: Exact discrete frequency responses Z_{09} and fitted third order transfer function Zf_{09} (m=2, N=3), with 03 iterations and internal floor heat source depth of 0.0225 m

Bode plot of operative transfer function X_{09}

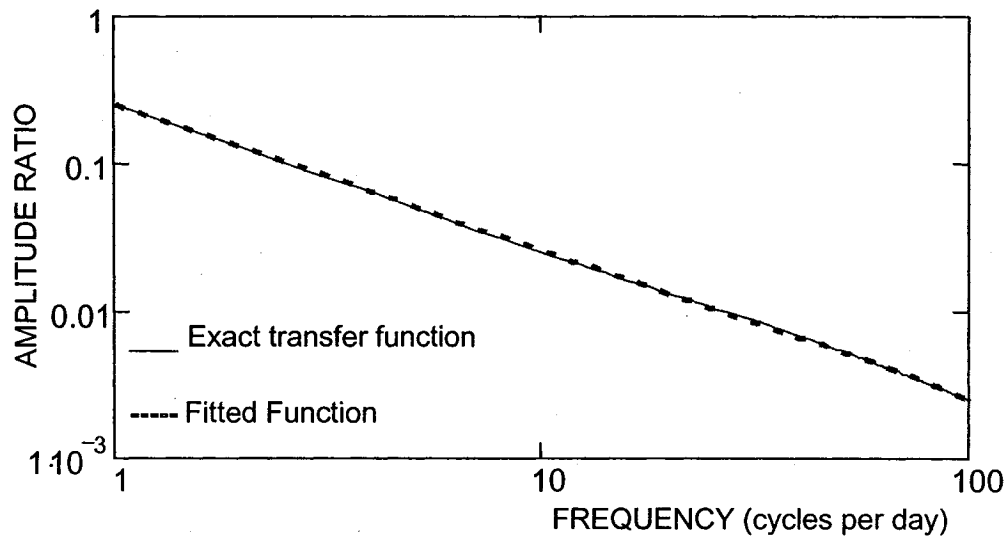

(a)

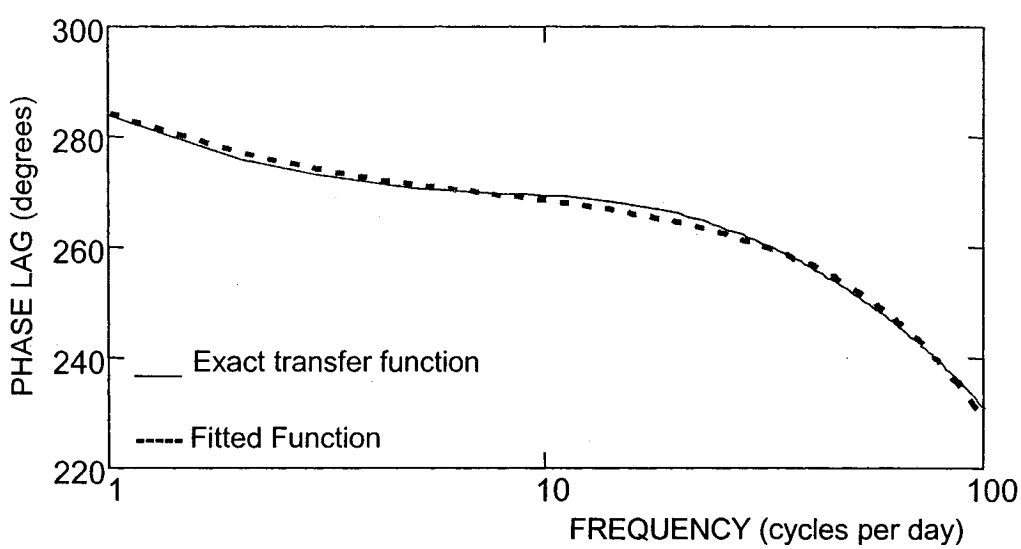

(b)

Figures 4.21a&b: Exact discrete frequency responses X_{09} and fitted third order transfer function Xf_{09} (m=2, N=3), with 03 iterations and internal floor heat source depth of 0.0225 m

CHAPTER 5

CONTROL

5.1. Introduction

The function of a building and its associated control system is to provide a comfortable environment. Bearing in mind that control is a problem embracing the whole building system and not just the extra hardware bolted onto it, thermal control studies are an important tool for the investigation of the appropriate control strategies. It allows the analysis of the building dynamic response and energy consumption associated with different parameters such as heating system options, different types and method of temperature control or building construction. The Building control system has a vital role to play in preventing waste of energy and ensuring a safe and efficient operation of the HVAC system.

The high thermal inertia of most building coupled with the slow response of traditional heating system has usually meant that reasonable stable temperature conditions can be achieved with simple control system. However the trend toward lighter building and the use of air handling system has increased the responsiveness of systems and so increased the possibility of instable conditions. When a controlled system running in a steady state is disturbed by a change in load, a change in a set point or some other disturbances, the system reacts. If the system is operating in a stable manner, it will sooner or later settle down in a new stable state. If the system is unstable, it will go into indefinite oscillations of increased amplitude. In practice, the size of the oscillation will de

limited by the size of the system and the system will continue oscillating or hunting.

5.2 System transfer functions

Analysis of a linear system are usually conducted in the frequency domain through numerous method all offering flexibility and ease of use. The standard method used to carry out building thermal analysis is based on the Laplace transform. The system is analyzed by setting up the differential equation that describes its dynamic. The building, HVAC system and control Laplace transfer functions are combined through block diagram algebra to obtain the overall system s-transfer functions. These transfer functions are then studied in the frequency domain ($s=j\omega$) for stability and other analyses or are used for transient analysis of overall system response to stepping and load variations using numerical inversion of Laplace transforms.

The transfer functions of the physical components, consisting of a controller, a sensor, a final controller element and a controlled device, of the building control system are based on established models described elsewhere and are as follows.

5.21 PID (Proportional-Integral-Derivative) controller

The transfer function for a PID (proportional-integral-derivative) controller is equal to the ratio of the controller output to the input (error) in the Laplace domain. Its output is proportional to the error, the integral of the error over time,

and the rate of change of the error. The transfer function of a PID controller is given by (Stephanopoulos, 1984):

$$G_c(s) = K_p\left(1 + \frac{1}{\tau_i s} + \tau_D s\right) \tag{5.1}$$

K_p is the proportional gain, τ_i the integral time and τ_D the derivative term

5.23 Temperature sensor

It is an essential element for detecting the deviation of controlled temperature from a set point. A transport delay may be included to reflect the time delay taken by the temperature change to be transmitted over the distance and the Laplace transfer function is:

$$G_s(s) = \frac{T_{measured}}{T_{actual}} \qquad G_s(s) = \frac{e^{-t_d s}}{\tau_s s + 1} \tag{5.2}$$

τ_s is the time constant and t_d the time delay due to the distance from the sensor to controller.

5.24 Final control element

The final control element, which may represents an on-off switch, a silicon-controlled rectifier (scr) to module the electric power supply or a valve for example, implement a control action upon reception of signal from the controller and its transfer functions is given by:

$$G_f(s) = K_{scr}\, e^{-t_{scr} s} \tag{5.3}$$

Where t_{scr} is the time delay and K_{scr} the magnitude ratio of the component.

5.25 Heater transfer function

The heating system falls generally into 02 categories, convective or radiative heating. The present case is confined to electric radiant panel heating and is expressed as:

$$G_m(s) = \frac{K_h}{\tau_h(s)+1} \tag{5.4}$$

K_h represents the capacity of the heating system and τ_h is the time constant of the heating system reflecting its thermal inertia.

5.26 Floor transfer function

The floor transfer function relates the floor internal auxiliary heat source the room air temperature. The equation derived previously is written is a non-dimensionalized quantity.

$$Z_{09}(s) = \frac{Tai(s)}{qr_{aux}(s)}$$

$$Z_{09}(s) = \frac{a_0 + a_1 s + a_2 s^2 + a_3 s^3 + a_4 s^4 + a_5 s^5}{1 + b_1 s + b_2 s^2 + b_3 s^3 + b_4 s^4 + b_5 s^5} \tag{5.5}$$

5.3 Overall feedback system Laplace transfer function

A block diagram is used to represent the composition of the system with simple feedback control and inputs-loads Q(j) (representing heat gains or losses) influencing room temperature Tair through transfer functions Z_{ij}. The transfer function relating temperature to auxiliary heat is Z_{0j}, which in the present case is Z_{09} for radiant floor heating or would be Z_{00} in the case of convective heating

analysis. As illustrated in Figure 5.1, the error signal Xe is processed by a controller which produces an output signal Y, which acts on the final control element, which in turn drives the HVAC controlled device i.e. a heating system, boiler, valves, resulting in a change in the controlled variable Tair. Assuming all the system components to be linear, the resulting room air temperature variation T_{ai} as a function of set point and load changes is then obtained through block diagram algebra as follows:

$$T_{ai}(s) = T_{sp}\frac{G_c\,G_f\,G_m\,Z_{09}}{1+G_c\,G_f\,G_m\,Z_{09}\,G_s} + \sum_j\left(Q(j)\frac{Z_{0,j}}{1+G_c\,G_f\,G_m\,Z_{09}\,G_s}\right) \qquad (5.6)$$

where j=0,1...8 surface number in the present case

T_{sp} is the set point and G the transfer functions indicated in the block diagram. All variables are a function of s. For operative temperature analysis, T_{ai}, Z_{09} and $Z_{0,j}$ are replaced respectively by their operative counterpart Top, X_{09} and $X_{0,J}$.

The first term indicates the room air temperature change due to set point

$$G_{sp}(s) = T_{sp}\frac{G_c\,G_f\,G_m\,Z_{09}}{1+G_c\,G_f\,G_m\,Z_{09}\,G_s} \qquad (5.6a)$$

The second term indicates the temperature response due to load change

$$\sum_j Q(j)\frac{Z_{0,j}}{1+G_c\,G_f\,G_m\,Z_{09}\,G_s} \qquad (5.6b)$$

An important item to equation (5.6) is that both denominators are identical, because any disturbance, no matter where it enters the system, will enter into the same closed loop. Therefore all disturbance due to external loads or and set-point terms will have the same denominator 1+ "the product of closed-loop blocks". The denominator $1+G_cG_fG_mZ_{09}G_s$ is the characteristic equation that

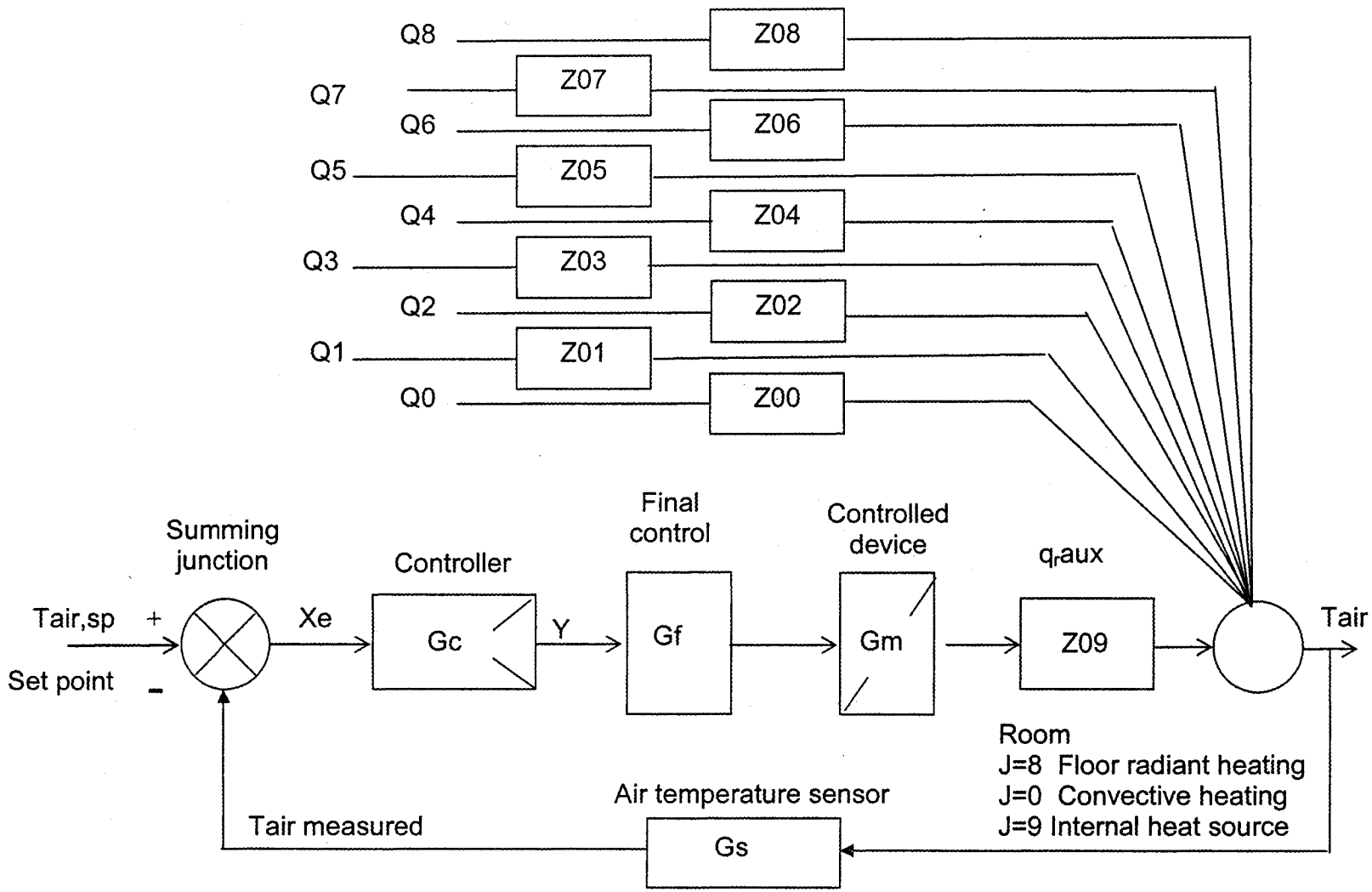

Figure 5.1: Block diagram for feedback thermal control

determines the stability of the heating control system and the open loop transfer function that can be used for stability analysis using the Nyquist criterion or the Bode criterion (Stephanopoulos 1981) is:

$$G_{OL} = G_c\, G_f\, G_m\, Z_{09}\, G_s \qquad (5.6c)$$

Most system are too complex for this analysis to be practical and empirical rules have been derived to assist in setting up a three term controller (PID) to achieve the desired compromise between stability and speed of response.

5.4 Temperature response using stepwise numerical Laplace transform inversion

After the control parameters have been determined, the system temperature response to set point and load changes can be investigated using numerical inversion of Laplace transform. Various numerical methods for numerical Laplace transform inversion are available. The advantage of the chosen approach is that it is easily incorporated into program dealing with frequency response analysis of linear system because the transfer functions are already determined as function of s and it is just a simple matter of substituting s with the frequency variable $j\omega$. This method developed and applied to circuits by Vlach (1969) and Singhal (1975) is particularly suitable for network solutions. It provides an efficient way for calculating the time domain response of system without determining poles of residues, that is transfer function which are transcendental and time delays without any artificial manipulation of the constants present.

It preserves the accuracy for large time by introducing in the original method a stepping algorithm so as to reset the time origin after each step. This method is based on the Paden approximation rational function $R_{N,M}(z)=P_N(z)/Q_M(z)$ where the poles z_i and residues K'_i were calculated once and for all with high precision and a selection is given in Appendix 3. In order to carry out evaluations, M and N must be chosen such that the function to be inverted $F(z)=V(z/t)R_{N,M}(z)$ has at least two more finite poles than zeros, $M \geq N+2$. The useful time interval can be increased by selection of higher M and N. Selection of the poles z_i and detailed description of the method can be found elsewhere (Vlach, J and K. Singhal, 1983).

For numerical inversion s is set equal to z_i/t where t is the time and z_i is a constant determined once and for all by VLach and Singhal (1969, 1975 and 1983). The overall closed loop transfer function do no need to be evaluated analytically but only at the selected time step, $s = z_i/t$ for time step, $s=z_i/(t+dt)$ for the next step. To reduce computations to one half, real time functions can be evaluated using the modified basic inversion formula as follows for M even and with Re denoting the real part of the complex conjugate:

$$\hat{u}(t) = -\frac{1}{t}\sum_{i=1}^{M'} \mathrm{Re}\left[K_i'(U(z_i/t)\right] \qquad (5.7)$$

where $M'=M/2$ and $K_i' = 2K_i$. When M is odd, $M'=(m+1)/2$ and $K_i' = K_i$.

This method applied first by Stylianou (1989) allows the use of transfer functions for the building envelope that model the thermal mass as distributed element.

5.5 Room temperature transient response to load change

The transient response of the room temperature without temperature control is obtained by introduction of a step input increase in heat gains directly in the room or through the floor internal heat source (floor radiant heating system) such as in the present case. This configuration, basically an open circuit with no feedback, can be used to compare the effects of different building characteristics such as different material and internal heat source depth of the floor mass, on the room temperature. The Laplace transfer function to be inverted is:

$$T_{ai}(s) = G_0(s)Z_{09}(s) \tag{5.8}$$

with Laplace transfer function for a load set input as:

$$G_0(s) = K_h/s \tag{5.8a}$$

K_h is the thermal capacity of the auxiliary source. Using equation (5.7), the room temperature time domain response over a time range t and with $s=z_i/t$ is:

$$T_{ai}(t) = -\frac{1}{t}\sum_{i=1}^{M'} \mathrm{Re}\left[K_i'(T_{ai}(z_i/t)\right] \tag{5.8b}$$

5.6 Room temperature response due to step input temperature change and stability analysis

The aim of tuning a controller is to restore control following a disturbance as quickly as possible and to achieve stable control with a small or zero offset from the set point. These criteria interact and increasing the speed of response risk introducing instability. The controller parameters must be set to values appropriate for the system.

Numerous methods for stability analysis are available, most of which are based on the characteristics equation. Tuning is usually performed on site for HVAC system because system parameters are usually not accurately known. The frequency response method developed by Ziegler and Nichols (1942) can be carried out on the control system. The method is based on the bode stability criterion which is used to determine the period and gain at the stability limit at which the phase angle of the open loop transfer function, corresponding to the crossover frequency ω_{co}, (for proportional control) is equal to 180 degree. The two parameters are known as the ultimate period P_u and ultimate gain K_u respectively and the recommended controller constants based on the Ziegler-Nichols method are:

Proportional (P): $K_p = 0.5K_u$

Proportional integral (P-I): $K_p = 0.45K_u \quad \tau_i = 0.8P_u$

Proportional integral derivative (PID): $K_p = 0.6K_u \quad \tau_i = 0.5P_u \quad \tau_D = 0125P_u$

The bode stability criterion is a reference that indicates the adjustment to be made in order to avoid system instability. To use this method, the integral and the derivative actions of the controller to be tuned are first disabled. The proportional gain K_p setting is then increased (i.e. the band is reduced) in small steps from a low value and at each value of the band, the system is given a small disturbance by adjusting the set point. At low values of the proportional gain, the controlled variables will settle down to a stable value when the set point is changed. As the gain is increased, a value will be reached when the system starts hunting. The oscillations should be steady with neither increasing nor

decreasing. The procedure is as follows:

1-Establish open Loop transfer function equation (5.6c) with proportional control $G_c = K_p$ and K_p is initially set equal 1.

$$G_{OL}(s) = K_p\, G_f(s) G_m(s) Z_{09}(s) G_s(s) \tag{5.9}$$

2-Determine from step 1 the phase angle and subsequently the crossover frequency ω_{co}.

3- Determine the ultimate gain Ku and the ultimate period P_u at cross-over frequency. The ultimate gain is determined based on the fact that at the crossover frequency the magnitude of the open loop transfer function (amplitude ratio) is equal to one at the stability limit.

$$K_u = \frac{1}{|G_{OL}(j\omega_{co})|} \tag{5.10}$$

$$P_u = \frac{2\pi}{\omega_{co}} \tag{5.11}$$

4- Select the controller parameters with regard to Ku, P_u and the PI controller constant from Ziegler Nichols method. In most HVAC application, the derivative term is not required and is disabled by setting the derivative time to zero, resulting in a PI controller with proportional term K_p=0.45·K_u and integral term τ_i =0.8 ·P_u.

4-The room transfer function is then derived from equation (5.62) as follows:

$$T_{ai}(s) = G_{sp}(s) T_{sp}(s) \tag{5.12}$$

with PI controller and step input temperature respectively as:

$$G_c(s) = K_p\left(1 + \frac{1}{\tau_i s}\right) \tag{5.12a}$$

$$T_{sp}(s) = \frac{1}{s} \tag{5.12b}$$

5-The time domain response of the room temperature response is then determined through numerical inverse transform over a time range t and $s=z_i/t$.

$$T_{ai}(t) = -\frac{1}{t}\sum_{i=1}^{M'} \mathrm{Re}\left[K_i'(T_{ai}(z_i/t)\right]$$

Unit step change in the set point is introduced and the value of the proportional gain K_p is varied with small step until the system oscillate continuously, always at cross over frequency.

5.7 Simulation results

The method is applied to analyze the thermal mass storage effect of a concrete floor and a concrete carpeted floor with different internal heat source depth in a room with characteristics as shown in Figure 3.1. The floor overall mass thickness remains the same (0.09m) and the impedance and operative transfer functions of interest for floor concrete without and with carpet cover are as indicated respectively in Tables 1 and 2. To comply with the requirement of the method, the coefficients chosen for this particular case are M=10 and N=8. The poles z_i and residues K'_i for inversion are as indicated in Appendix 3.

5.71 Room transient response to load change

Figures 5.2 to 5.13 illustrate the effect of radiative step heat input (8.4KW) through the floor internal heat source with different depths. Figures 5.2 to 5.7 depict the effect of concrete floor while Figures 5.8 to 5.11 show the effect due to

concrete carpeted floor. All the Figures show the equivalent first order time constant obtained from the transient response at the time by which room temperature reaches 63% of its steady state.

As expected, Figure 5.2 reveals that with concrete floor and low bottom floor insulation (1 RSI), room air temperature takes longer to reach steady state with internal heat source at a depth of 0.0675 m than at smaller depth of 0.045 m (15.34 hr versus 15.13hr), consequently the temperature rise is slightly lower. The same conclusions are drawn for operative temperature (15.22hr versus 15.13hr in the same depth order) as shown by Figure 5.3. On the other hand, Figures 5.6 & 5.7 show, that with high bottom floor insulation (56 RSI and step heat input equal to 5000 kW), transient response remains the same whatever the floor internal heat source depth for operative and air temperature. This shows the influence of bottom floor insulation and indicates that it is an important parameter to be taken into account, particularly at the design stage. Figures 5.4&5.5 show the steady state of operative temperature to be higher than that of air temperature (40.59 degrees versus 38.88 degrees), confirming again the operative control to be a more appropriate mode for radiant heating system.

Figures 5.8 to 5.11 show that for concrete carpeted floor, variation of the internal heat source depth produces the same general room response. However Figures 5.10 and 5.11 indicate that the steady state temperature interval between operative and air temperature is higher than that of concrete floor (3.45 degrees versus 1.71 degrees). This shows that carpeted floor has a higher impact on air temperature response and that operative control mode is even more appropriate.

Figures 5.12 and 5.13 show the room temperature response with concrete floor and with concrete carpeted floor and confirm that carpet cover with floor radiant heating system induces a lower room temperature response. As expected, room temperature takes longer to reach steady state with carpeted floor than concrete floor (15.63hr versus 15.13 hr and 15.66 hr versus 15.13 hr respectively for operative and air temperature for a depth of 0.045m). However, the steady state temperature interval between the two configurations is higher for air (2.17 degrees) than for operative temperature (0.42 degree). Overall this shows that depth of installation of internal heat source and thermal properties of floor slab have an impact on the resulting room response and confirm again more that operative control mode is more appropriate for radiant heating.

5.72 Room temperature response to set point increase

Figures 5.14 to 5.21 show samples of room temperature responses to one degree temperature step rise in the set point for concrete and carpeted floor. The objectives of the simulation being to investigate the effect of variation of the depth of the floor internal heat source, the same parameters were used throughout the samples; no attempt was made to act on the proportional gain except to maintain room temperature oscillation within 2 degrees. The floor thickness remains constant (0.09m), proportional integral control with recommended controller constants was used with air sensor for both air and operative temperature. The time constants are set equal to 20 seconds for the internal heat source and 15 seconds for the air temperature sensor.

Floor concrete

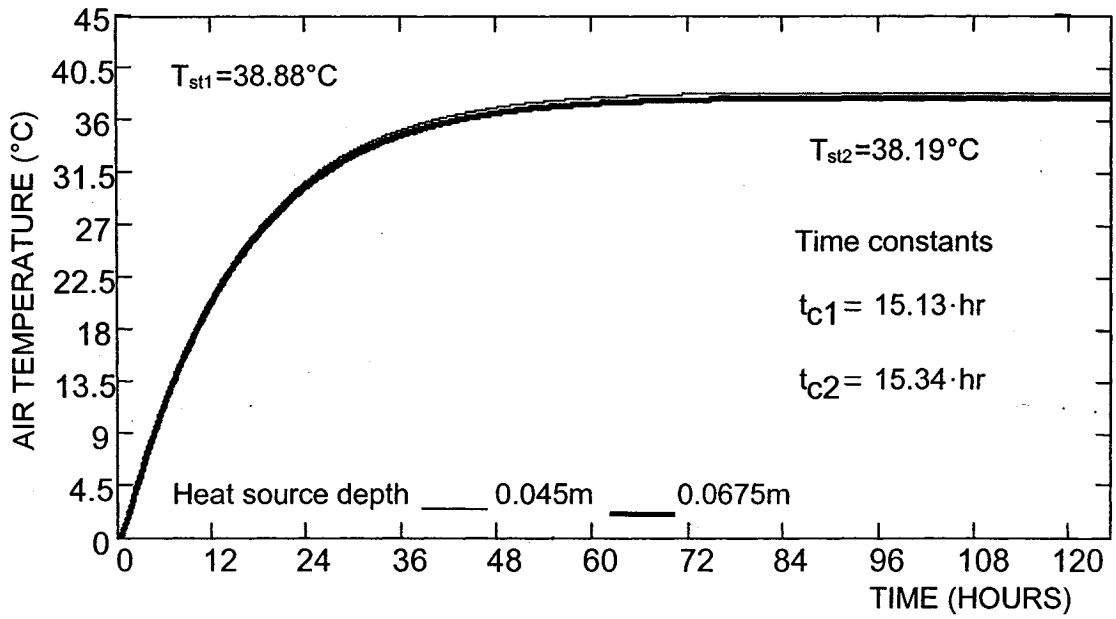

Figure 5.2: Air temperature response to step input of radiative gain

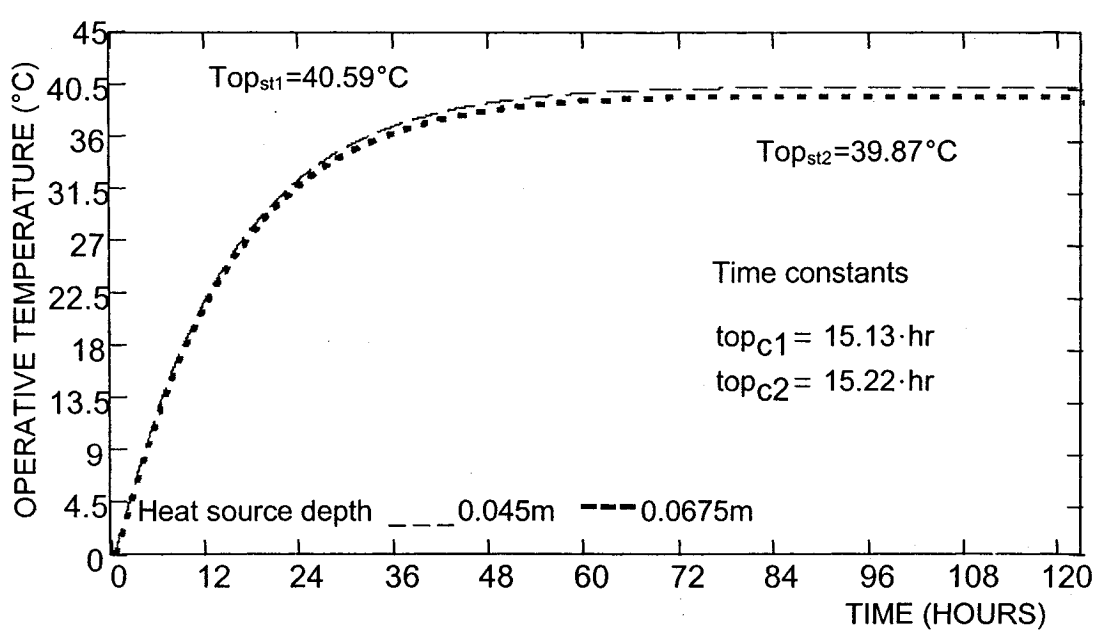

Figure 5.3: Operative temperature response to step input of radiative gain

Floor concrete

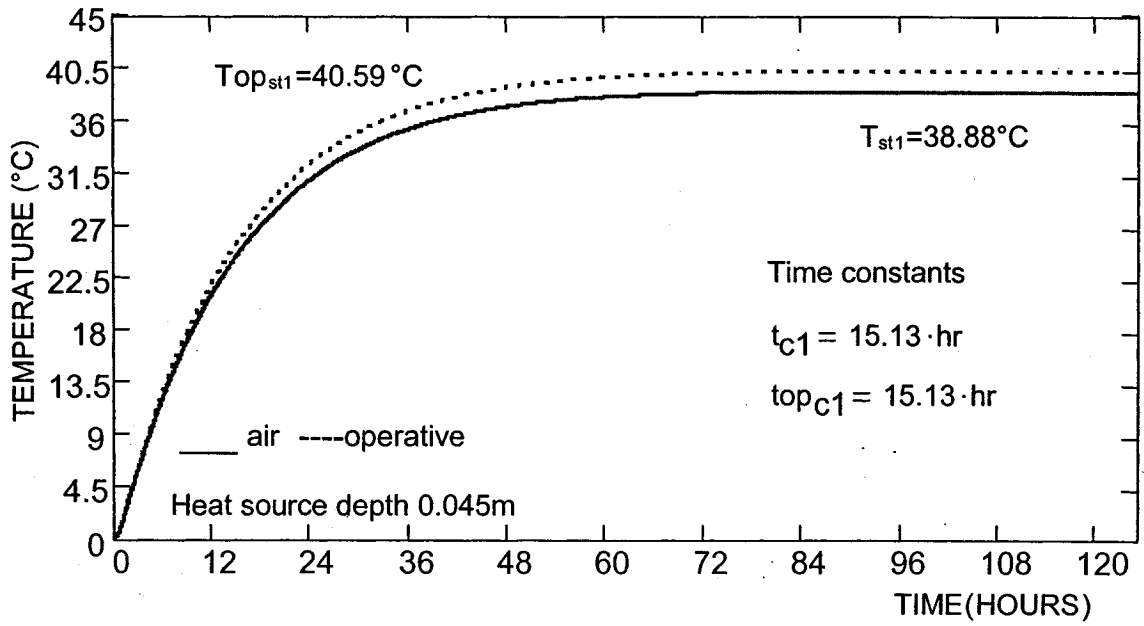

Figure 5.4: Operative and air temperature response to step input of radiative gain with heat source depth equal to 0.045m

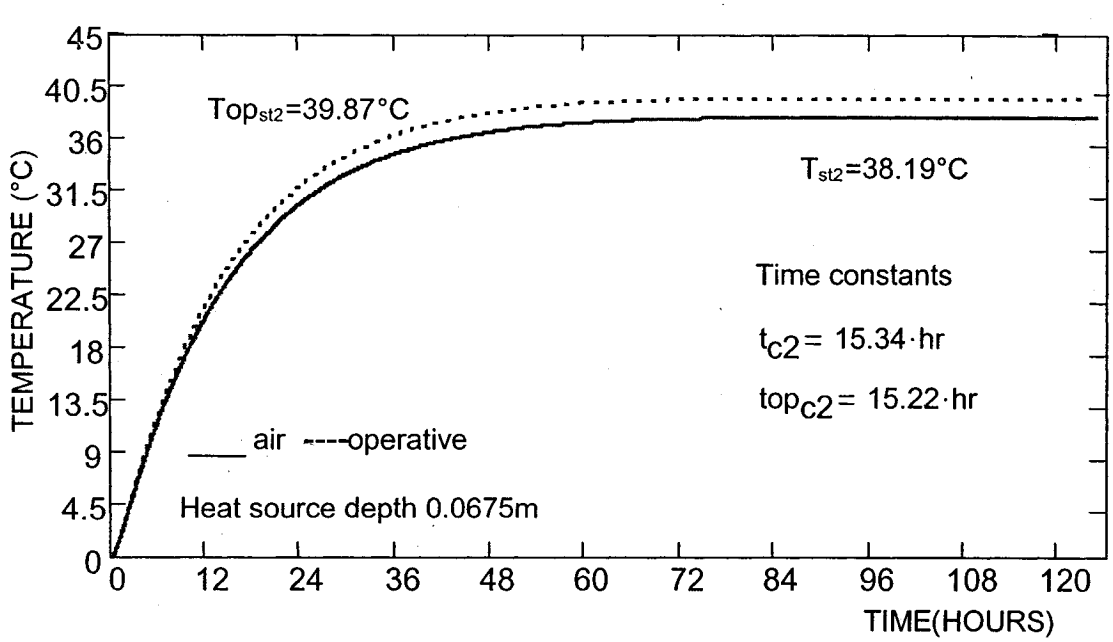

Figure 5.5: Operative and air temperature response to step input of radiative gain with heat source depth equal to 0.0675m

Floor concrete

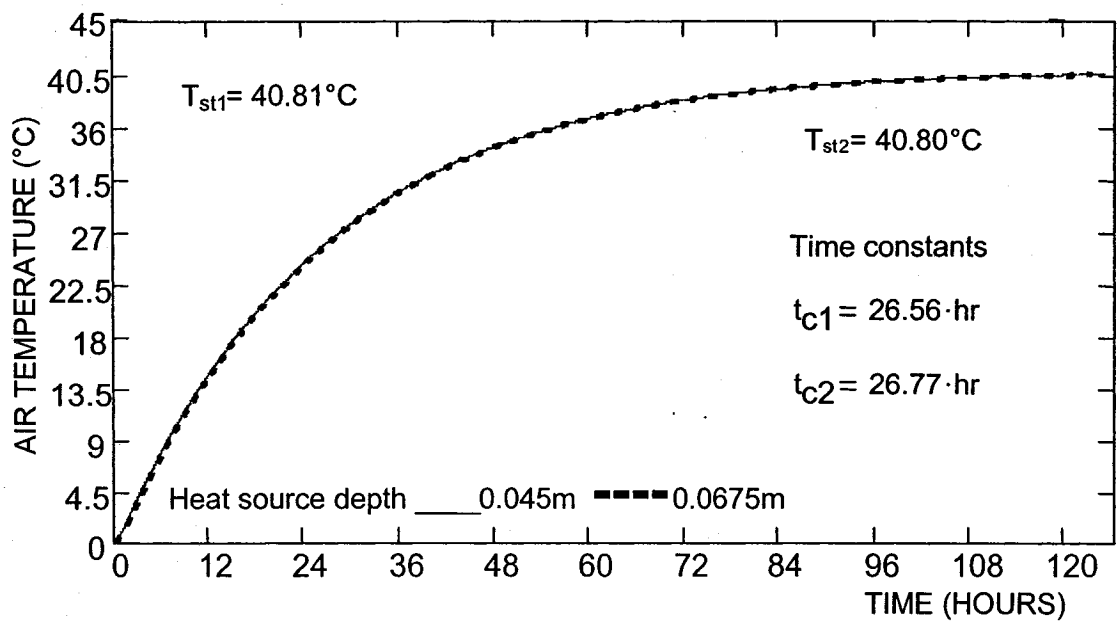

Figure 5.6: Air temperature response to step input of radiative gain with high bottom floor insulation (56 RSI)

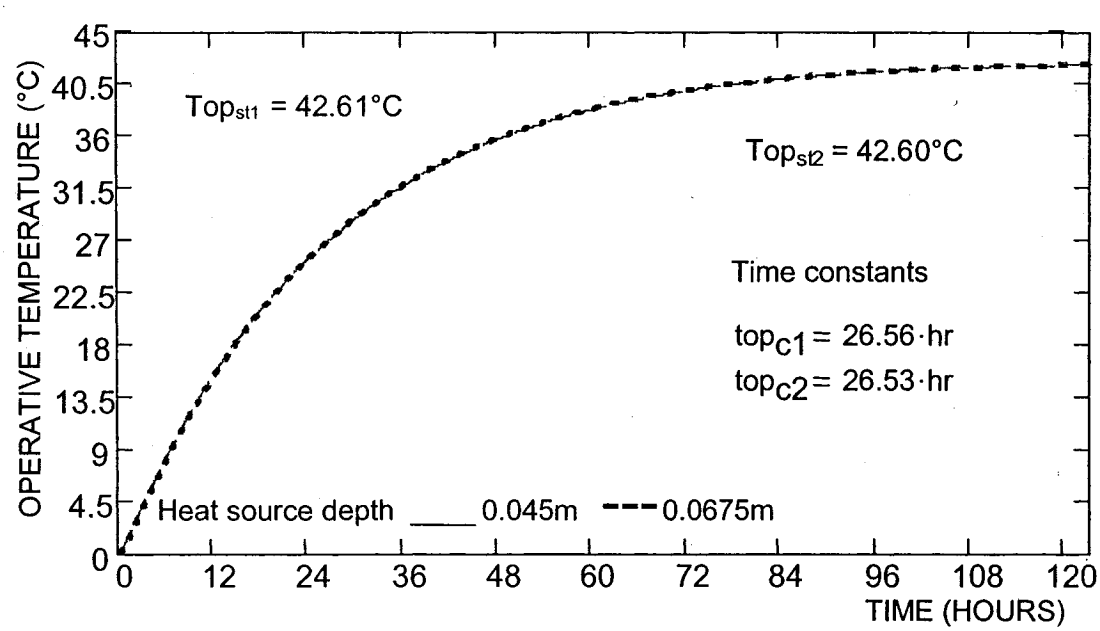

Figure 5.7: Operative temperature response to step input of radiative gain with high bottom floor insulation (56 RSI)

Floor concrete with carpet cover

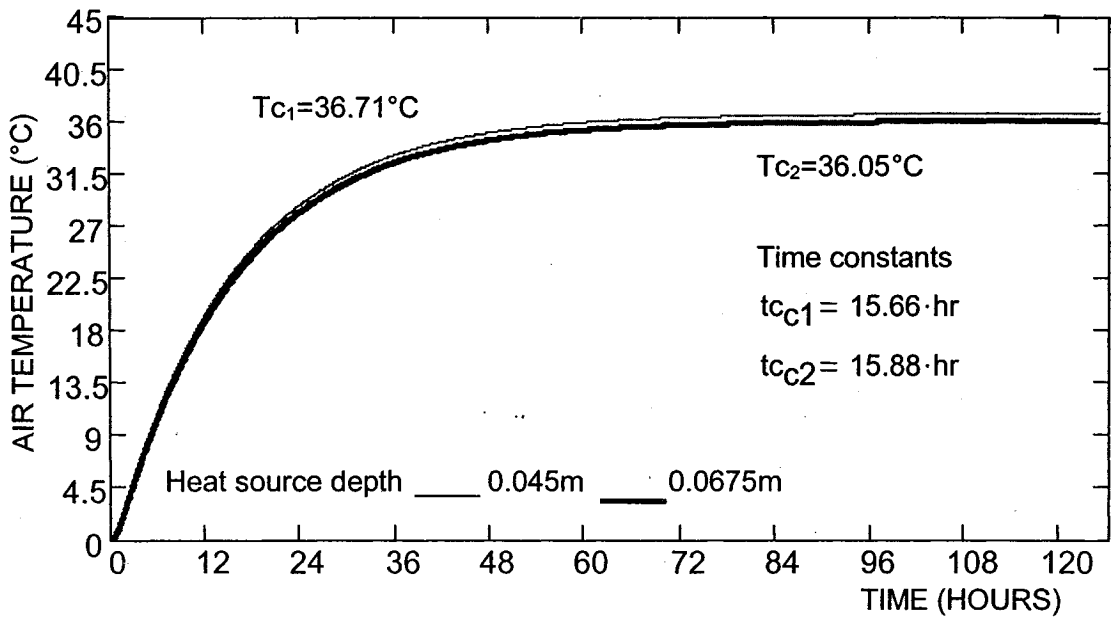

Figure 5.8: Air temperature response to step input of radiative gain

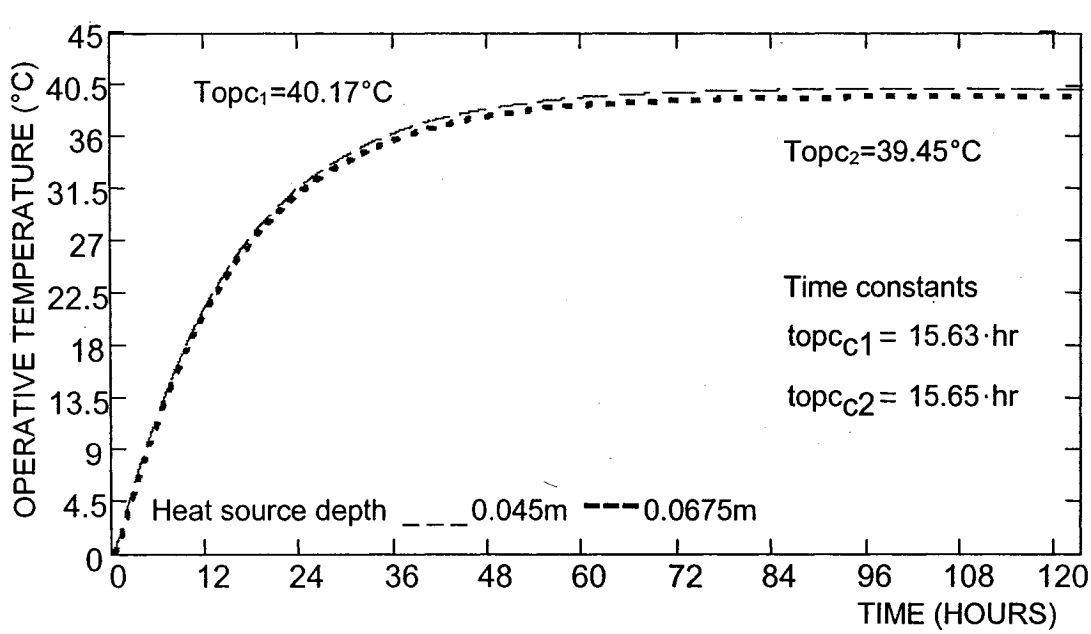

Figure 5.9: Operative temperature response to step input of radiative gain

Floor concrete with carpet cover

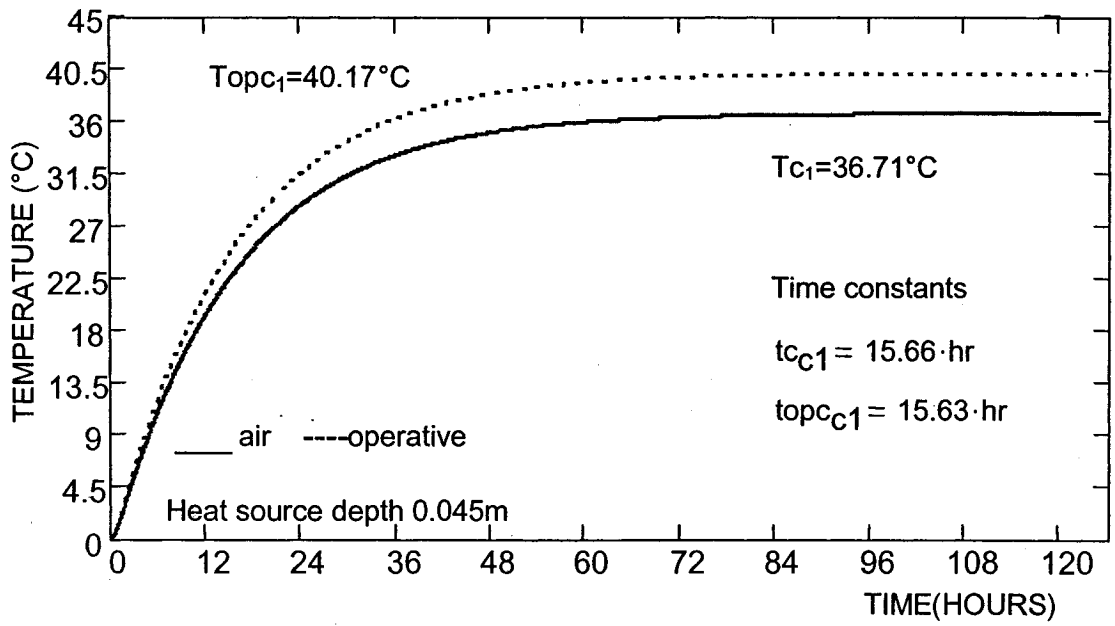

Figure 5.10: Operative and air temperature response to step input of radiative gain with heat source depth equal to 0.045m

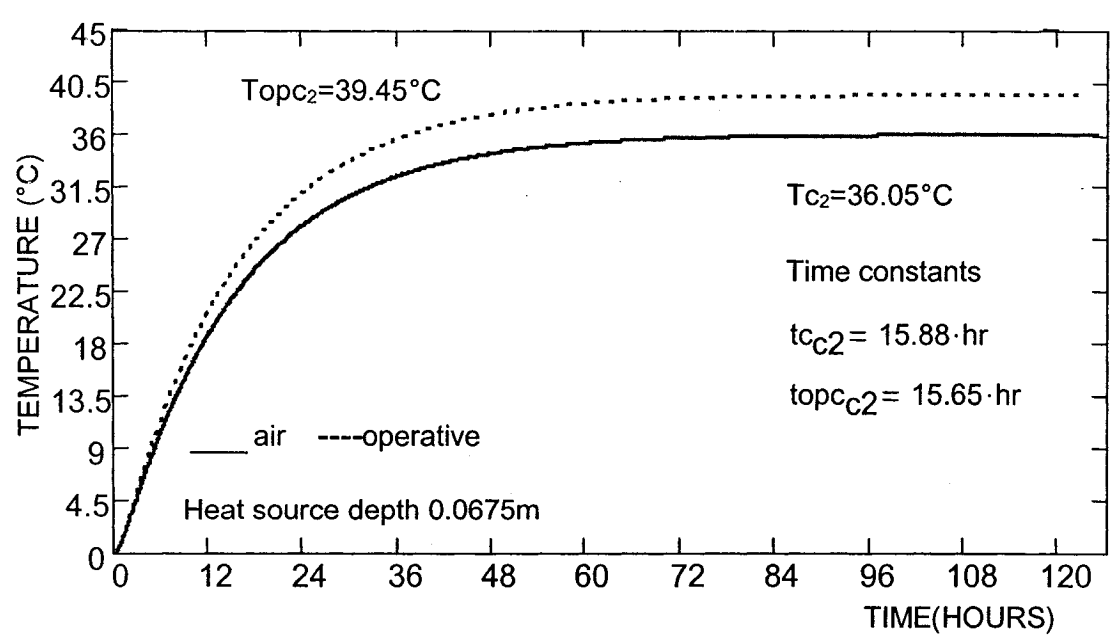

Figure 5.11: Operative and air temperature response to step input of radiative gain with heat source depth equal to 0.0675m

Concrete versus carpet

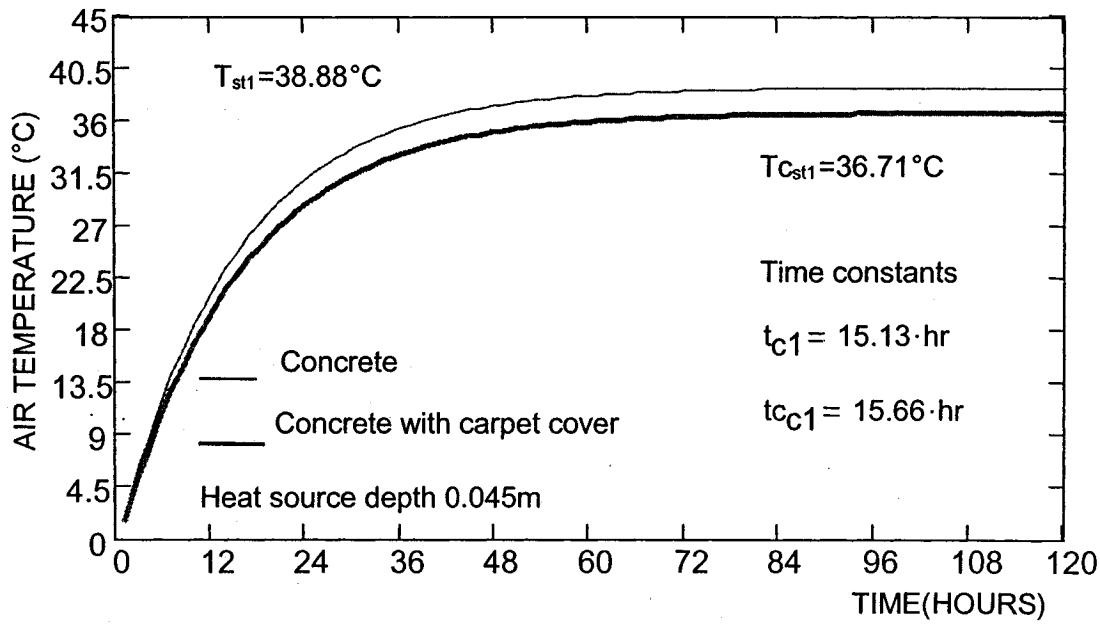

Figure 5.12: Air temperature response to step input of radiative gain

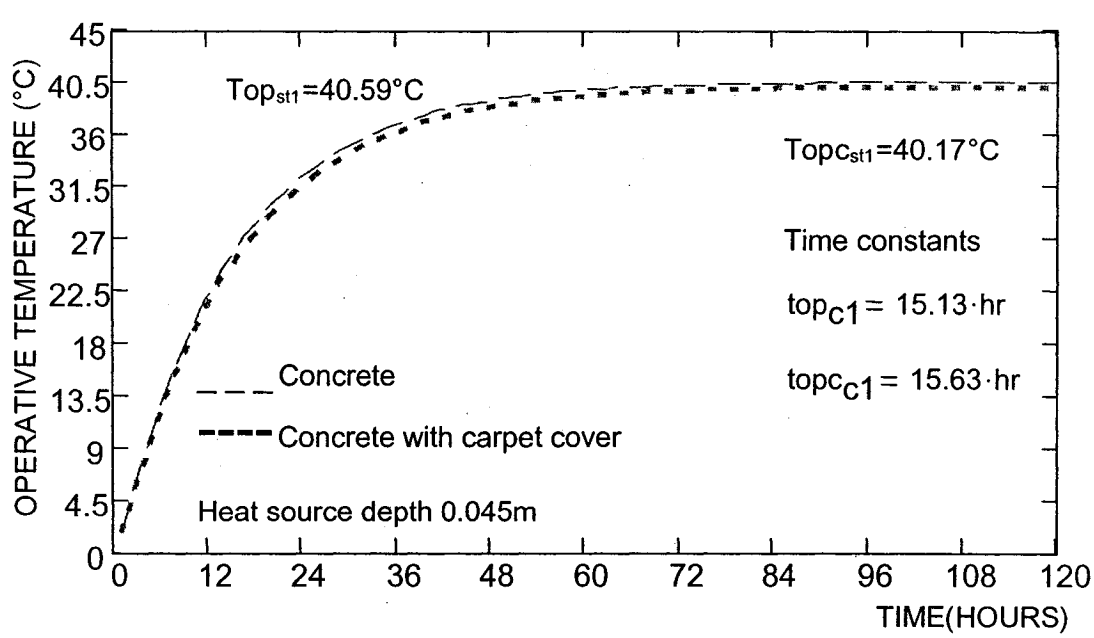

Figure 5.13: Operative temperature response to step input of radiative gain

The time delay transportation between heater and thermostat seconds is set to 30 seconds and for simplicity the SCR constant K_{scr} is combined with the proportional control constant K_p to give the modified gain K=2 watts/°C.

Figures 5.14 and 5.15 indicate that the deeper the internal heat source within the floor concrete slab, the higher the temperature overshoot and the longer the settling time which represents the time required for a step response to be within 0.95 and 1.05 degree around the set point. However, temperature overshoot variation due to installation depth is not very significant; but the settling time is more important. As expected, room temperature reaches stable state faster with lower internal heat source depth. Figures 5.16 and 5.17 reveal that operative temperature overshoot and its settling time are slightly higher than for air temperature.

For concrete carpeted floor, Figure 5.19 reveals that operative temperature follows the same pattern described above whereas Figure 5.18 indicates, on the opposite, that the deeper the internal heat source within the floor slab, the lower the air temperature overshoot and the longer the settling time. Figure 5.20 shows that, for a depth of 0.045m, overshoot and corresponding settling time higher are lower in the case of operative temperature than for air temperature. On the other hand, Figure 5.21 shows that, for a depth of 0.0675m, the overshoot for operative temperature is slightly higher than for air temperature but still with lower settling time. It can be noted that temperature overshoot is higher with carpeted floor due to the thermal resistance introduced by the carpet but the difference with concrete floor decreases with increasing internal heat source depth.

Floor concrete

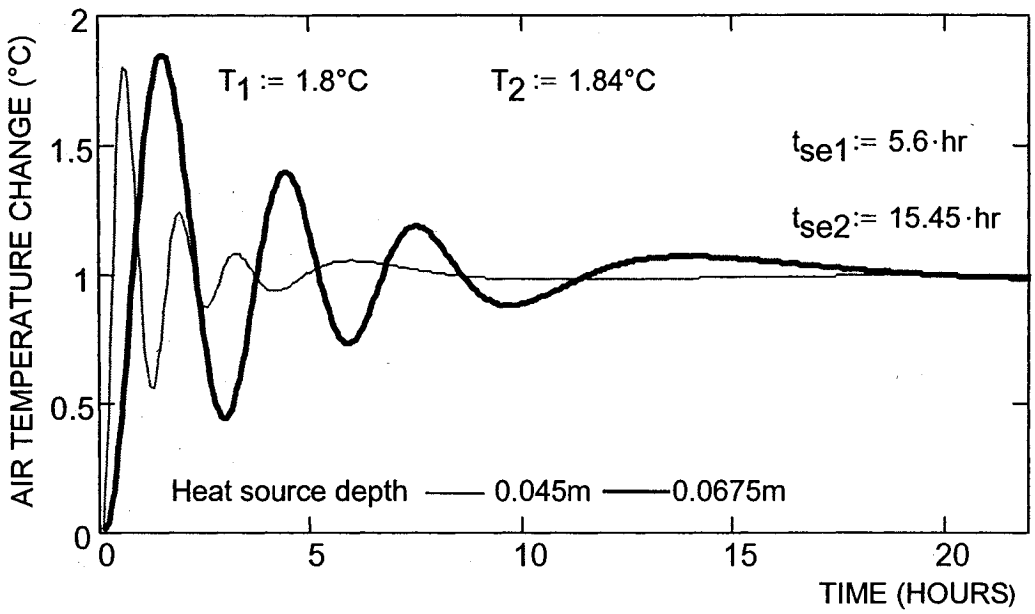

Figure 5.14: Air temperature response to unit step change rise in the set point with air temperature sensor and proportional integral control

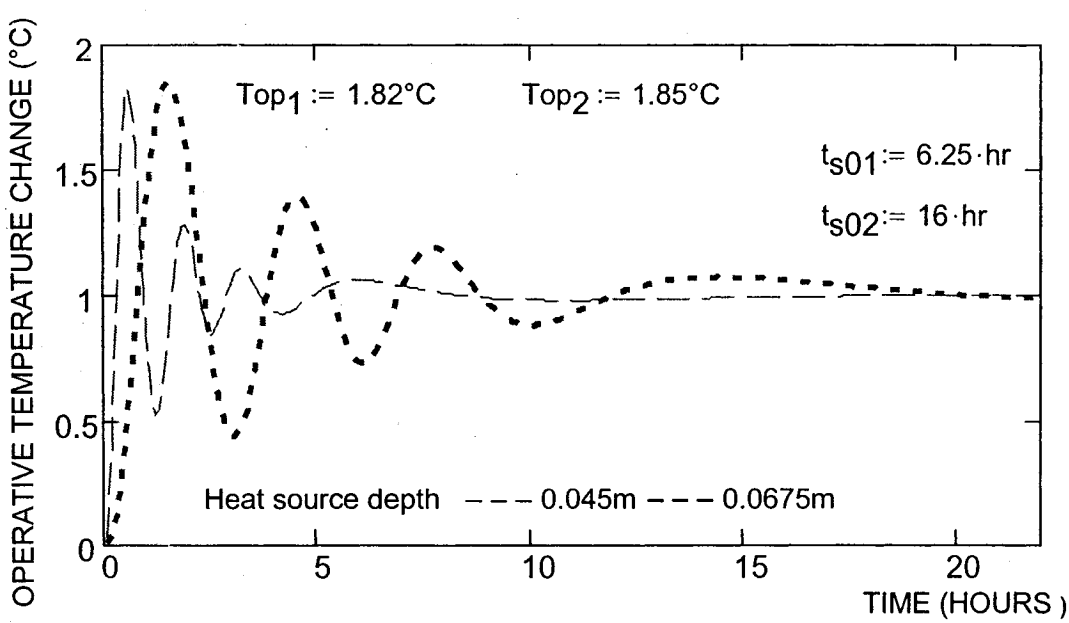

Figure 5.15: Operative temperature response to unit step change rise in the set point with air temperature sensor and proportional integral control

Floor concrete

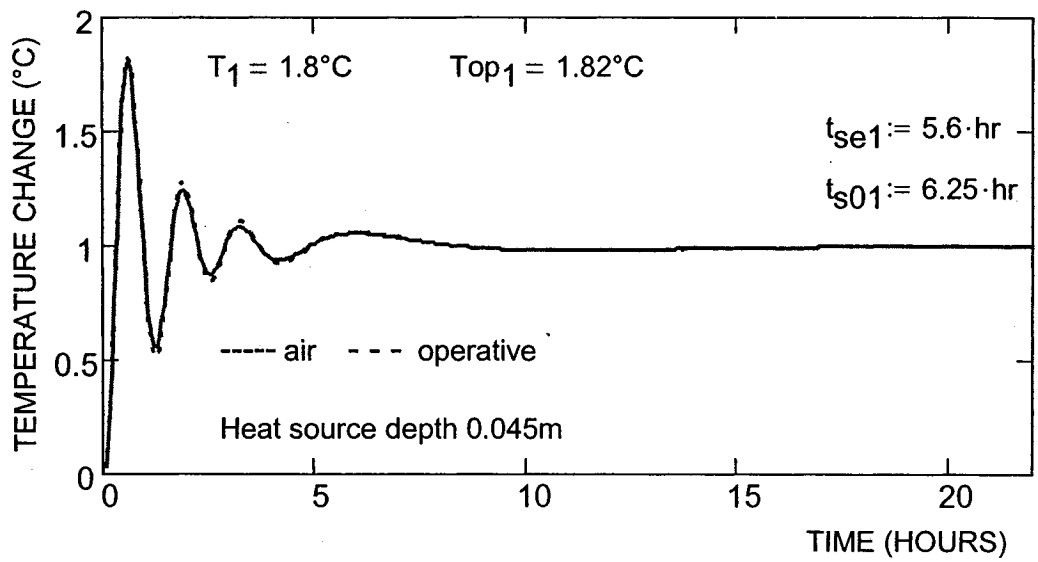

Figure 5.16: Operative and air temperature response to unit step change rise in the set point with P.I. control and heat source depth equal to 0.045m

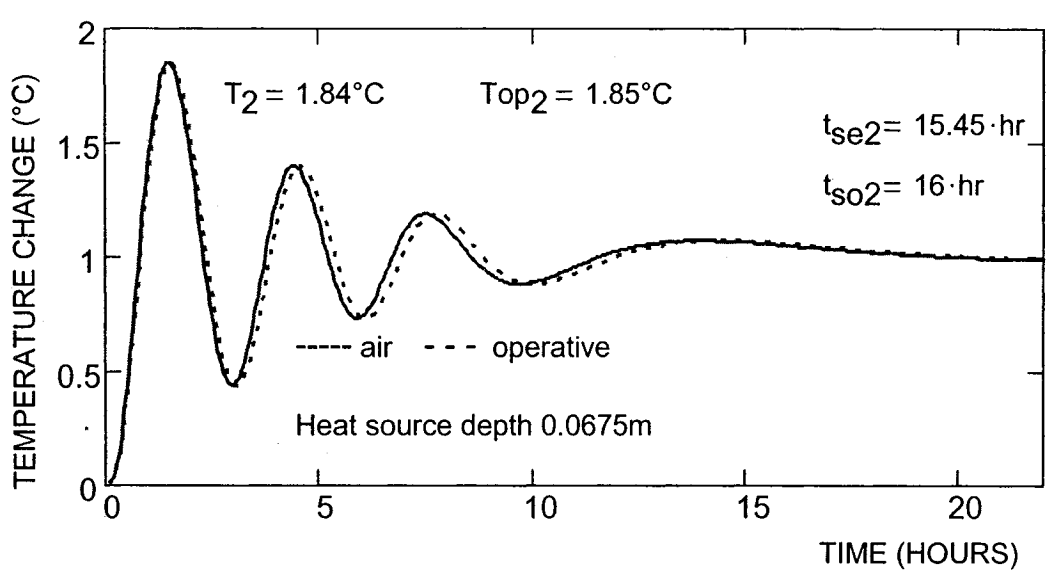

Figure 5.17: Operative and air temperature response to unit step change rise in the set point with P.I. control and a heat source depth equal to 0.0675m

Floor concrete with carpet cover

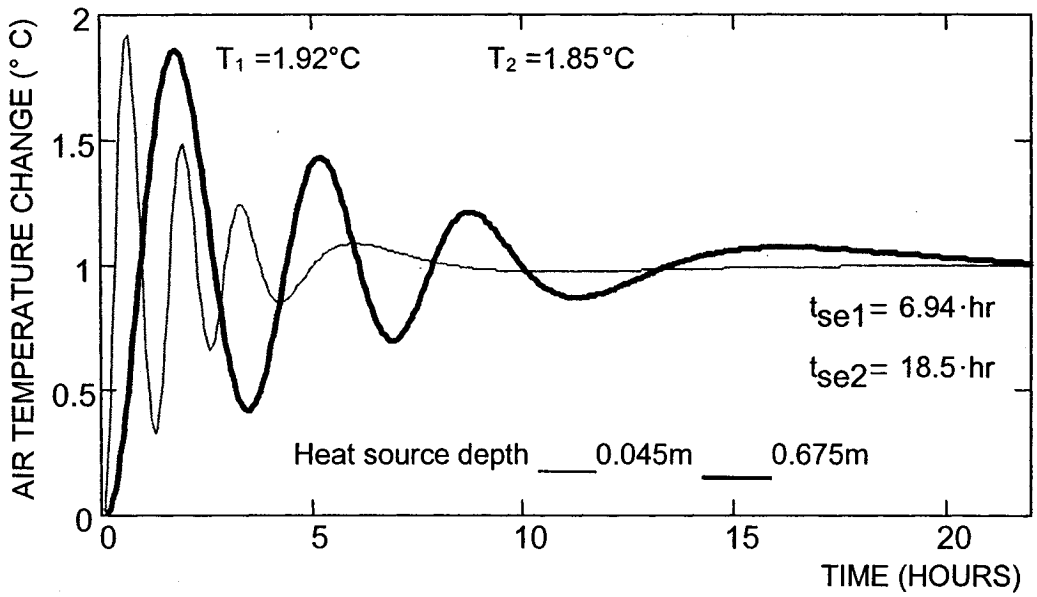

Figure 5.18: Air temperature response to unit step change rise in the set point with air temperature sensor and proportional integral control

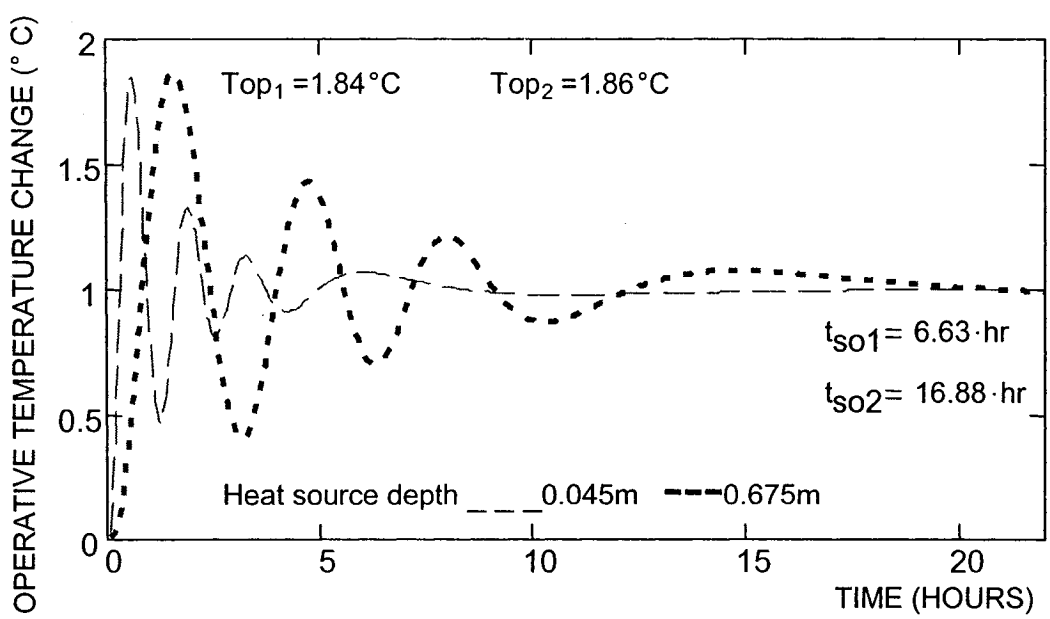

Figure 5.19: Operative temperature response to unit step change rise in the set point with air temperature sensor and proportional integral control

Floor concrete with carpet cover

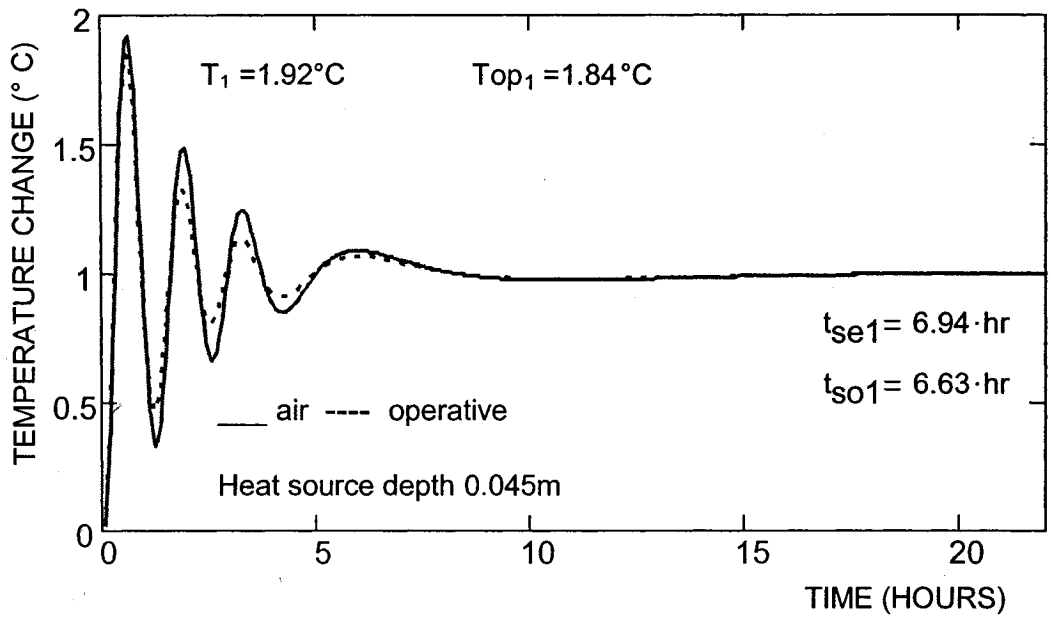

Figure 5.20: Operative and air temperature response to unit step change rise in the set point with P.I. control and heat source depth equal to 0.045m

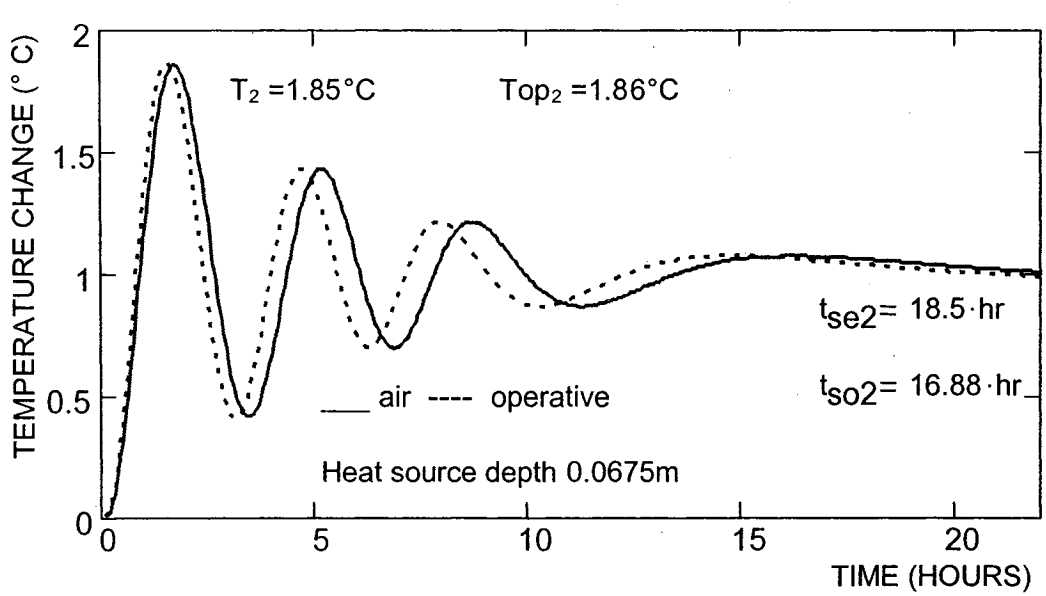

Figure 5.21: Operative and air temperature response to unit step change rise in the set point with P.I. control and a heat source depth of 0.0675m

Overall, this indicates that with air temperature sensor, the overshoot and the corresponding settling time of the room temperature response increase with increasing depth of heat source within the floor slab, thereby may cause a higher waste of energy. The interval difference between air temperature and operative temperature response decreases with increasing depth. Operative control mode is confirmed to be more appropriate with carpeted carpet.

5.8 Model validation

Validation of the frequency domain based model presented in this thesis is carried out by comparing room air transient response obtained with the numerical inversion method to that obtained with a one-dimensional explicit finite difference model developed by Athienitis (1997) and appropriately modified for the circumstances as described in Appendix 1. Simulations are carried out with different floor internal heat source depths for concrete and carpeted floor. The same conditions are used with the finite difference model which however assumes all the unheated surfaces as one surface and does not represent in detail infrared radiation between room interior surfaces. Care has been taken so as to maintain the same room parameters and heat transfer coefficients. Simulations conducted with the finite difference method with time step of 300 seconds (just below the minimum required) confirmed the steady state temperature results but with much higher time constant (20.5 hr). Adequate results were obtained with time step set to 56.25 seconds for both methods as shown by Figures 5.22a&b.

Figure 5.22a reveals that for floor internal heat source depth of 0.0225 m, results obtained with the explicit finite difference method are higher by 2.53°C and 3.76°C for the steady state temperature respectively for concrete and carpeted floor and 0.74 and 0.5 hour for the time constant in the same order.

Figure 5.22b follows the same pattern with a 0.0675 m floor internal heat source depth of 0.0675. The explicit method results simulation are higher by 2.27 degrees steady state temperature and 0.69 hour time constant for concrete, 3.63 degrees and 0.49 hr for carpeted floor.

The results are consistent and the discrepancies between the two approaches are probably due the difference in the level of heat loss coefficients modeling though it is known that finite difference generally provide a more accurate estimation of temperature and heat flows due to its capability to model both linear and non-linear system. Overall the results are confirmed and we conclude that:

1-the model used in the present case is adequate for thermal control analysis.

2-Discretization of a wall into two layers (capacitances) with low time step (100 seconds or less) is sufficient to conduct estimation of thermal analysis with the explicit finite difference method. The room Laplace transfer functions, derived in this research paper through the least square method required only one iteration at the most.

Validation of the transient results
Numerical Laplace transform inversion versus finite difference method

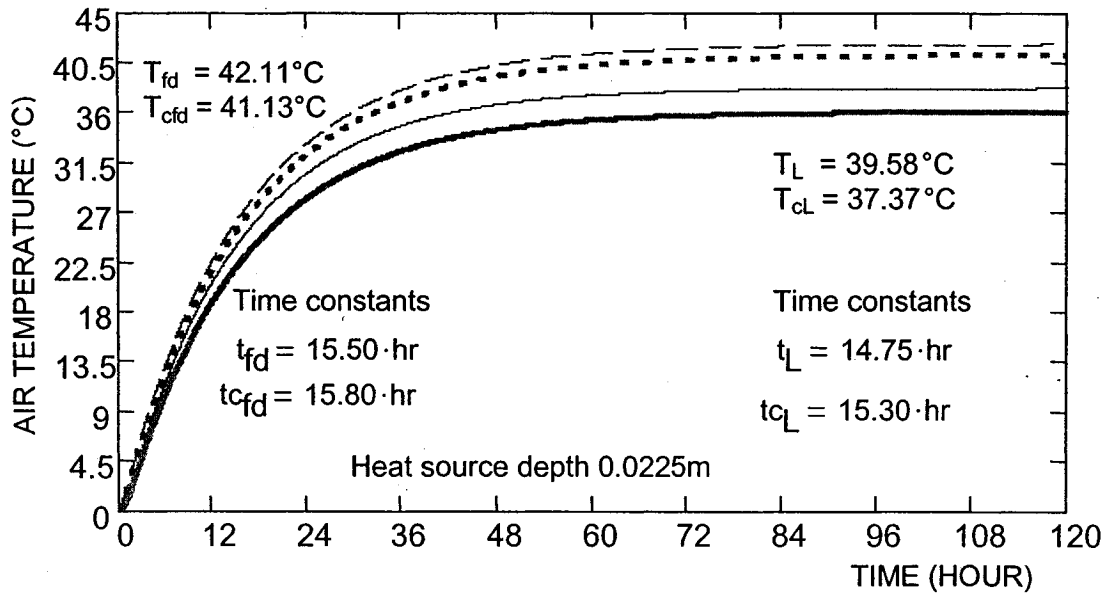

(a)

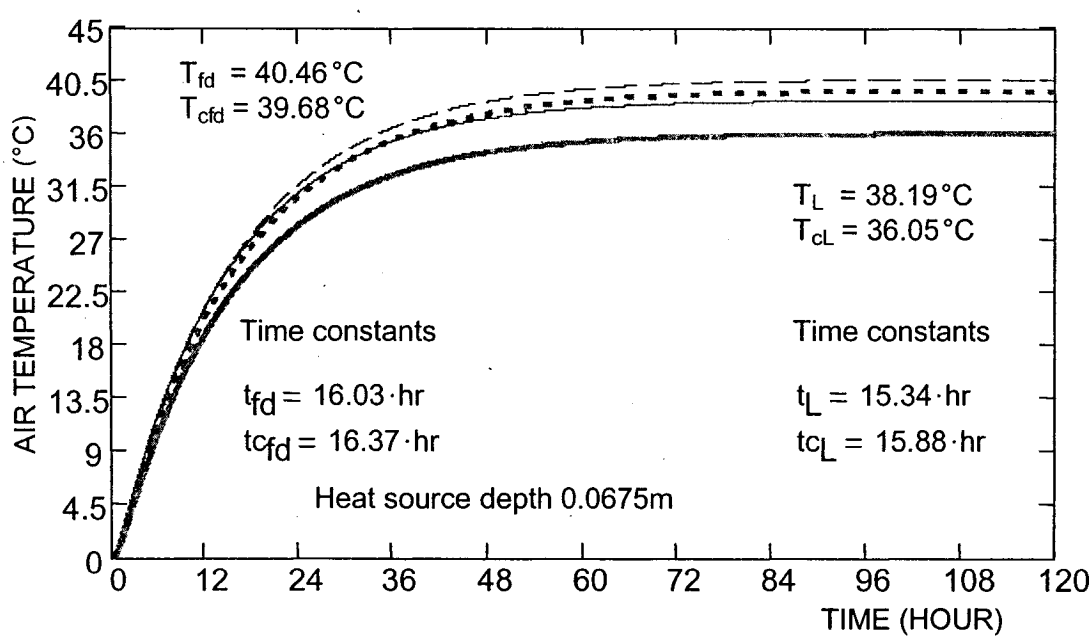

(b)

Numerical Inversion method —— Concrete (T_L) — — Carpet cover (Tc_L)
Finite difference method —— Concrete (T_{fd}) - - - Carpet cover (Tc_{fd})

Figures 5.22a&b: Air temperature response to step input of radiative gain

5.9 Feedforward-feedback control

The previous analysis and subsequent discussion showed that feedback control is insensitive to model approximation and is negatively affected by the presence of significant dead time resulting in high overshoot and sluggish response to disturbances. On the other hand, feedforward control takes care of this dead time by taking action before the effect of disturbance is felt by the system. Combination of anticipatory and feedback effect constitutes one of the approaches to counter the problems caused by the thermal lag effect and time delay associated with heat storage directly when dealing with radiant heating design .

Feedback control loops can never achieve perfect control of the air room temperature at the desired set point value in the presence of load or set point change for the simple raison that a feedback controller reacts only after it has detected a deviation in the value of the measured room air (or operative) temperature from the desired set point.

Unlike the feedback systems, a feedforward control configuration measures the disturbance (load due to outside weather conditions) directly and takes control action to eliminate its impact on the inside room air temperature. Feedforward control would seem to be a more appropriate control system for floor radiant heating systems.

The control objective is to keep the room air temperature at the desired value (set point) despite any change in outside weather conditions. It measures the outside temperature (or eventually the solar radiation), anticipate its effect on

the room air temperature then adjust appropriately the output of the manipulated variable (heating system) to eliminate the impact of the disturbance (change in outside weather conditions) on the controlled variable (room air or operative temperature). Basically unlike conventional system, control action starts immediately after a change in outside conditions has been detected.

An essential characteristic is that the design of a feedforward controller arises directly from the model of a process, the better a model represents the behaviour of a process, and the better the resulting feedforward controller will be. Feedforward control has the potential for perfect control but also suffers from several inherent weaknesses such as:

-Identification requirement of all possible disturbances and their direct measurement, which is not always possible

-Any change in the parameters of the building thermal characteristics (i.e. higher infiltration rate) cannot be compensated by a feedforward controller because their impact cannot be detected.

A combined feedforward-feedback control system will retain the superior performance of the first and the insensitivity of the second to uncertainties and inaccuracies. The deviation caused by the various weakness of the feedforward control will be corrected by the feedback controller. This is possible because feedback control loop directly monitors the room air temperature. The block diagram (Figure 5.23) shows the configuration of a combined feedforward-feedback control system (the final control element G_f and the controlled device G_f shown in Figure 5.1 are combined as G_m). The overall system Laplace transfer

function describing the contribution of each input is as follows:

$$T_{ai}(s) = T_{sp}\frac{Z_{09}\,G_m\,(G_{c1}+G_{c2}\,G_{sp})}{1+G_{c1}\,G_m Z_{09}\,G_{s1}} + \sum_j \left(Q(j)\frac{(Z_{0,j} - Z_{09}\,G_m\,G_{c2}\,G_{s2})}{1+G_{c1}\,G_m\,Z_{09}\,G_{s1}} \right) \quad (5.13)$$

Where j=0,1...8 surface number in the present case

Where T_{sp} is the set point and G is the transfer functions indicated in the block diagram. All variables are a function of s. For operative temperature analysis, T_{ai}, Z_{09} and $Z_{0,j}$ are replaced respectively by their operative counterpart Top, X_{09} and $X_{0,J}$.

Examination of this transfer function reveals that the stability of the closed loop response is determined by the root of the characteristic equation which depends on the transfer functions of the feedback loop only. Therefore the stability characteristics of a feedback system will not change with the addition of a feedforward loop and remains as identified previously:

$$G_{OL}(s) = 1 + Z_{09}\,G_{c1}\,G_m\,G_{s1}$$

Consequently anything affecting the stability of the feedback loop, such as delays in the sensing elements would have the same impact on a feedback-feedforward loop. Thus the low values of the proportional gain and high values of the integral time would have to be maintained. The transfer functions of the feedforward loop are as follows:

Transfer function of the feedforward controller

$$G_{c2} = \frac{\sum_j Z_{0,j}}{Z_{09}\,G_m\,G_{s2}} \quad (5.14)$$

Transfer function of the set point element

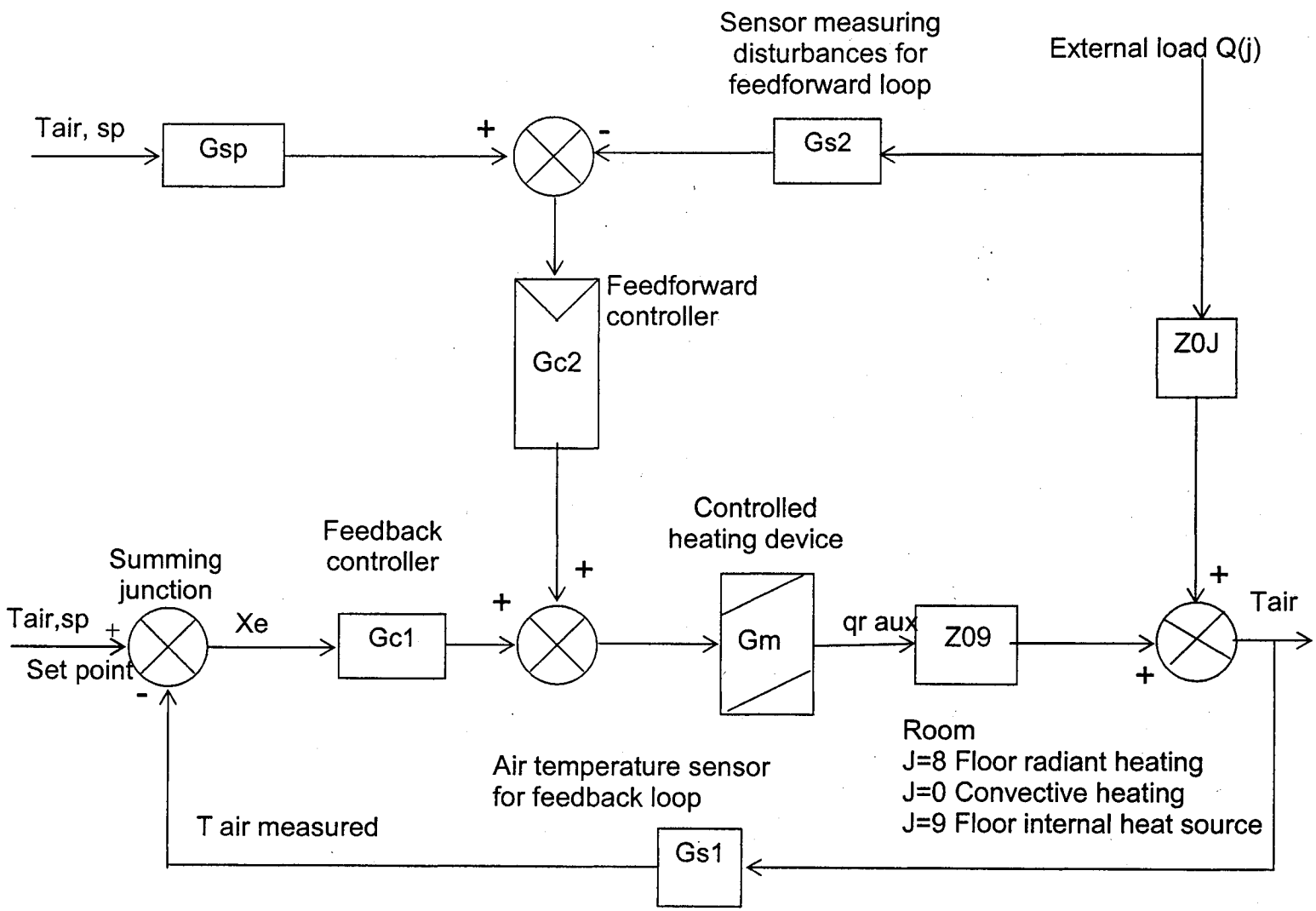

Figure 5.23 Block diagram for feedforward-feedback control

$$G_{sp} = \frac{G_{s2}}{\sum_j Z_{0,j}} \tag{5.15}$$

If the design equation Z_{09}, $Z_{0,J}$, G_m and G_{s2} are known exactly (which is not practically possible), the feedforward loop can compensate completely for disturbances in the outside weather or set point changes and the feedback controller remains idle since T_{sp}-T_{air}=0

If any of Z_{09}, $Z_{0,J}$, G_m and G_{s2} are known only approximately, then:

$$Z_{0,j} - Z_{09}\, G_{c2}\, G_m\, G_{s2} \neq 0 \tag{5.16}$$

and/or

$$Z_{09}\, G_{c2}\, G_{sp}\, G_{s2} \neq 1 \tag{5.17}$$

In such case the feedforward loop does not provide perfect control Tsp-T_{air} # 0, then feedback loop is activated and offers the necessary compensation.

The same method based on the numerical Laplace transform inversion in combination with the Ziegler and Nichols method is used to perform the room temperature response and stability analysis to step input and load change.

5.91 Discussion

Simulations are carried out with the assumption that the feedforward transfer functions are know exactly and equal to equations (5.14) and (5.15). This means that the feedforward loop compensates completely for disturbances due outside load or set point change. The design parameters used previously remains unchanged and because of the assumptions made, there is no need to know the time constant for outside air temperature sensor.

Examination of the Figures 5.24 to 5.27 shows that the overshoot and the settling time are considerably reduced with feedforward-feedback control compared to feedback control. The overshoot is mainly due to the temperature sensor time and associated transport delay in the detection and the transmission of the deviation of the controlled temperature. Rapid response temperature sensor will reduce this overshoot. We observe that room temperature response overshoot and time constant decrease with floor internal heat source depth suggesting that this control mode is appropriate for floor radiant heating. We note that with air sensor, the operative temperature overshoot is higher than air temperature whereas the time constants are the same. This confirms that feedforward-feedback control system, combining stability and improved system performance, can be an effective approach to comfort problems caused by the combined effect of various time delays during building operation. This underlines the advantages of a unified approach taking into account the interaction between the building shell, the HVAC system and the control system.

Floor concrete

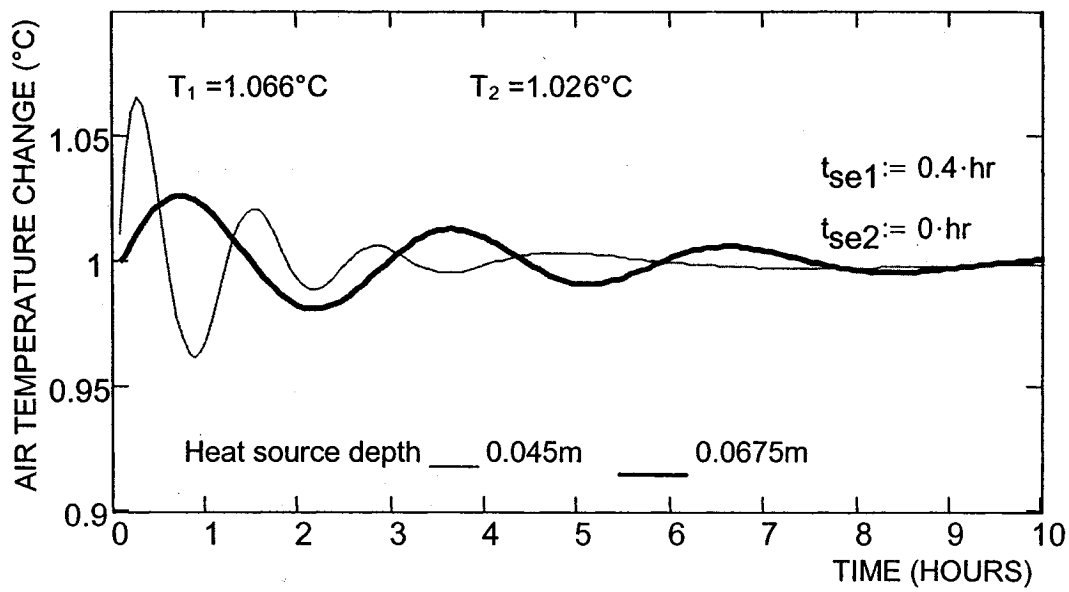

Figure 5.24: Air temperature response to unit step change rise in the set point with feedforward-feedback control

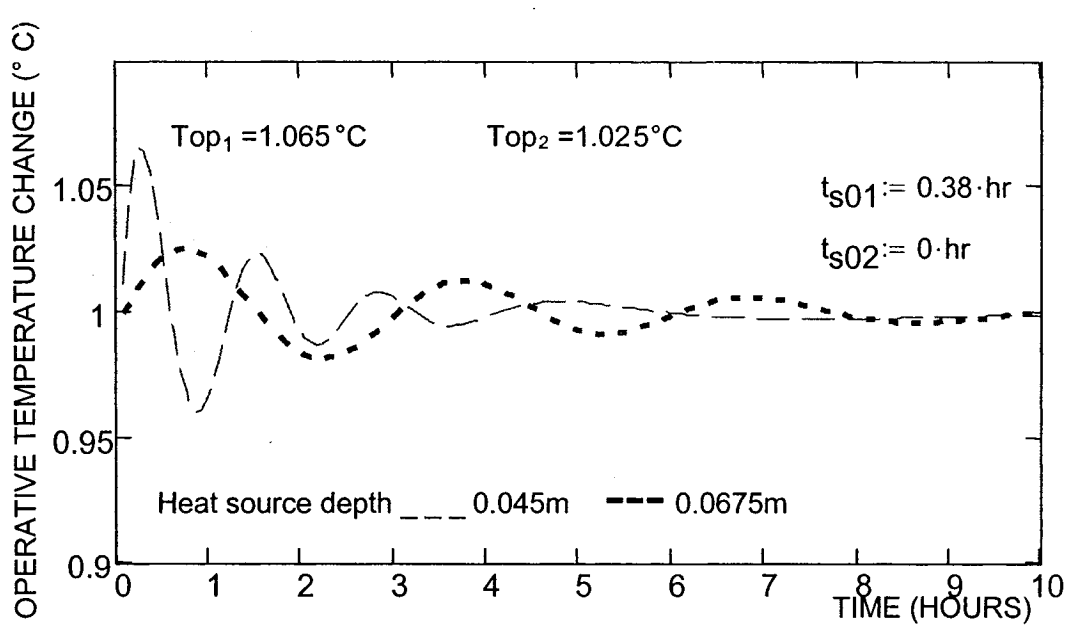

Figure 5.25: Operative temperature response to unit step change rise in the set point with and feedforward-feedback control

Feedforward-feedback control versus Feedback control
Floor concrete

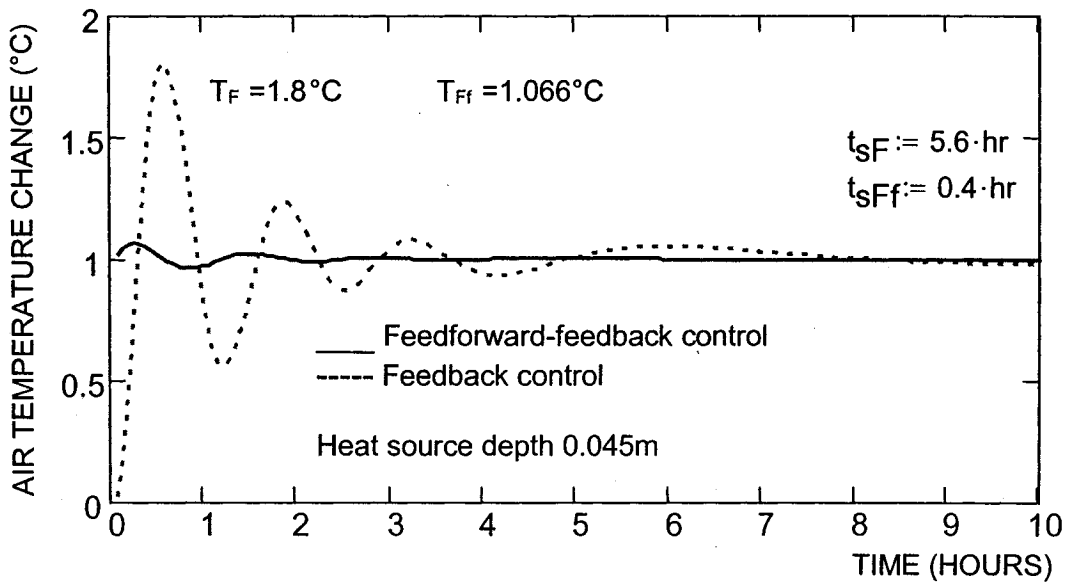

Figure 5.26: Air temperature response to unit step change rise in the set point

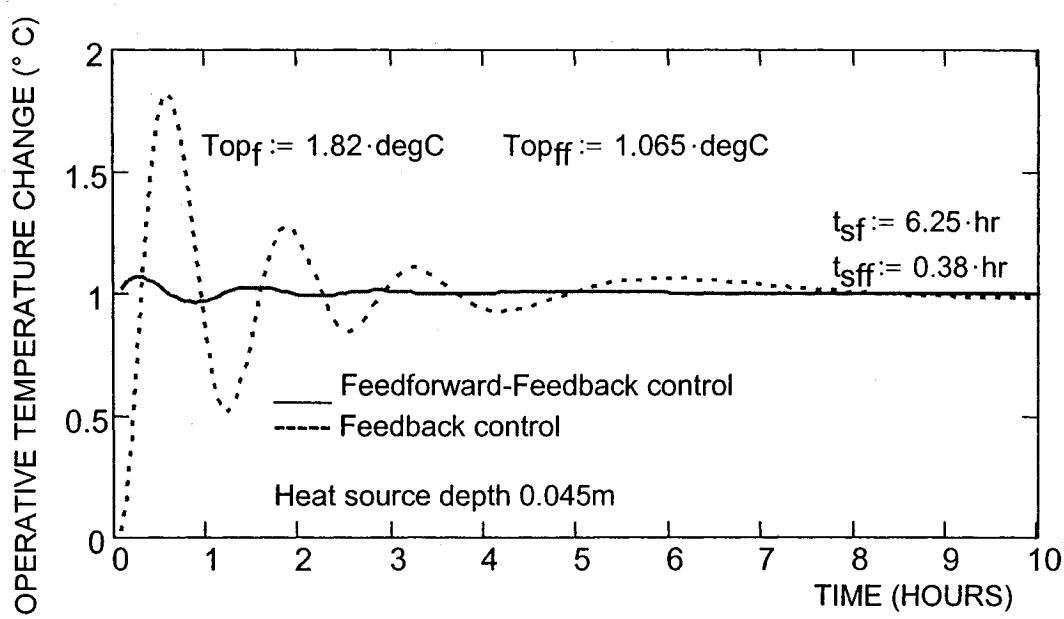

Figure 5.27: Operative temperature response to unit step change rise in the set point

Impedance transfer function

Heat source depth=0.045m

$$Z_1(s)=\frac{4.63\times10^{-3}+5.191\,s-2.324\times10^{-6}\,s^2-1.394\times10^{4}\,s^3+6.806\times10^{5}\,s^4-1.426\times10^{7}\,s^5}{1+5.584\times10^{4}\,s+1.351\times10^{8}\,s^2+4.282\times10^{10}\,s^3-4.211\times10^{12}\,s^4+1.347\times10^{14}\,s^5}$$

Heat source depth=0.0675m

$$Z_2(s)=\frac{4.547\times10^{-3}+5.224\,s-3.316\times10^{-4}\,s^2-6.827\times10^{4}\,s^3+7.093\times10^{6}\,s^4-3.831\times10^{8}\,s^5}{1+5.664\times10^{4}\,s+1.798\times10^{8}\,s^2+1.486\times10^{11}\,s^3+3.354\times10^{13}\,s^4+2.47\times10^{15}\,s^5}$$

Operative transfer function

Heat source depth=0.045m

$$X_1(s)=\frac{4.833\times10^{-3}+5.135\,s+55.288\times10^{-9}\,s^2-15.735\times10^{3}\,s^3+880.366\times10^{3}\,s^4-27.945\times10^{6}\,s^5}{1+55.825\times10^{3}\,s+136.029\times10^{6}\,s^2+43.207\times10^{9}\,s^3+4.23\times10^{12}\,s^4+126.468\times10^{12}\,s^5}$$

Heat source depth=0.0675m

$$X_2(s)=\frac{4.747\times10^{-3}+8.847\,s-628.812\times10^{-3}\,s^2-114.814\times10^{3}\,s^3+11.087\times10^{6}\,s^4-657.877\times10^{6}\,s^5}{1+56.866\times10^{3}\,s+227.448\times10^{6}\,s^2+237.734\times10^{9}\,s^3+55.542\times10^{12}\,s^4+4.339\times10^{15}\,s^5}$$

TABLE 1: Floor concrete

Impedance transfer function

Heat source depth=0.045m

$$Zc_1(s)=\frac{4.372\times10^{-3}+3.88\,s+3.27\times10^{-3}\,s^2+2.58\times10^{4}\,s^3-3.484\times10^{6}\,s^4+2.139\times10^{8}\,s^5}{1+5.755\times10^{4}\,s+1.463\times10^{8}\,s^2+4.786\times10^{10}\,s^3+5.619\times10^{12}\,s^4+4.835\times10^{14}\,s^5}$$

Heat source depth=0.0675m

$$Zc_2(s)=\frac{4.293\times10^{-3}+5.869\,s-3.029\times10^{-3}\,s^2-8.063\times10^{4}\,s^3+8.594\times10^{6}\,s^4+5.153\times10^{8}\,s^5}{1+5.88\times10^{4}\,s+2.183\times10^{8}\,s^2+2.257\times10^{11}\,s^3+5.478\times10^{13}\,s^4+1.075\times10^{15}\,s^5}$$

Operative transfer function

Heat source depth=0.045m

$$Xc_1(s)=\frac{4.783\times10^{-3}+4.973\,s-2.136\times10^{-7}\,s^2-1.458\times10^{4}\,s^3+7.849\times10^{5}\,s^4-2.299\times10^{7}\,s^5}{1+5.755\times10^{4}\,s+1.469\times10^{8}\,s^2+4.708\times10^{10}\,s^3+4.643\times10^{12}\,s^4+1.44\times10^{14}\,s^5}$$

Heat source depth=0.0675m

$$Xc_2(s)=\frac{4.697\times10^{-3}+9.059\,s+0.168\,s^2-1.18\times10^{5}\,s^3+1.141\times10^{7}\,s^4-6.794\times10^{8}\,s^5}{1+5.86\times10^{4}\,s+2.466\times10^{8}\,s^2+2.7\times10^{11}\,s^3+6.383\times10^{13}\,s^4+5.021\times10^{15}\,s^5}$$

TABLE 2: Floor concrete with carpet cover

CHAPTER 6

TEMPERATURE AND HEATING LOAD CALCULATION

6-1 Introduction

Heating systems are generally separated into two main categories; convective heating system that heat primarily the room air and the radiant or panel heating system in which the source is integrated in the building envelop. Further to its advantages compared to convective heating, a floor heating system is potentially highly compatible in operation with a direct gain passive solar system, which would also store solar gains within the floor mass. The solar gains are absorbed at the top surface of the floor slab while the auxiliary heat is applied at the bottom or within the floor slab with different lag effect in either case. Radiant heating system operates on a mode similar to direct gain relying on a high surface temperature (up to 29°C for floor heating) and a low air temperature. However, design and control of radiant heating system are still based on room air temperature overlooking the effect of the mean radiant temperature on comfort conditions even tough several studies suggested that it would be more rational to control the operative temperature (Athienitis, 1998).

Design of floor heating system requires several important decisions such as the maximum heating device output, type and thickness of the thermal mass integrated in the floor heating system and appropriate control strategies for the system to maintain desired thermal conditions in the heated space and prevent floor surface from exceeding 29°C as required by current standard (ASHRAE,

1992). Room overheating and floor surface exceeding comfort limits are the main problem with the performance of a passive solar building with floor heating system. This occurs particularly when a significant amount of solar radiation is incident on the floor while its thermal storage mass is already warm from continuous auxiliary heating input during the night and in the early morning. Several alternatives have been proposed to address this problem such as temperature set back at night involving anticipatory or predictive control or increasing thermal storage (Athienitis, 1997). Calculation of peak heating and cooling loads should take into account building thermal storage capacity and dynamic variation of solar radiation and outdoor conditions in order to avoid over sizing of auxiliary heating or cooling systems. Room temperatures and heating load calculations can be performed by means of frequency domain technique in conjunction with Fourier series.

6.2 Modeling of a Temperature controlled heat source (TCHS)

In the theory of building thermal network, heat sources such as auxiliary heating sources, can be equivalently transformed into dependent heat flow sources controlled by temperature variables and are designated as temperature controlled heat source (TCHS). Temperature controlled heat source is analogue to electrical voltage controlled current source and can thus be directly included in both the nodal formulation (Vlach and Singhal 1983). Consequently, the auxiliary radiant heating system may be modeled as a dependent heat source with heat flow q_{aux} proportional to the difference between the desired temperature T_{sp} and

the room air temperature T_a as follows:

$$q_{aux} = Kp(T_{sp} - T_a) \quad \text{or} \tag{6.1}$$

$$q_{aux} = Q_1 - Kp\,T_a \quad \text{with} \quad Q_1 = Kp\,T_{sp}$$

Where kp is the source constant (W/K). In the frequency domain, the above quantities are phazors. Thus, the auxiliary power, as a function of time and under periodic conditions is given by

$$q_{aux}(t) = \sum_n q_{aux,n}(j\omega_n)\exp(j\omega_n t) \quad \text{where} \tag{6.2}$$

$$q_{aux}(j\omega_n) = kp(T_{sp,n} - T_{a,n}) \tag{6.2a}$$

$T_{a,n}$ and $T_{sp,n}$ are the phazors for the two temperatures for frequency equal to ω_n. The actual air temperature T_a is determined before applying the above equation to determine q_{aux}. Application of this method as part of the detailed model Figure 3.1 with floor radiant heating acting on node air 0 through floor surface node 8 is developed as follows:

Considering the two nodes network shown in Figure 6.1 representing the floor heating system under consideration, node 0 and 8 correspond respectively to room air and floor surface temperature and the independent source Q_1 together with the proportional control heat source kpT_a represent the THCS source as described by equation (6.1). Applying a heat balance at the two nodes yields:

Node 0 $$Y_0\,Ts_0 + U_{8,0}(Ts_0 - Ts_8) - Q_2 = 0 \tag{6.3}$$

Node 8 $$Y_8\,Ts_8 + U_{0,8}(Ts_8 - Ts_0) - Q_1 + Kp\,Ts_0 = 0 \tag{6.3a}$$

Expressed in nodal form:

$$\begin{bmatrix} Y_0 + U_{8,0} & -U_{8,0} \\ -U_{0,8} + Kp & Y_8 + U_{0,8} \end{bmatrix} \begin{bmatrix} Ts_0 \\ Ts_8 \end{bmatrix} = \begin{bmatrix} Q_2 \\ Q_1 \end{bmatrix} \tag{6.3b}$$

Q_2 and Y_0 represent respectively the other heat sources and admittances/conductances related to the air node 0 and $U_{0,8}$ is the convective conductance between floor surface node 8 and air node 0. Thus with regard to the general matrix equation (4.12) developed in chapter 4, the nodal admittance matrix entry $Y(0,8) = -U_{0,8}$ before the source is connected is modified as follows:

$$Y(0,8) = Y(0,8) + Kp = -U_{0,8} + Kp \tag{6.4}$$

The heat source vector has an extra source $Q_1 = Kp\,T_{sp}$ added to its entry:

$$Q(8) = Q(8) + Kp\,T_{sp} = Qeq + Kp\,T_{sp} + Sn_8 \tag{6.5}$$

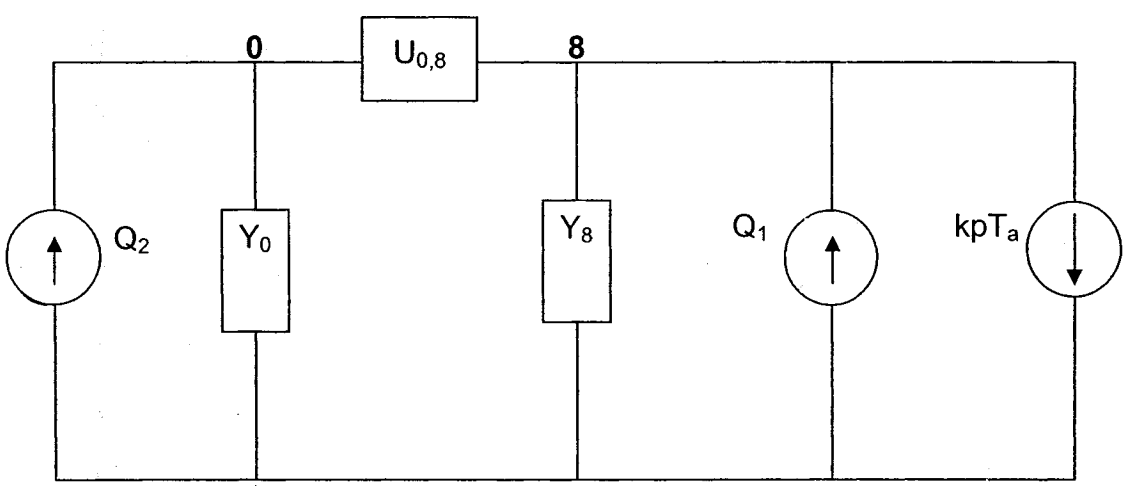

Figure 6.1: Temperature controlled heat source through floor radiant heating acting on air node 0 through floor surface node 8.

The above operations are performed for all harmonics except for kp which is not a function of frequency. As can be noted, the matrix is not symmetric because the THCS depends on two distinct nodes. It would have been otherwise if the TCHS was directly acting on the node air such as with convective heating. In

such case, the admittance matrix would still be symmetric because the TCHS does not depend on other node temperature apart from that of node air.

6.3 Choice of Kp for TCHS

The source constant Kp may be related to the capacity of heating or it may simply be treated as a numerical quantity which can be suitably chosen for analysis and design, depending on the objective of the analysis. Different analysis may be performed with regard to chosen values of the TCHS constant kp. kp equal to zero can be used to study the building passive behavior while increasing it to a sufficiently high value will simulate a specified temperature source. Because the present work doe not go into the second aspect, it will be just related to the heating capacity $Yz_0\ \Delta T$ and chosen accordingly to the desired room temperature. ΔT being the temperature differential between ambient and design room air (or operative) temperature and Yz_0 the room overall U value.

6.4 Load and temperature calculation

Temperature and heating load calculations are performed by means of discrete Fourier series using the same building transfer functions employed in frequency response and thermal control studies (chapters 4 and 5). The transfer functions are calculated at discrete frequency and a discrete Fourier transform (DFT) of the weather data and other sources or specified temperature such as that of the basement is performed. The frequency domain response is then evaluated through complex algebra and the time domain load and room temperatures

variation are subsequently obtained through an Inverse discrete Fourier transform (IDFT). Adequate representation of the different inputs such as absorbed solar radiation, internal heat gains or ambient temperature can usually be obtained with five to nine harmonics for design day analysis. This approach (Athienitis, 1993) based on the superposition principles allows effects of various inputs to be studied conjointly or separately. Passive solar analysis for example can be carried out by setting the auxiliary heating source to zero

The THCS is introduced in the matrix equation (4.12) and resulting surface and air temperature are obtained through an inverse matrix $T_s=[Y]^{-1}\cdot[Q]$.

$$\begin{pmatrix} Ts_0 \\ Ts_1 \\ Ts_2 \\ Ts_3 \\ Ts_4 \\ Ts_5 \\ Ts_6 \\ Ts_7 \\ Ts_8 \end{pmatrix} = \begin{bmatrix} \sum_j U_{0,j} + U_{inf} & \cdots & -U_{8,0} \\ \vdots & & \\ \vdots & & \\ \vdots & & \\ \vdots & & \\ \vdots & & \\ \vdots & & \\ \vdots & & \\ -U_{0,8} + kp & \cdots & Ys_8 + \sum_j U_{8,j} \end{bmatrix}^{-1} \begin{pmatrix} TonU_{inf} + Qg \\ TonA_1u_W \\ TonA_2u_W \\ Teq_3Yt_3 + Sn_3 \\ Teq_4Yt_4 + Sn_4 \\ Teq_5Yt_5 + Sn_5 \\ Teq_6Yt_6 + Sn_6 \\ Teq_7Yt_7 + Sn_7 \\ TbYt_8 + KpT_{sp} + Sn_8 \end{pmatrix} \tag{6.6}$$

$Tb\cdot Yt_8+Kp\cdot T_{sp}$ represent basically the equivalent heat source Qeq. Performing an inverse discrete Fourier series over the range of frequency and for each time step yields the following results:

$$Tr_i(t) = T_{s0} + 2\sum_{n=1}^{12} Re(T_{sn})\exp(j\omega_n t) \tag{6.7}$$

with $T_{s,0}$ representing the mean value

The equivalent source capacity delivered at the floor surface to match the load with no restriction concerning floor surface temperature or cooling load is performed as follows:

$$Qeq = Kp(T_{sp} - Ts_0) \quad \text{with room air temperature} \tag{6.8}$$

The same equation can be used with room operative temperature Ts_{op} instead of the air temperature Ts_0. Using equation (4.10), the auxiliary floor radiant heating source related to this equivalent source is:

$$qr_{aux} = Qeq \frac{Y10}{Y8 + Ybs + Y10} - Ybt\,Tb \tag{6.9}$$

The solution for each time step is obtained through an inverse discrete Fourier series:

$$qr_{aux}(t) = qr_{aux0} + 2\sum_{n=1}^{12} Re(qr_{aux,n}) \exp(j\omega_n t) \tag{6.10}$$

However, these results may not reflect the reality as shown by simulation because the resulting room air (or operative) temperature is artificially maintained at the set point T_{sp} without maximum floor surface temperature restriction and whatever the room load requirements which may include heating and/or cooling load.

In practice such as with simple feedback proportional control, room temperature is maintained near set point with control of the heat source according to the detected room temperature error offset, basically starting or shutting off the auxiliary heating system with no cooling involved. However, due to building thermal lag time and other inputs variables such as ambient temperature or solar radiation, room and floor surface temperatures may go over

the desired set points. If those variables were taken into account using appropriate control strategies such as predictive control with/or combined use of radiant/convective heating system, the heating capacity could be modulated in an efficient way in order to reduce or avoid building overheating and consequent waste of energy. To simulate this conditions, the following logic statements are introduced to determine approximately the heating capacity required with regard to the set point.

Heating effect only (no cooling)

$$\text{If}\left(Ts_0(t) > T_{sp}(t)\right), qr_{aux}(t) = 0 \qquad (6.11)$$

The 29°C maximum floor surface temperature recommendation is achieved by shutting or modulating down the auxiliary radiant heating system upon reaching this temperature. A sensor within the floor slab should anticipate the floor surface temperature and act on the heating system so as to minimize the effect of the floor thermal lag.

$$\text{If}\left(Ts_8(t) > 29\,\text{deg}C\right), qr_{aux}(t) = 0 \qquad (6.12)$$

Anticipatory control such as temperature reset set point due to solar radiation and/or ambient temperature may be represented by shifting the cooling load theoretically required otherwise (to keep room air temperature within set point requirement) to other period of the day. This cooling load represents basically the amount of energy which, with appropriate control, could also be recuperated for example to heat some other part of the building or domestic hot water. The time shift may be simulated as follows:

$$q_{cool}(t) = q_{cool0} + 2\sum_{n=1}^{12} Re(q_{cool,n}) \exp\left(j\omega_n (t - \frac{\arg(\phi)}{w_1}) \right) \tag{6.13}$$

arg(Φ) may represent the argument of the main harmonic of solar radiation incident on the floor surface or any time shift required to modulate the load efficiently. The resulting auxiliary heat source with conditions as established by equations (6.11) to (6.13) would be equal to:

$$q_{aux} = qr_{aux}(t) + q_{cool}(t) \tag{6.14}$$

The cooling load is subtracted from the heating load and the equivalent heat source at the floor surface is:

$$Qeq = q_{aux} \frac{Y8 + Ybs + Y10}{Y10} + Ybt\,Tb \tag{6.15}$$

The equivalent heat source Qeq thereby modified and taking in account all the conditions dictated by equations (6.11) to (6.13) is reintroduced in the original matrix equation (4.12) for calculation of the room temperatures using the same procedure as described above. The inverse matrix would be as follows:

$$\begin{pmatrix} Ts_0 \\ Ts_1 \\ Ts_2 \\ Ts_3 \\ Ts_4 \\ Ts_5 \\ Ts_6 \\ Ts_7 \\ Ts_8 \end{pmatrix} = \begin{bmatrix} \sum_j U_{0,j} + U_{inf} & \cdots & -U_{8,0} \\ \vdots & & \\ \vdots & & \\ \vdots & & \\ \vdots & & \\ \vdots & & \\ \vdots & & \\ \vdots & & \\ -U_{0,8} & \cdots & Ys_8 + \sum_j U_{8,j} \end{bmatrix}^{-1} \cdot \begin{pmatrix} TonU_{inf} + Qg \\ TonA_1 u_W \\ TonA_2 u_W \\ Teq_3 Yt_3 + Sn_3 \\ Teq_4 Yt_4 + Sn_4 \\ Teq_5 Yt_5 + Sn_5 \\ Teq_6 Yt_6 + Sn_6 \\ Teq_7 Yt_7 + Sn_7 \\ Qeq + Sn_8 \end{pmatrix} \tag{6.16}$$

The energy balance could also include radiant heating system combined

with convective heating Q_v directly at the node air which would provide rapid heat loss recovery whenever needed. This combination may be used to lower down the floor surface temperature or with predictive control to reduce the heat provided by the floor heating system and stored in the floor thermal mass so as to make full use of solar radiation.

The auxiliary heating consumption would be:

$$Q_{cons} = \sum_{t} q_{aux}(t) \tag{6.17}$$

The room temperatures of interest are derived from the above inverse matrix through an inverse discrete Fourier series as follows:

Air temperature

$$Tr_i(t) = Ts_{0,0} + 2\sum_{n=1}^{12} Re(Ts_{n,0})\exp(j\omega_n t) \tag{6.18}$$

Mean radiant temperature using equation (4.21)

$$Tmr(t) = \langle D_{mr} \rangle \{T_{s,0}\} + 2\sum_{n=1}^{12} Re(\{D_{mr}\}\{T_{s,n}\}) \exp(-j\omega_n t) \tag{4.19}$$

Operative temperature using equation (4.22)

$$Top(t) = \langle D \rangle \{T_{s,0}\} + 2\sum_{n=1}^{12} Re(\{D\}\{T_{s,n}\}) \exp(-j\omega_n t) \tag{4.20}$$

6.5 Discussion

Numerical simulation was performed for sunny and cloudy cold days to determine potential passive solar savings for a floor thickness of 0.09m with different internal heat source depths. Control based on air temperature and

operative temperature with air sensor was also investigated. The conditions established for the room thermal network Figure 3.1 were as follows: typical cold day for Montreal, Canada, latitude 45 North, January with sinusoidal outdoor temperature variation:

$$T_o(t) = T_{om} + \Delta T_o \cos(\omega t - 5\pi/4) \tag{4.21}$$

Where $T_{om} = -12°C$ mean outside temperature

$\Delta T_o = 8°C$ amplitude of $T_o(t)$ and ω=2л/(86400s)

Two set point profiles were considered in the simulations:

1-Constant set point $T_{sp} = 20°C$

2-An optimal profile based on results of previous studies (Athienitis, 1994, Athienitis and Chen, 1998) expressed in sinusoidal form.

$$T_{sp}(t) = T_{sp,low} + \Delta T_{sp} \cos\pi\left(\frac{t-(t_{end}+t_{start})/2}{t_{end}-t_{start}}\right) \tag{6.22}$$

Where $T_{sp,low} = 18°C$ and $\Delta T_{sp} = 4°C$

T_{start}=3 hours after midnight (start of half-sinusoid)

T_{end}=3 hours after midnight (end of half-sinusoid)

The basement temperature variation was also considered as follows

$$Tb(t) = Tbn + \Delta T_o \cos(\omega t - 5\pi/4) \tag{6.23}$$

With $Tbn = 0°C$ and $\Delta T_o = 2°C$

Solar radiation data is generated using the Hourly clearness index as shown in Appendix 2. The resulting sources are modeled over the day time period as a half-sinusoid from sunrise to sunset. High (655 watts/m^2) and low

(100 watts/m^2) instantaneous solar radiation transmitted through the windows and respectively equivalent to sunny and cloudy days with same ambient temperature profile are considered.

The auxiliary heating system is assumed to have a capacity of 8400 watts based on the maximum steady heat loss and is operated under proportional control. The infiltration conductance is estimated based on an infiltration rate equal to one air change per hour (ACH) as follows:

$$U_{inf} = \frac{ACH \times \text{Room Volume}}{3600\,s} \rho_{air}\, c_{air} \tag{6.24}$$

With $\rho_{air} = 1.2 \frac{kg}{m^3}$ and $c_{air} = 1000 \frac{joule}{kg\,°C}$

Simulations were performed using simple feedback control of room air (and operative) temperature with and without floor surface temperature control (shut-off control based on a maximum floor surface temperature set to 29°C)

6.51 Concrete floor

Examination of Figures 6.2 to 6.9 representing room temperatures responses with air sensor reveals as expected that the room MRT and consequently the operative temperature are respectively higher by up to 2.35°C and than 1.6°C than room air temperature, particularly during sunny days. Athienitis and Chen (1993) concluded that MRT may differ significantly from room air temperature often by more than 3°C and therefore in order to improve thermal comfort, particularly in building with high radiant gains, it is preferable to use operative control. Figures 6.2, 6.4, 6.6 and 6.8 reveal that overheating is

experimented during periods of high solar radiation for both air and operative temperature and that floor surface temperature may exceeds the recommended temperature by up to 1.8°C with any heat source depth within the floor slab.

Maximum floor surface is reduced significantly from 30.8°C to 29.4°C with floor reset control as shown by Figures 6.6 to 6.9. Floor surface overheating problem would be more easily resolved with operative temperature control. However, we observe that peak air and operative temperature are over set point reaching up to 24.5°C with floor reset control. This may result from the high floor thermal mass thickness (9cm) causing a higher room temperature swing as it transmits heat slower than medium mass, requiring the heating system to be on for longer period of time along with higher output due to proportional control. This explains the fact that although the heating system is off when there is significant solar gains (Figures 6.10 and 6.12), a significant amount of heat still travels from the bottom of the slab to the surface and together with solar gains, causes a higher room temperature swing. This shows the needs for more appropriate control and integrated building energy analysis in the design stage in order to maximize the solar gains and avoid overheating.

Figures 6.4 and 6.8 indicates that half sinusoid set point profile results in improving overall performance as compared to a constant set point on sunny days particularly with operative temperature control which reduces floor surface temperature (down to 28.8°C) and maintains room temperature within the set point. However, the results are different for cloudy day as shown by Figures 6.5 and 6.9, where we observe overheating of floor surface (up to 29.7°C) with no

improvement of the overall air or operative temperature. This is explained by the fact that change in set point requires high heating rates when the transmission losses are high. The high heat transfer rate and the thermal lag effect results in a delayed rise of the floor surface temperature, particularly at the end of the temperature setback point (t_{end}=3hours after midnight).

Examination of Figures 6.10 to 6.13 representing the energy consumption confirms the effect of thermal mass on energy savings due to solar gains. We observe that there is about 25% to 30% reduction of heating load respectively for constant set point and optimal profile control temperature. The energy consumption is reduced from 48 MJ to 35 MJ and from 46 MJ to 34 MJ respectively for constant set point and optimal profile for sunny day compared to cloudy day. Floor overheating is resolved by the floor reset temperature control which shuts off the system when temperature is higher than 29°C.

Figures 6.14 to 6.17 reveal as expected that that the floor internal heat source depth has no impact of the room steady state temperatures surface. Room temperature above design set point values are observed for sunny day.

Figures 6.18 to 6.23 show that energy consumption increases with increasing depth of the heat source within the floor slab. This is due to the low bottom insulation (1 RSI), which allows heat to flow downwards.

6.52 Carpeted floor

Carpet cover is simulated as a resistance in series with the floor inside air film (Uc=0.6 m^2.°C/watt). Examination of Figures 6.22 and 6.23 reveals that with

constant set point profile, floor surface temperature (around 34.5°C) without reset control is above recommended limit in order to maintain air temperature at the set point for both sunny and cloudy day. Figures 6.26 and 6.27 indicate that with floor reset control and the same control parameters as for concrete floor, floor surface temperature surface (30.5°C) is still above recommended limit with, in this case, a resulting room air temperature under desired temperature set point (down to 16.5 °C on cloudy day), thereby requiring supplementary heat (auxiliary convective heat source) to be provided. Optimal profile, as represented by Figures 6.24, 6.25, 6.28 and 6.29, does improve slightly the room response which, however, remains outside design limits.

All these figures reveal that the mean radiant temperature differs significantly from the room air temperature by up 4.5°C for sunny day and 4.7°C for cloudy days. These observations are similar to that already made for concrete floor and confirm that control based on operative temperature will be more appropriate under these conditions.

Figures 6.30 to 6.33 indicate that energy consumption with carpeted floor is about 6% higher than with concrete floor. On the other hand with floor control reset, the energy consumption is respectively lower by 3% and 4% for constant and variable set point due to the fact that the heating system shuts off upon maximum floor surface temperature is reached but however without room temperature reaching its set point. Floor covering has a certain impact of floor surface temperature due to its restriction effect on the heat flow towards the heated space which may lead floor slab to overheat with possible resulting

damage on the building structure. Particular attention should be given to this detail in the design stage.

6.53 Conclusion:

The half sinusoid set point profile gives the best response when both temperature and energy consumption are considered. Variation in setpoint from day to night is confirmed as an effective control alternative for increased passive solar gains. Control of radiant heating based on operative temperature reduces both maximum floor surface and maximum operative temperature, particularly for carpeted floor. It reduces energy consumption particularly on sunny day and improves thermal comfort.

Appropriate control strategies for radiant heating system with weather anticipation and more effective use of the passive solar gains is required to maintain the room air (or operative) and the floor surface temperature within the desired temperature.

Concrete floor

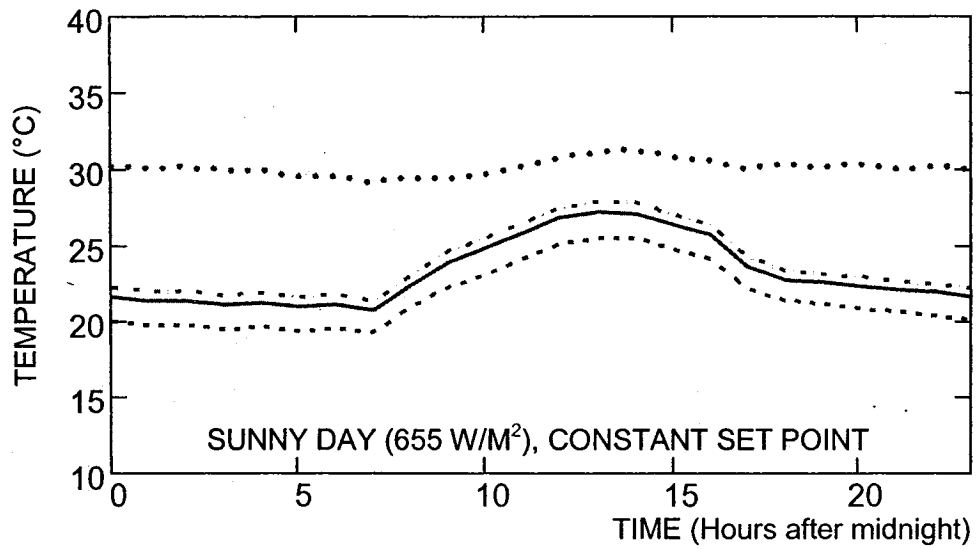

Figure 6.2: Temperature response with no floor surface reset control

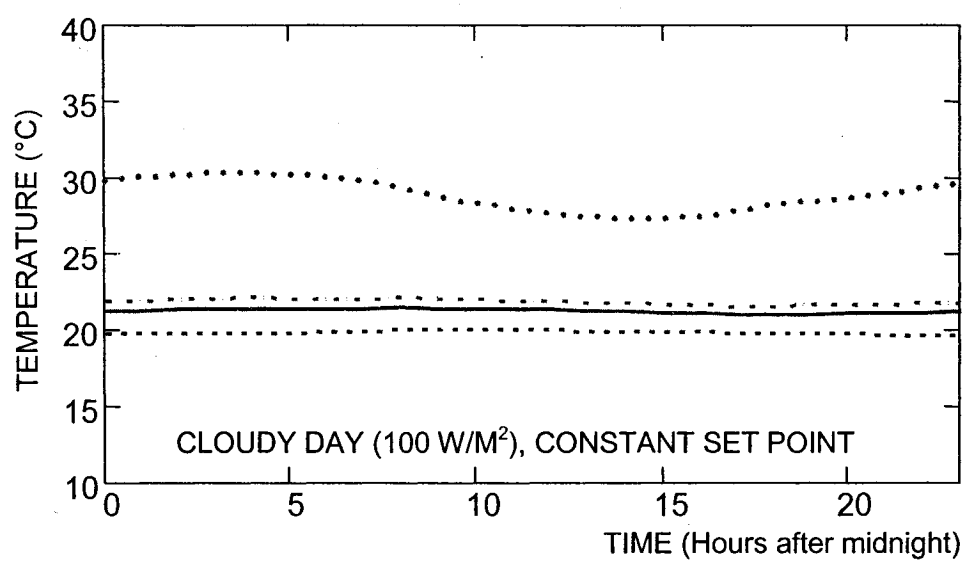

Figure 6.3: Temperature response with no floor surface reset control

••••• Floor temperature
—— Operative temperature
—·—·— Mean radiant temperature
····· Air temperature

Concrete floor

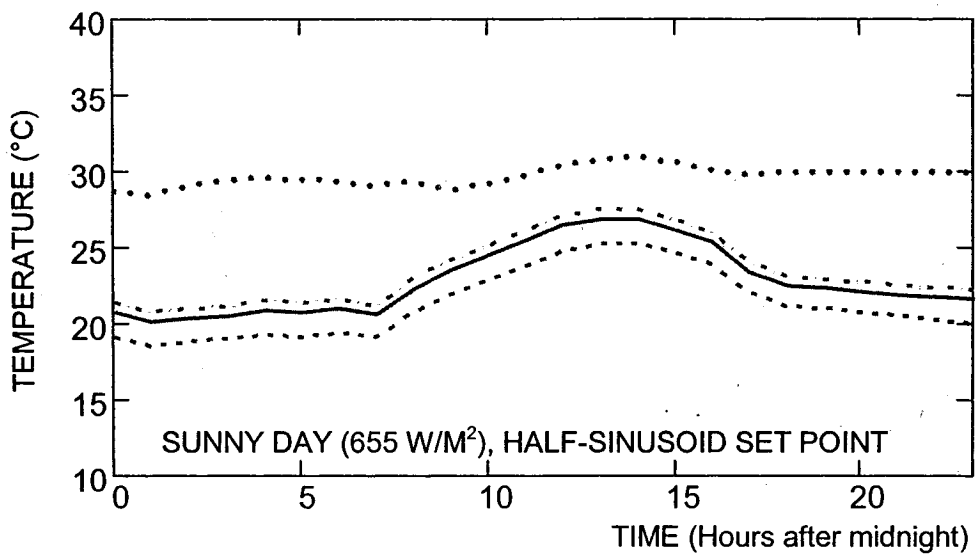

Figure 6.4: Temperature response with no floor surface reset control

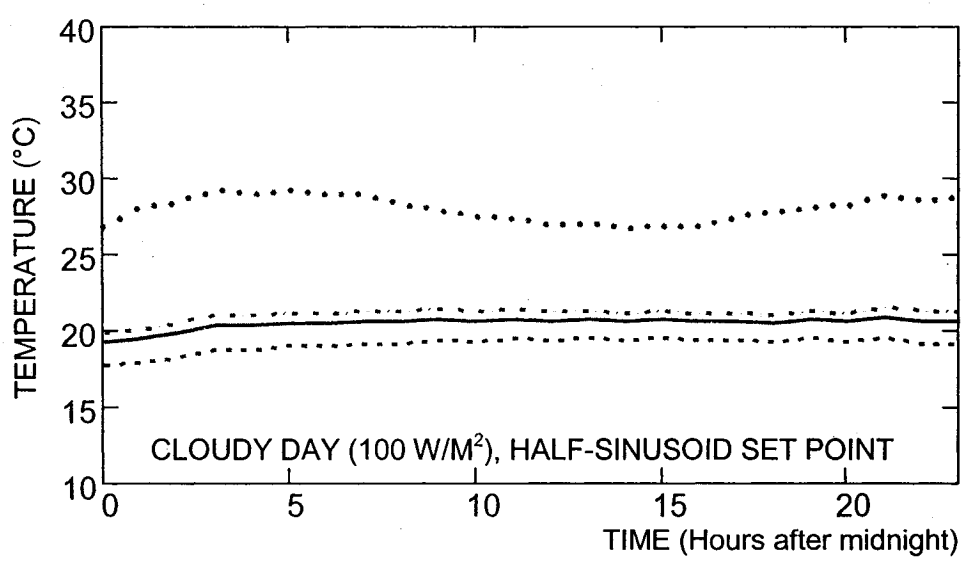

Figure 6.5: Temperature response with no floor surface reset control

••••• Floor temperature
—— Operative temperature
—·—·— Mean radiant temperature
····· Air temperature

Concrete floor

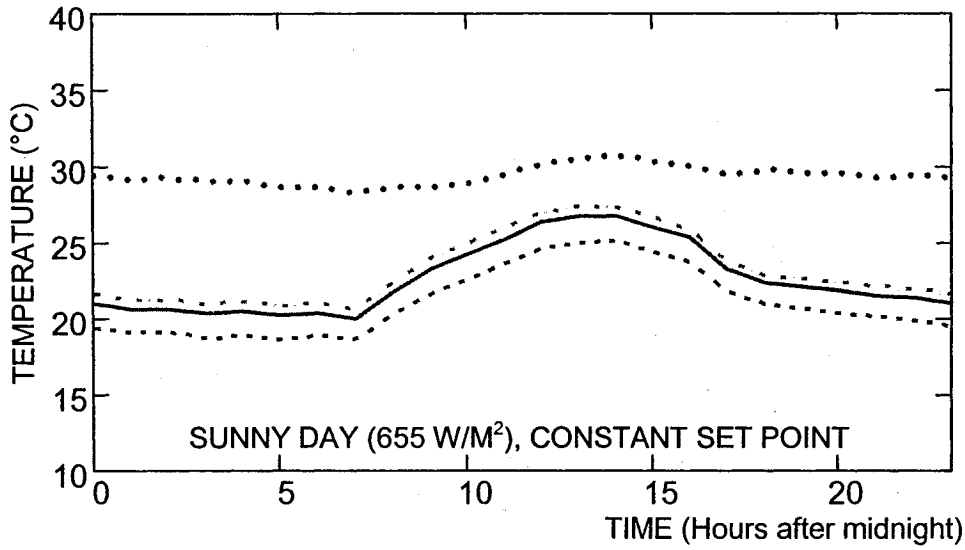

Figure 6.6: Temperature response with floor surface reset control

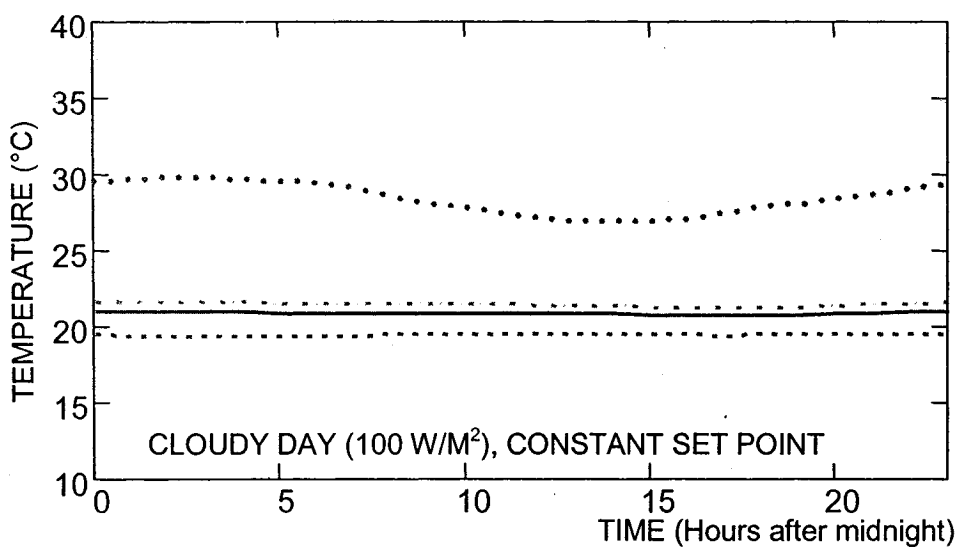

Figure 6.7: Temperature response with floor surface reset control

••••• Floor temperature
—— Operative temperature
-·-·-· Mean radiant temperature
····· Air temperature

Concrete floor

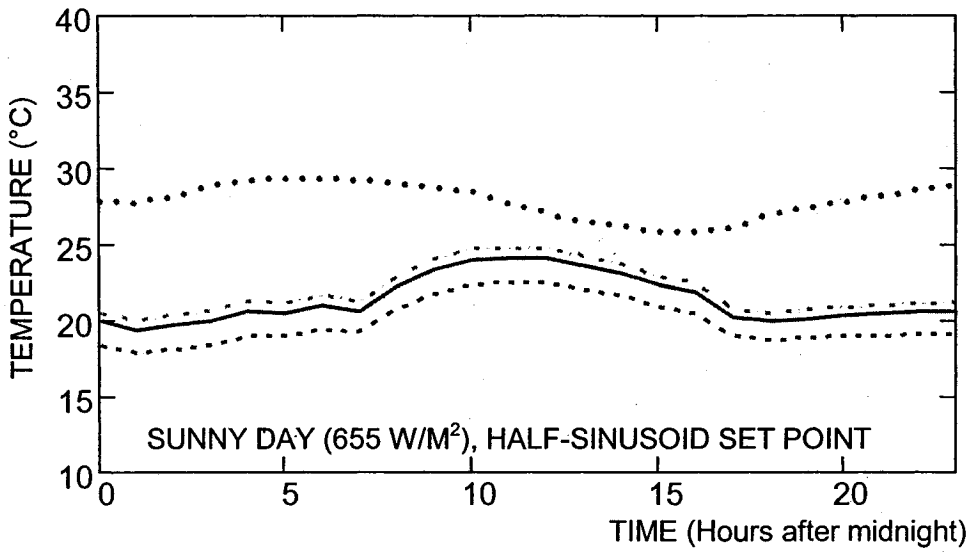

Figure 6.8: Temperature response with floor surface reset control

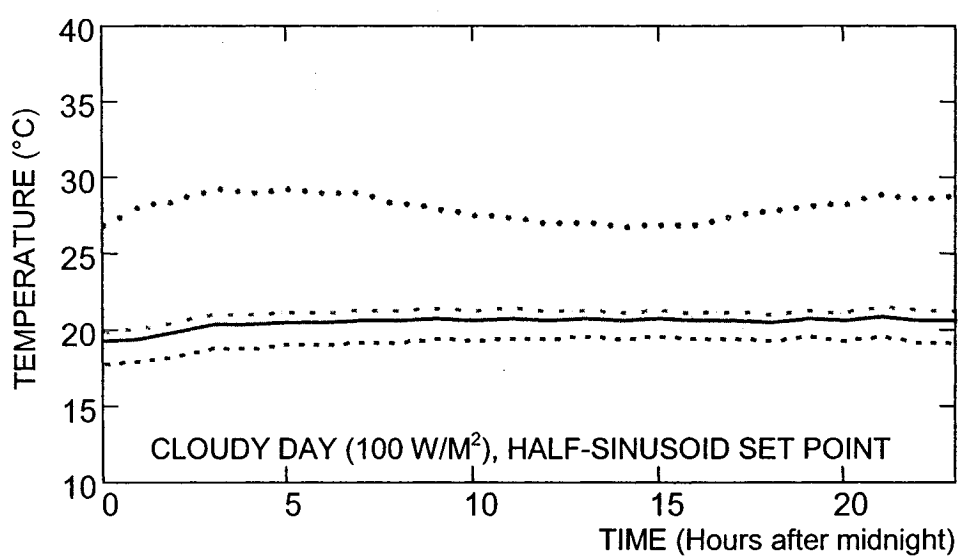

Figure 6.9: Temperature response with floor surface reset control

••••• Floor temperature
—— Operative temperature
—·—·— Mean radiant temperature
····· Air temperature

Concrete floor

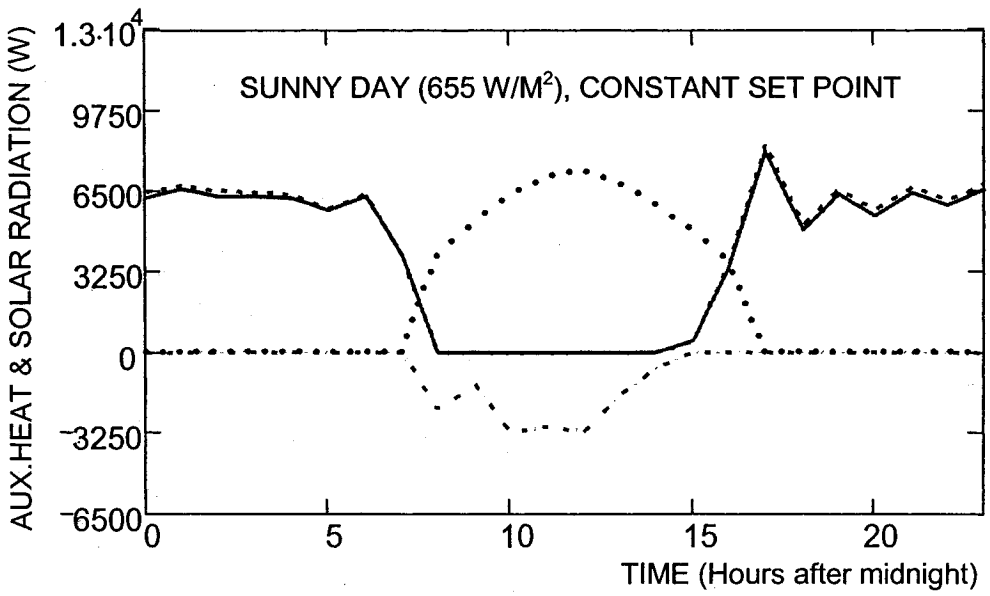

Figure 6.10: Auxiliary heat source output

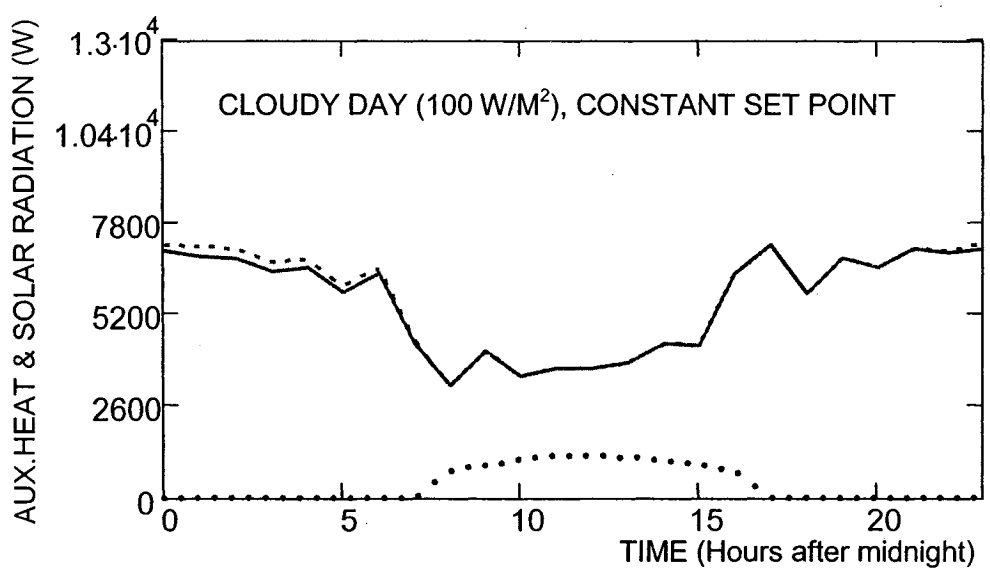

Figure 6.11: Auxiliary heat source output

- - - No floor reset control
••••• Solar radiation
—— Floor reset control (≤29.degC)
- - - Potential floor thermal mass solar gains

Concrete floor

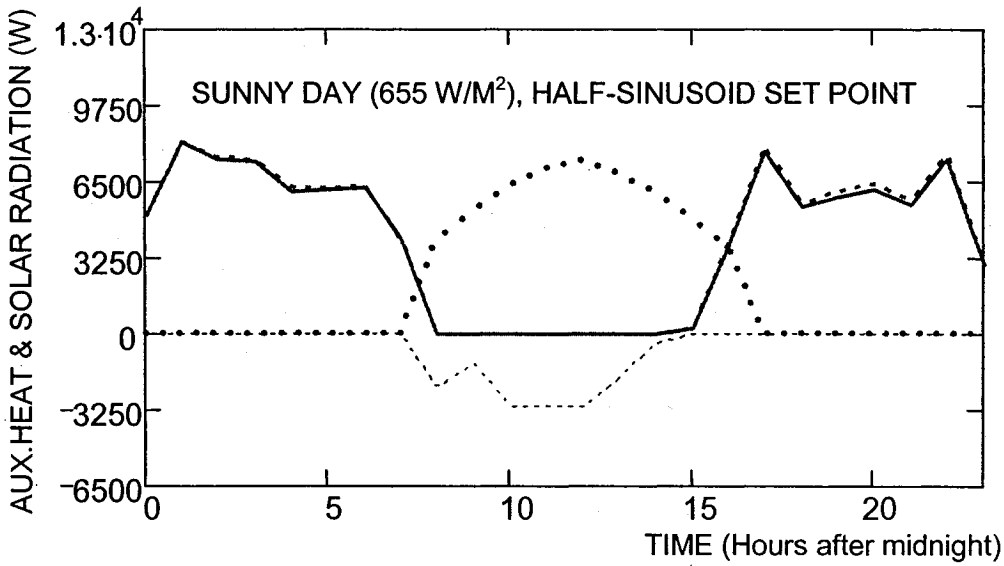

Figures 6.12: Auxiliary heat source output

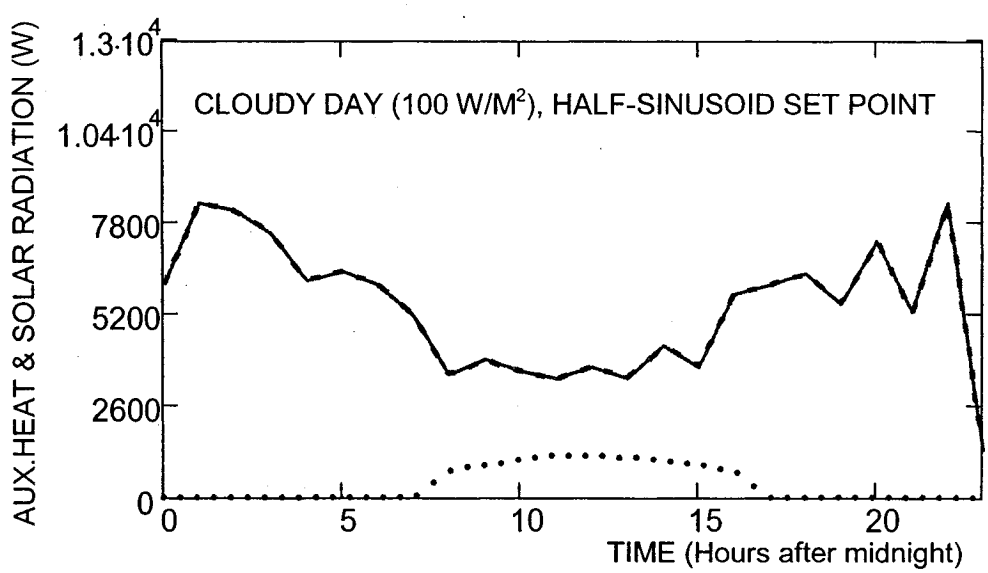

Figure 6.13: Auxiliary heat source output

- - - No floor reset control
•••• Solar radiation
—— Floor reset control (≤29.degC)
- - - Potential floor thermal mass solar gains

Concrete floor

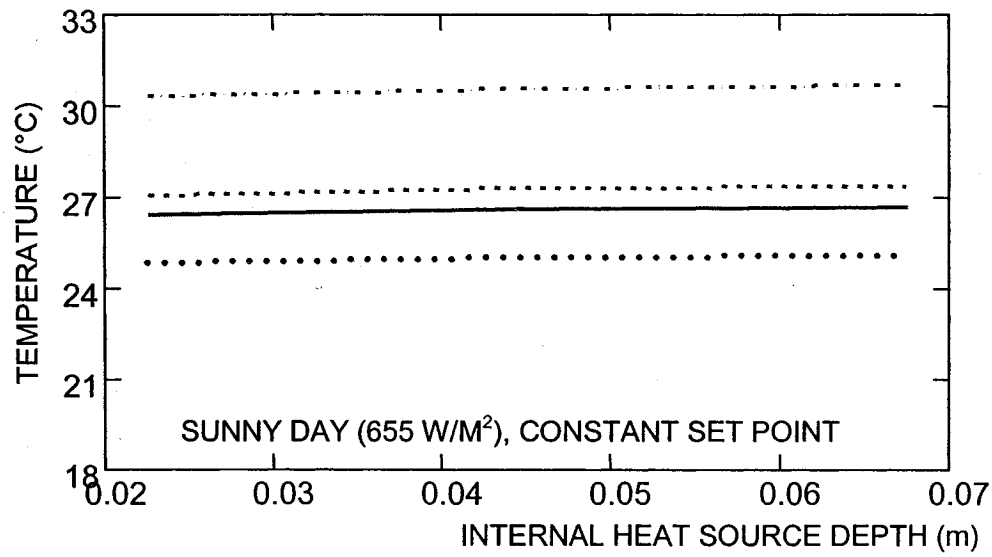

Figure 6.14: Temperature response versus floor internal heat source depth and no floor surface reset control (time: 14 hours)

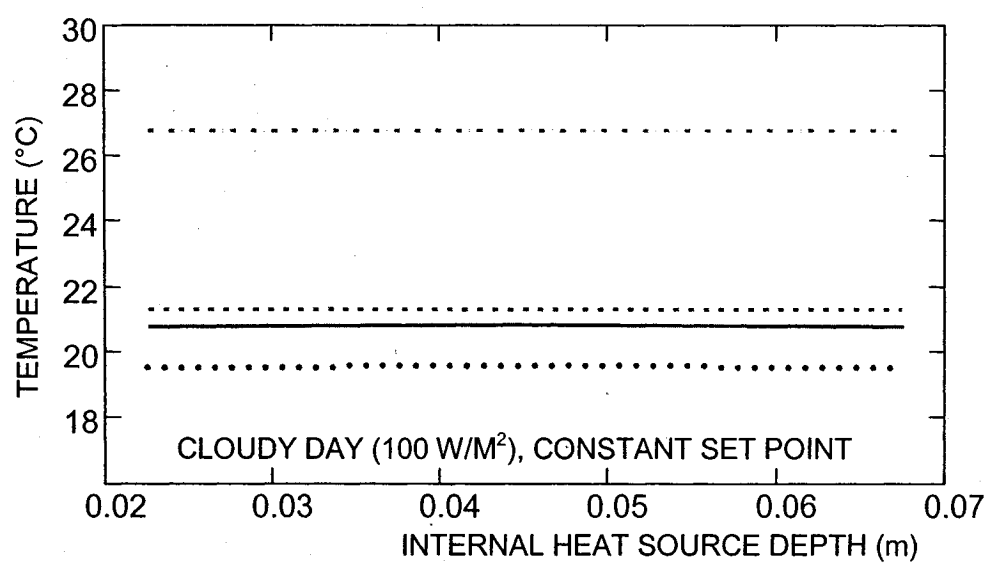

Figure 6.16: Temperature response versus floor internal heat source depth and no floor surface reset control (time: 14 hours)

••••• Air temperature
—— Operative temperature
—·—·— Floor temperature
····· Mean radiant temperature

Concrete floor

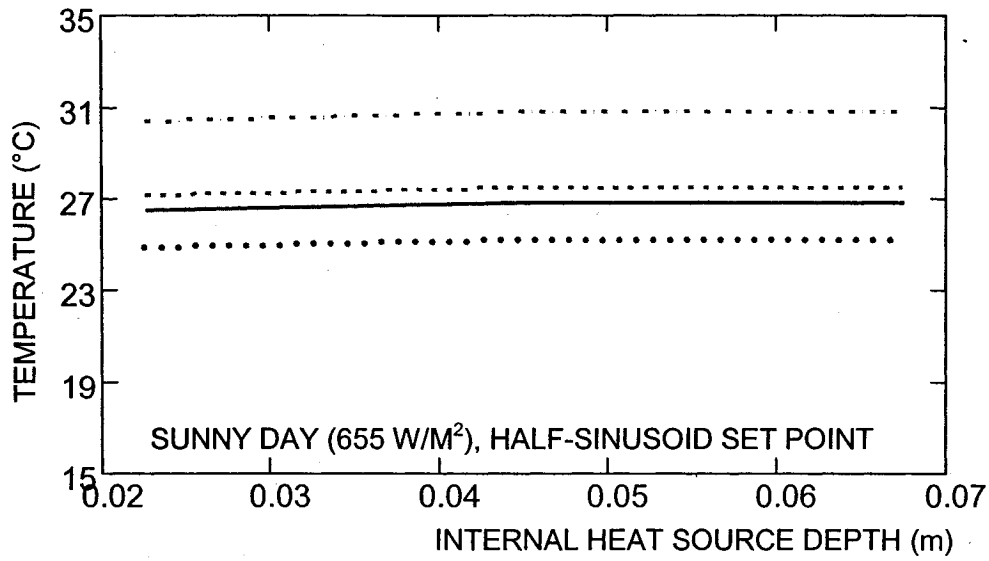

Figure 6.16: Temperature response versus floor internal heat source depth and no floor surface reset control (time 14 hours)

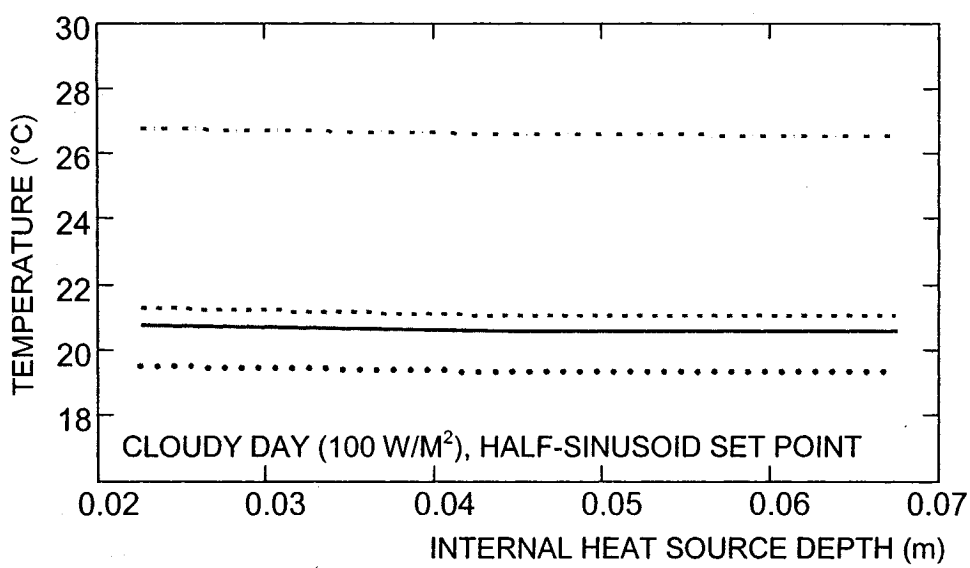

Figure 6.17: Temperature response versus floor internal heat source depth and no floor surface reset control (time 14 hours)

••••• Air temperature
—— Operative temperature
–·–·– Floor temperature
····· Mean radiant temperature

Concrete floor

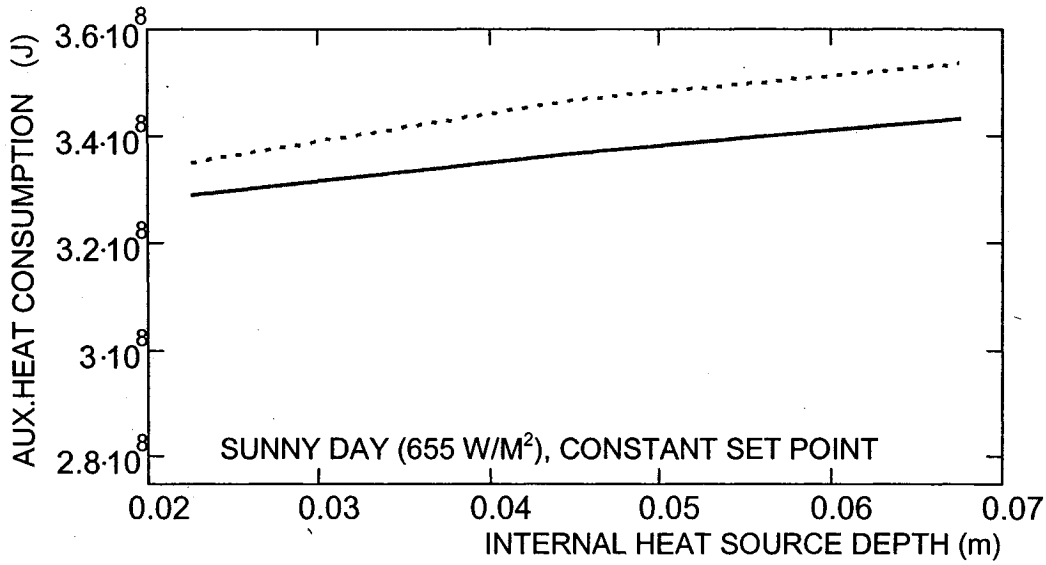

Figure 6.18: Energy consumption versus floor internal heat source depth

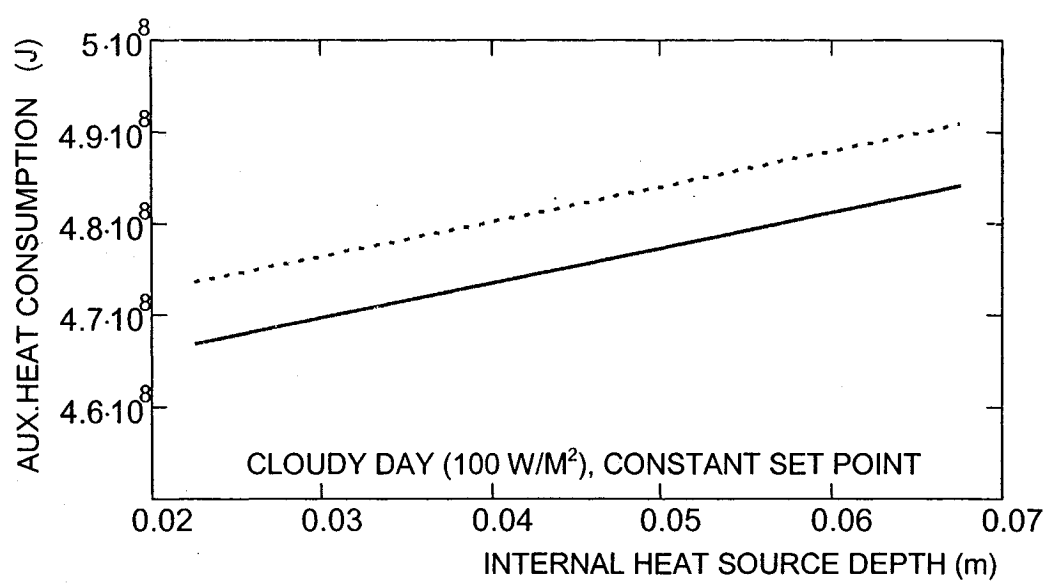

Figure 6.19: Energy consumption versus floor internal heat source depth

------ No floor reset control —— Floor reset control (≤29.degC)

Concrete floor

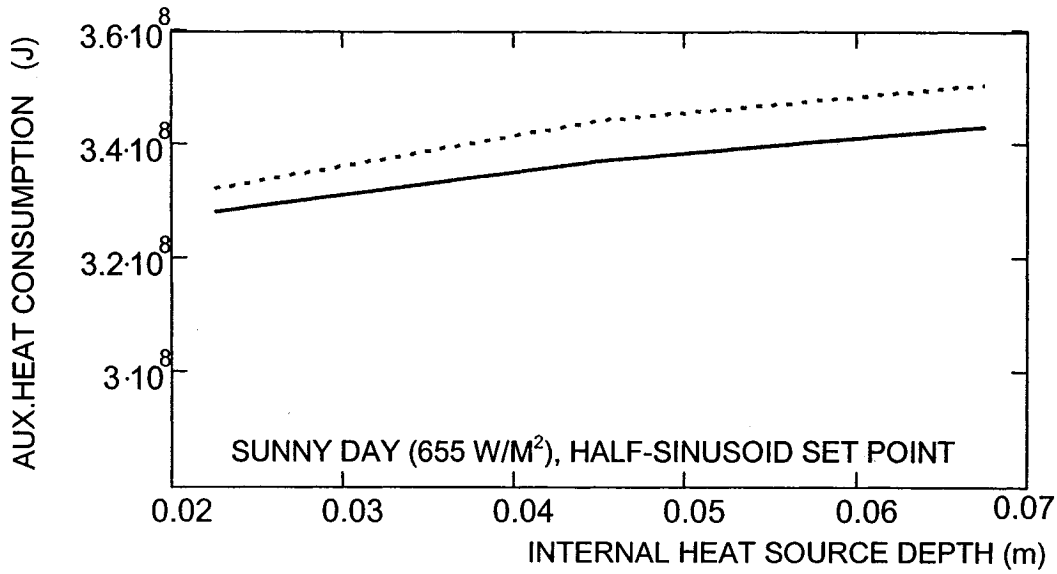

Figure 6.20: Energy consumption versus floor internal heat source depth

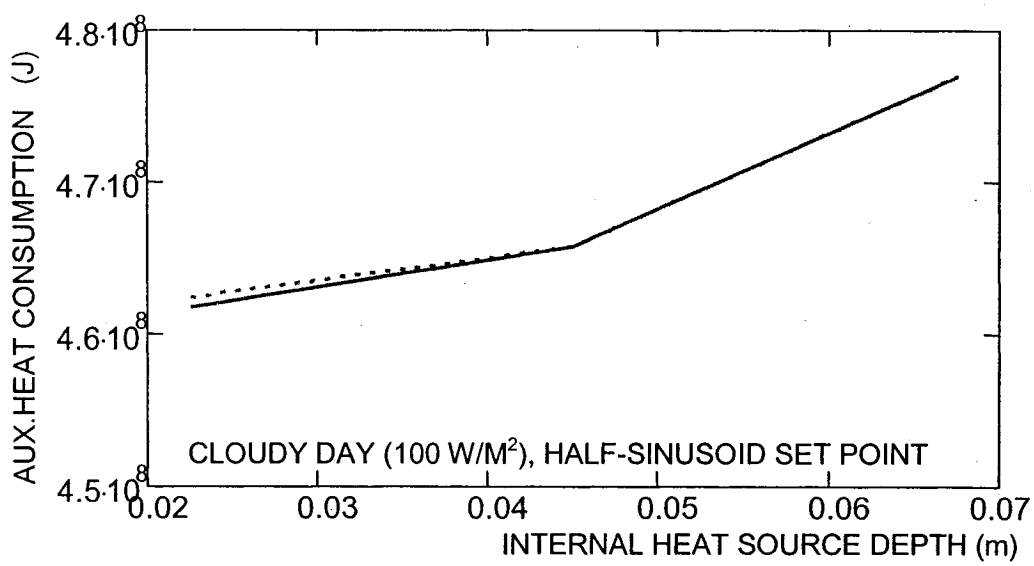

Figure 6.21: Energy consumption versus floor internal heat source depth

------ No floor reset control —— Floor reset control (≤29.degC)

Carpeted floor

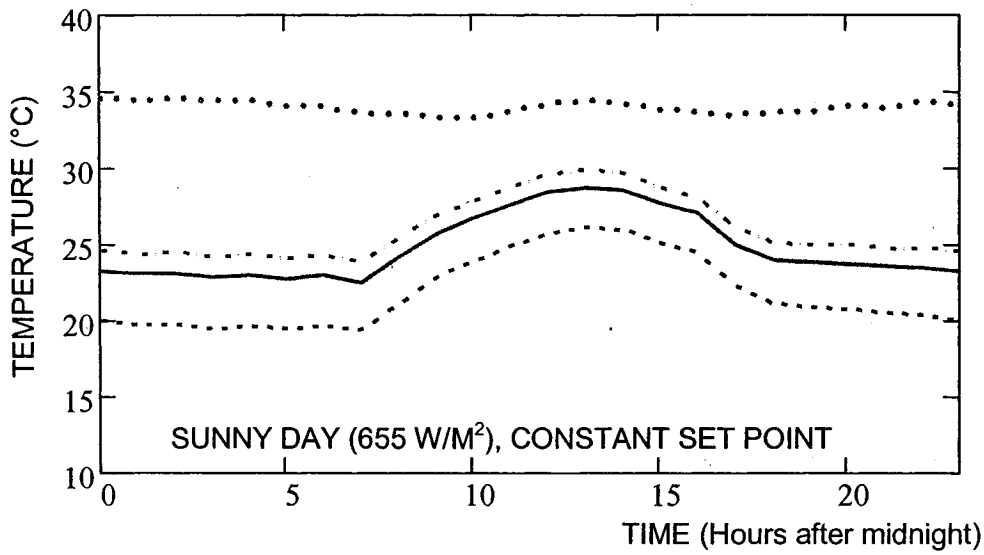

Figure 6.22: Temperature response with no floor surface reset control

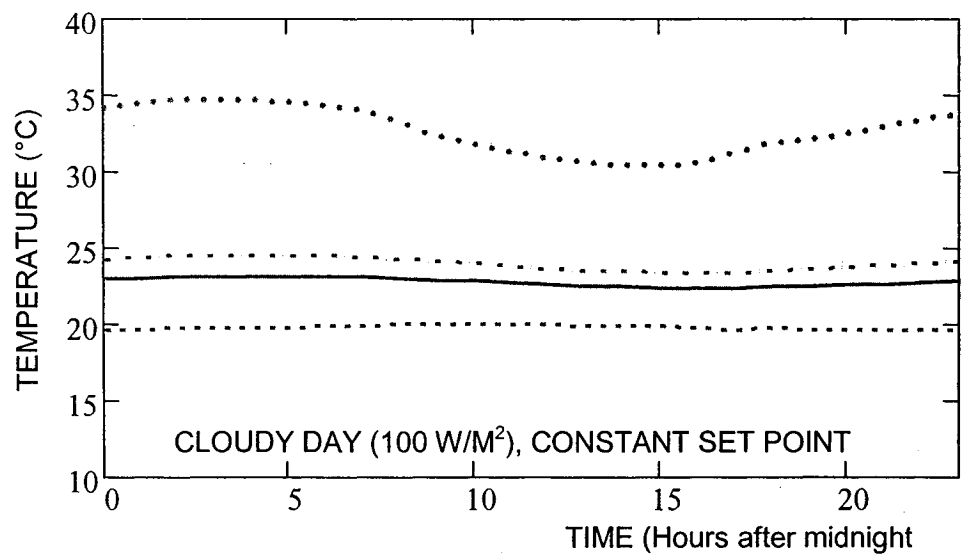

Figure 6.23: Temperature response with no floor surface reset control

••••• Floor temperature
—— Operative temperature
–·–·– Mean radiant temperature
····· Air temperature

Carpeted floor

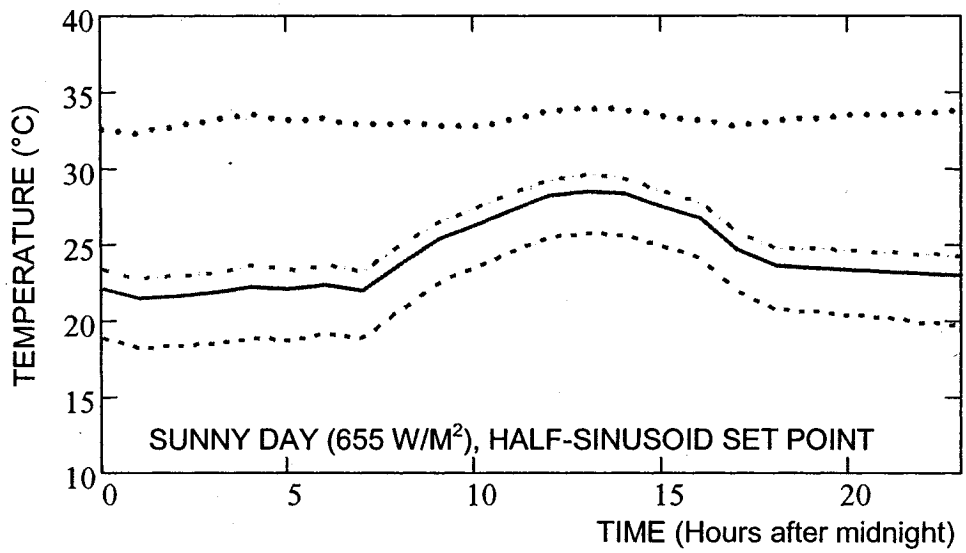

Figure 6.24: Temperature response with no floor surface reset control

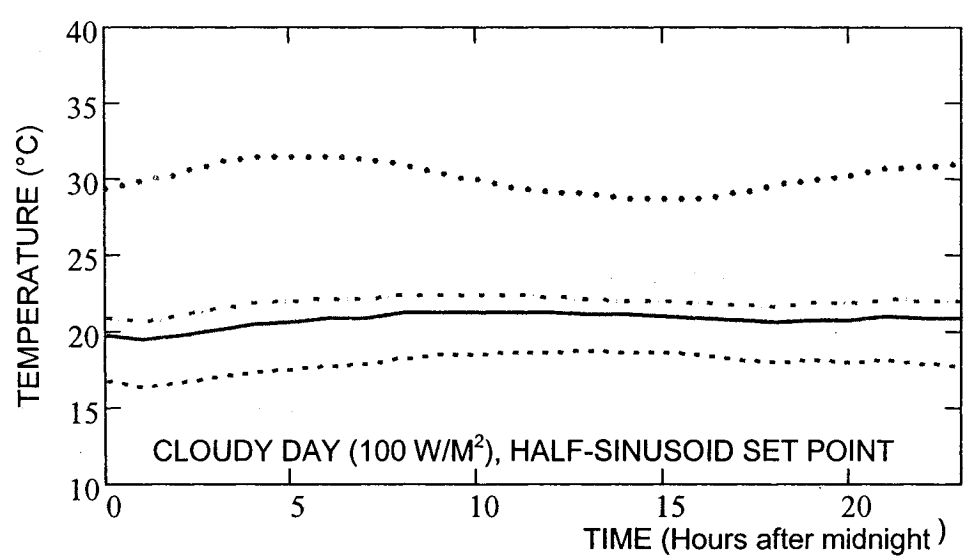

Figure 6.25: Temperature response with no floor surface reset control

••••• Floor temperature
—— Operative temperature
—·—·— Mean radiant temperature
····· Air temperature

Carpeted floor

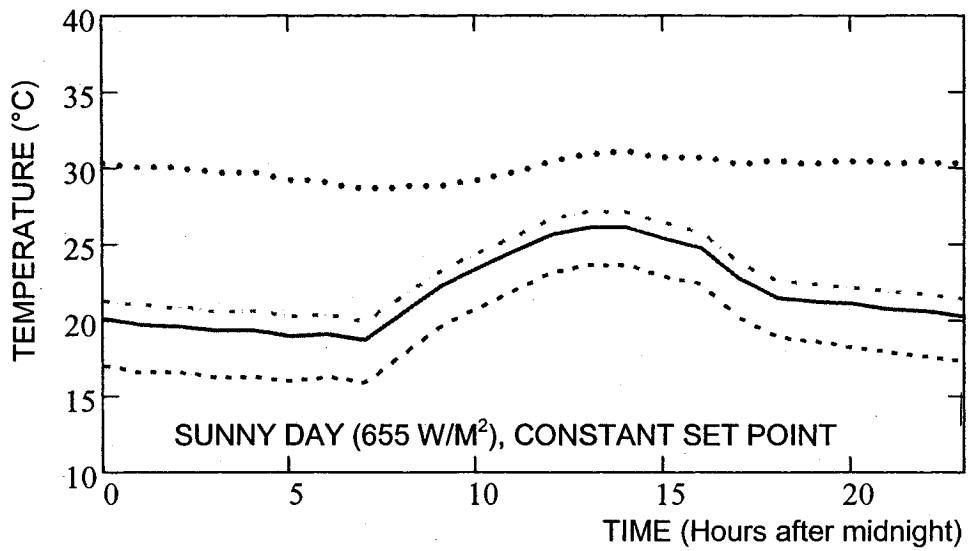

Figure 6.26: Temperature response with floor surface reset control

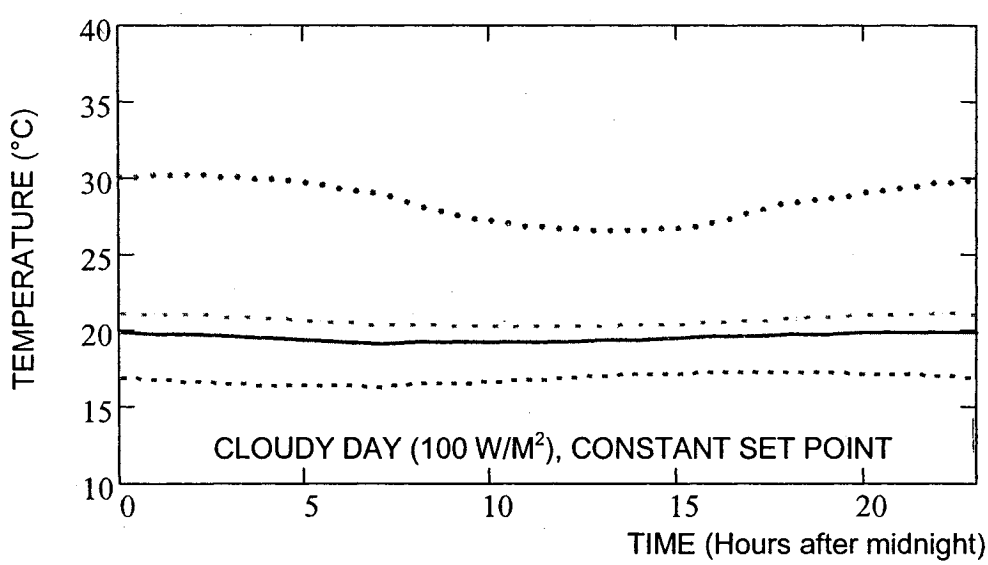

Figure 6.27: Temperature response with floor surface reset control

••••• Floor temperature
—— Operative temperature
–·–·– Mean radiant temperature
····· Air temperature

Carpeted floor

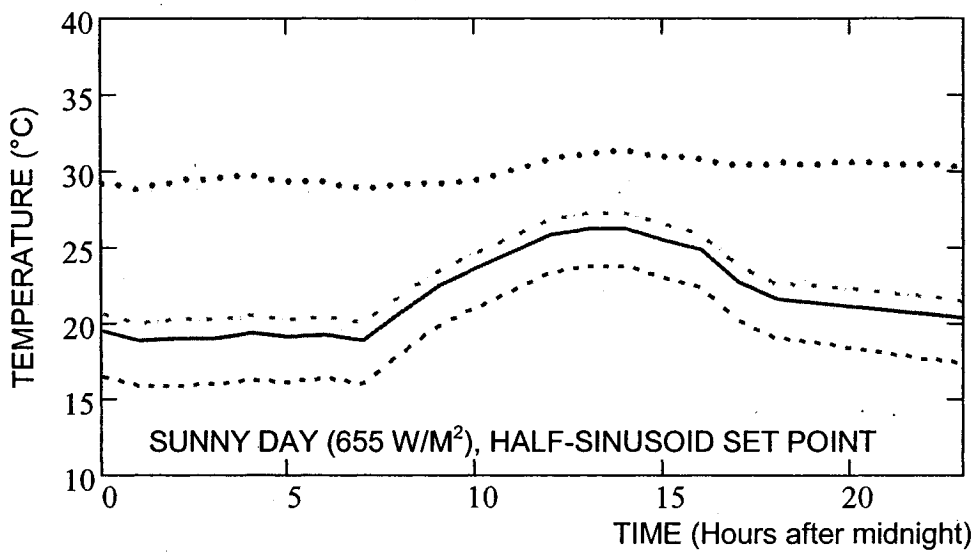

Figure 6.28: Temperature response with floor surface reset control

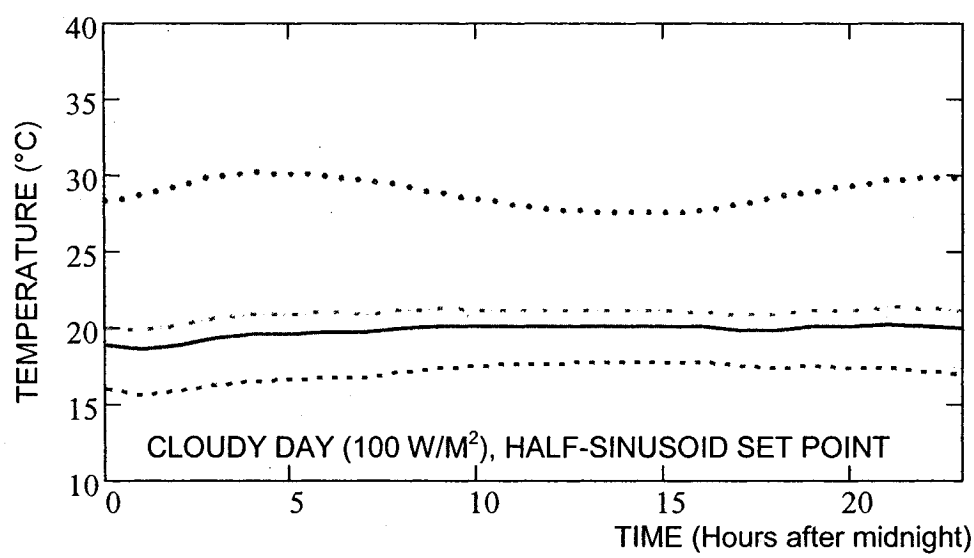

Figure 6.29: Temperature response with floor surface reset control

••••• Floor temperature
—— Operative temperature
—·—·— Mean radiant temperature
····· Air temperature

Carpeted floor

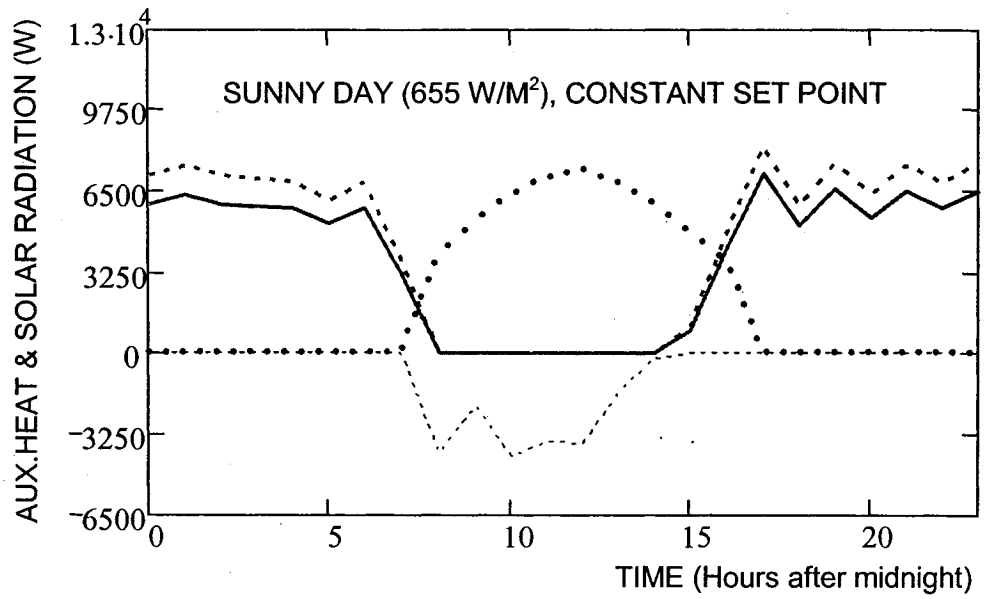

Figure 6.30: Auxiliary heat source output

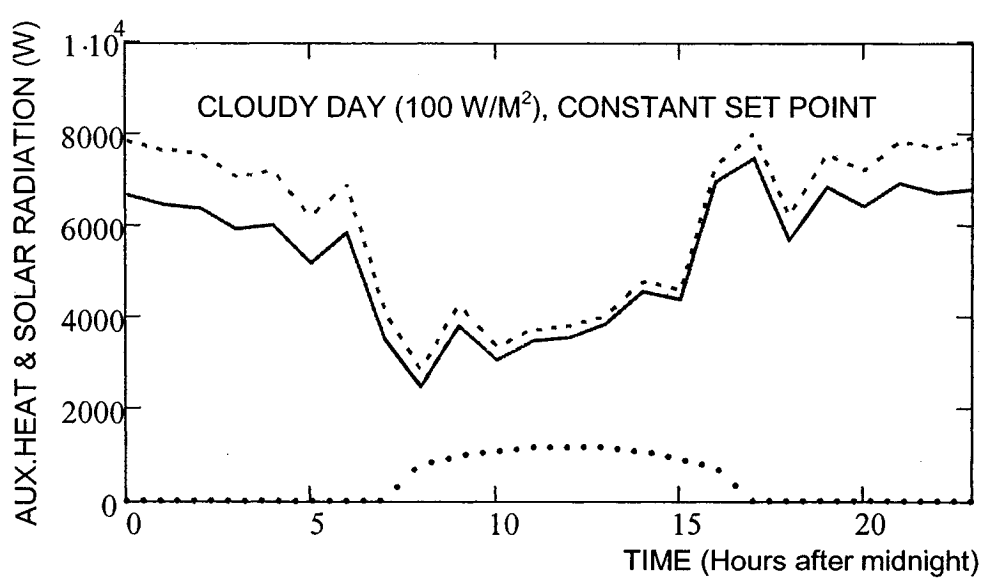

Figure 6.31: Auxiliary heat source output

- - - No floor reset control
•••• Solar radiation
—— Floor reset control (≤29.degC)
- - - Potential floor thermal mass solar gains

Carpeted floor

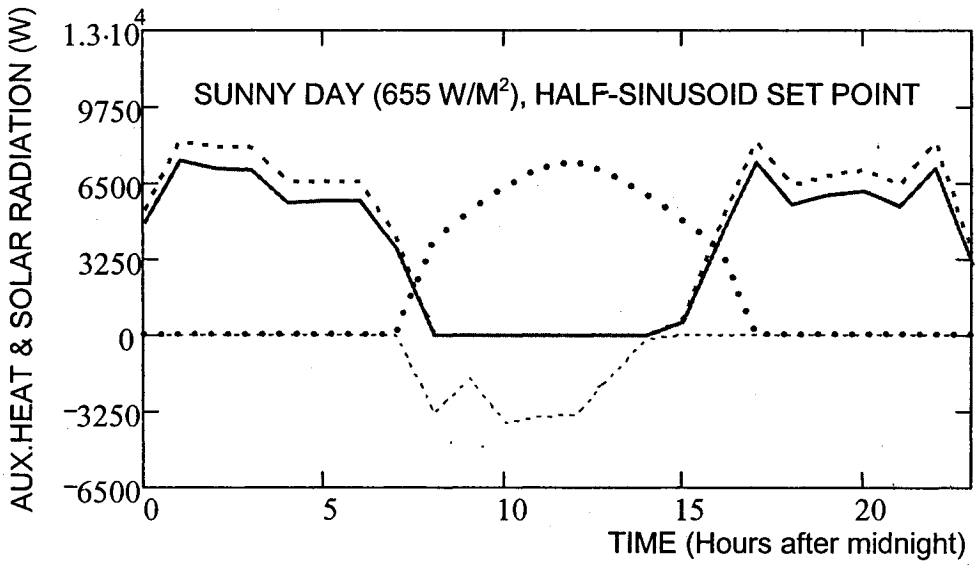

Figure 6.32: Auxiliary heat source output

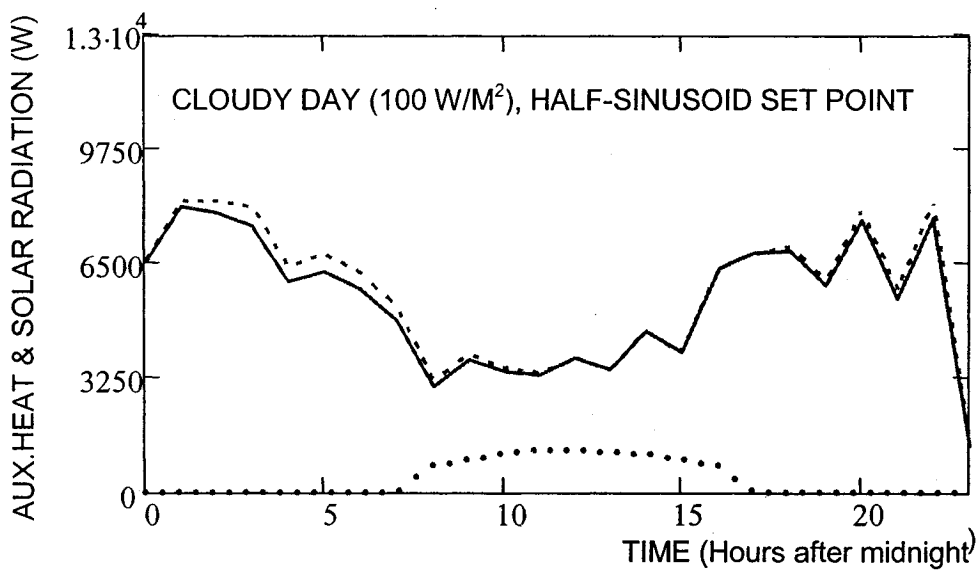

Figure 6.33: Auxiliary heat source output

- - - No floor reset control
••••• Solar radiation
—— Floor reset control (≤29.degC)
- - - Potential floor thermal mass solar gains

CHAPTER 7

CONCLUSIONS

7.1 Conclusions

An integrated methodology based on frequency domain technique in conjunction with Laplace transform and associated Fourier series has been developed and applied to investigate the thermal dynamics of a floor radiant heating–direct gain passive solar system. A detailed room thermal network model with both distributed and lumped parameters including accurate interior radiant exchanges was considered. A heat balance, involving accurate calculation of conductive, convective and radiative parameters along with inside and outside heat sources, is performed at all nodes. Floor radiant heating system with variable installation depth within the slab is modeled using the diakoptic method. This technique allows the floor heating system to be fully integrated and handled like any other surface within the heat balance framework.

Building dynamic thermal response is investigated through the study of important frequency domain transfer functions, such as the admittance transfer function, the impedance transfer function obtained by inversion of the system admittance matrix and the operative transfer function, in terms of magnitude and phase lag and as a function of frequency, thermal properties and geometry for analysis of the effects on room temperature of weather variables such as solar radiation and outside temperature.

The s-domain transfer functions, required for the control analysis, are obtained through a modified least-squares polynomial fit to the discrete frequency responses obtained by inversion of the same system admittance matrix. The building, floor radiant heating system and control transfer functions are combined through block diagram algebra to obtain the overall system s-transfer functions. Analysis of system transient thermal response to load and temperature change, feedback and feedforward-feedback control is performed through numerical inversion of Laplace transforms. Stability studies are carried out in the frequency domain.

Load and temperature calculations, under various control strategies involving constant and sinusoidal room set-point profile, are performed by means of discrete Fourier series associated with the floor internal heat source equivalently transformed into a dependent heat flow source controlled by temperature variables.

Results of the simulations are summarized as follow:

1-An integrated frequency domain based dynamic model of a floor radiant heating has been developed and validated using explicit finite difference transient results.

2- Discretization of a wall into two layers (02 capacitances) with small time step (100 seconds or less) was found to be sufficient to conducted estimation of thermal analysis with the explicit finite difference method.

3-There is an optimum floor mass thickness that reduces most the temperature fluctuations, which is an important relationship in passive solar

design.

4-The effect of thermal mass is minimal in the low frequency long-term dynamics (less than a minute). For low frequencies such as one to four cycles per day, the magnitude and phase angle of the impedance and operative transfer functions are a strong function of room construction.

5-Depth of heat source within the floor slab is shown to have higher effect in the high frequency range short term dynamics response of the room.

6-Carpet cover induces higher thermal lag with resulting effect on room temperature requiring longer time to reach steady state. This effect intervenes in the short term, medium to high frequency range, tends to decrease with floor internal heat source depth and has higher impact, though limited, on the air temperature than on the operative temperature.

7-Feedforward-feedback control is a more effective control compared to feedback control with floor radiant heating system. Temperature overshoot and settling time due to step input temperature change are considerably reduced.

8-Thermal mass reduces energy consumption by 25% to 30% on sunny days while carpet cover reduces this energy gain by up to 6%.

9-Mean radiant temperature and operative temperature with floor concrete mass may differ from air temperature respectively by up to 2.5°C and 1.6°C and carpet cover increases floor surface temperature by up to 2°C and the room mean radiant temperature by to 2.35°C.

10-The half sinusoid set point profile for proportional control of the room air or of the operative temperature gives the best response when both

temperature and energy consumption are considered. Variation in setpoint from day to night is confirmed as an effective control alternative for increased passive solar gains. Control of radiant heating based on operative temperature reduces both maximum floor surface and maximum operative temperature, particularly for carpeted floor, thereby improving thermal comfort. Furthermore, it reduces energy consumption particularly on sunny day.

7.2 Recommendations for future work

-Development, implementation and field testing of a predictive control model adapted to thermal mass characteristics, building load variations and weather anticipation in order to improve performance of floor heating in terms of comfort level and effective use of its solar gains to ensure maximum energy savings.

-Analysis of the transfer function identification method showed a high level of accuracy up to a frequency of 100 cycles a day, however further investigation is needed in order to establish simple and reliable criterions for determining the required polynomial order that will allow reaching acceptable accuracy level for both magnitude and phase lag at any frequency range.

REFERENCES

ASHRAE 1989. Handbook – Fundamentals.

ANSI/ASHRAE standard 55-1992. 1992. Thermal environmental conditions for human occupancy.

ASHRAE - 1987. Handbook of Systems and applications: 13-19

Adelman, D. 1988. Some control strategies for radiant floor heating. Radiant times. March: 4-5.

Athienitis, A.K., Sullivan, H.F and K.G.T. Hollands, 1987. Discrete Fourier series models for building auxiliary energy loads based on network formulation techniques. Solar energy 39: 203-210.

Athienitis, A.K., M. Stylianou and J. Shou. 1990. A Methodology for Building thermal dynamics studies and control application. Building and Environment 28(4): 483-496.

Athienitis, A.K., J.G. Shou. 1991. Control of radiant heating based on the operative temperature. ASHRAE Transactions 97(2): 787-784.

Athienitis, A.K. and T. Chen. 1993. Experimental and theoretical investigation of floor heating with thermal storage. ASHRAE Transactions 99(2): 1049-1057.

Athienitis, A.K. 1993. A Methodology for integrated building HVAC system thermal analysis. Building and Environment 28(4): 483-496.

Athienitis, A.K. 1994. A Numerical Model of a Floor Heating System", ASHRAE Transactions 100(1): 1024 1030.

Athienitis, A.K. 1997. Investigation of thermal performance of a passive solar building with floor radiant heating. Solar Energy 61(5): 337-345.

Athienitis, A.K. and Y. Chen. 1998. A Three-Dimensional numerical investigation of the effect of cover materials on heat transfer in floor heating system. ASHRAE Transactions 104(2): 1350-1355.

Athienitis, A.K. 1998. Building Thermal Analysis, 3rd edition. Concordia University, Montreal.

Athienitis, A.K. and Y. Chen. 2000. The Effect of solar radiation on dynamic thermal performance of floor heating systems. Solar energy 69(3): 229-237.

Athienitis, A.K. and Y. Chen. 2002. Comparison Of control strategies for floor heating systems. ASHRAE Transactions 108(1): 1005-1016.

Athienitis, A.K. and M. Santamouris. 2002. Thermal analysis and design of passive solar buildings. Concordia University, Montreal.

Balcomb, J.C. 1992. Passive solar building. Cambridge, Mass. MIT Press.

Bohle, J. and H. Klan. 2000. Design of panel heating and cooling systems. ASHRAE transactions 103(1): 677-683.

Brameller, A., M.N. John and M.R. Scott. Chapman & Hall Ltd. Practical diakoptics for electrical networks.

CEN, 1994. EN 1264, Floor heating-Systems and components. European Committee for Standardization.

Chapman, K.S., and P. Zhang. 1995. Radiant heat exchange calculations in radiantly heated and cooled enclosures. ASHRAE transactions 101(1): 1236-1247.

Chapman, K.S., and P. Zhang. 1996. Energy transfer simulation calculations in radiantly heated and cooled enclosures. ASHRAE transactions 102(1): 76-84.

Chapman, K.S., J.M. DeGreef and R.D. Watson. 1997. Thermal comfort analysis using BCAP for retrofitting a radiantly heated residence. ASHRAE transactions 103(1): 959-965.

Chen, T. 1997. A methodology for thermal analysis and predictive control of building envelope heating systems. Ph. D. Thesis, Centre for Building Studies, Concordia University, Montreal, Canada.

Chen, T. 2002. Application of adaptive predictive control to a floor heating system with a large thermal lag. Energy and buildings 34(1): 45-51.

Cho, S.H. and M. Zaheer-uddin.1997. Temperature regulation of radiant floor heating systems using two-parameter on-off control: An experimental study. ASHRAE Transactions 103(1): 966-980.

Cho, S.H. and M. Zaheer-uddin. 2003. Predictive control of intermittently operated radiant floor heating systems. Energy Conversion and Management 44: 1333-1342

Clarke, D.W. 1985. HVACSIM^{+} Building systems and equipment simulation program. Reference manual. National Bureau of Standard, Gaithersburg. MD

U.S.

Dale, J.D. and M.Y. Ackerman. 1993. The thermal performance of a radiant panel floor heating system. ASHRAE Transactions 9(1): 23-34.

De Carli, M. and B.W. Olesen. 2002. Field measurements of operative temperatures in buildings heated or cooled by embedded water-based radiant systems. ASHRAE Transactions 108(2): 715-725.

Fisk, D.J. 1981. Thermal control of buildings. Applied Science Publishers, London.

Freestone, M. and W.M. Worek,.1996. Radiant panel perimeter heating options: Effectiveness and thermal comfort, ASHRAE Transactions 102(1): 667-674.

Gibbs, D.R. 1994. Control of multi-zone hydronic radiant floor heating systems, ASHRAE Transactions 99 (1): 1003-1010.

Haghighat, F. and A.K. Athienitis.1988. A comparison between Time domain and Frequency domain computer program for building energy analysis. Computer Aided Design 20(9): 525-532.

ISO Standard 7730, 1994. Moderate thermal environments - Determination of the PMV and PPD indices and specification of the conditions for thermal comfort. Geneva. International organization for Standardization.

36. Jones, B., and K.S. Chapman, 1994. Simplified method to factor mean radiant temperature (MRT) into building and HVAC system design. Final report of ASHRAE research project RP-657.

Kilkis, B.I., M. Eltez and S. Sager. 1995. A simplified model for the design of radiant in-slab heating panels, ASHRAE Transactions 101(1): 210-216.

Kilkis, B.I., and M. Coley. 1995. Development of complete software for hydronic floor heating of buildings. ASHRAE Transactions 101(1): 1201-1213.

Kilkis, B.I., and M. Sapci. 1995. Computer-aided design of radiant sub-floor heating systems. ASHRAE Transactions 101(1): 1214-1220.

Kimura, K. 1977. Scientific Basis for Air Conditioning" Applied Science Publishers Ltd.

Leigh, S.B. and C.R. MacCluer. 1994. A Comparative study of proportional flux-modulation and various types of temperature-modulation approaches for radiant floor heating system control. ASHRAE Transactions 100(1): 1040-1052.

Leal, R.L.V. and P.L. Miller. 1972. An Analysis of the transient temperature distribution in pavement heating installations. ASHRAE Transactions 78(2): 71-78.

MacCluer, C.R. 1989. The control of radiant slabs. ASHRAE Journal. September: 28-33.

MacCluer, C.R. 1991. The response of radiant heating systems controlled by outdoor reset with feedback. ASHRAE Transactions 97(2): 795-799.

Olesen, B.W. 1994. Comparative experimental study of performance of radiant floor heating systems and a wall panel heating system under dynamic conditions. ASHRAE Transactions 100(1): 1011-1023.

Olesen, B.W. 2002. Radiant floor heating in theory and practice. ASHRAE Journal. July: 19-26.

Scheatzle, D.G. 2003. Data set for validating simulation tools for radiant/convective system systems. ASHRAE Transactions. 109(1): 583-596

Shou, J.G. 1991. A Computer technique for heating control analysis and application to radiant heating. M.A.Sc. Thesis. Centre for Building Studies, Concordia University. Montreal, Canada.

Simmonds, P. 1996. Practical applications of radiant heating and cooling to maintain comfort conditions, ASHRAE Transactions. 102(1): 659-665.

Tse, W.L. 2003. Knowledge-based algorithm for daily thermal load prediction of a building. Building Engineering 100(5): 6-28.

Strand R.K. and C.O. Pederson. 1997. Implementation of a radiant heating and cooling model into an integrated building energy analysis program, ASHRAE Transactions 103(1): 949-958.

Strand R.K. and C.O. Pederson. 2002. Modeling radiant systems in an integrated heat balance based energy simulation program. ASHRAE Transactions 108(2): 979-987.

Vlach, J and K. Singhal, 1983. Computer methods for circuit analysis and design. Van Nostrand Reinhold Company. New York

Younger, M.S. Handbook for linear regression DUXBURY PRESS

Zhang Z. and M.B. Pate. 1986. A numerical study of heat transfer in a hydronic radiant ceiling panel, in numerical methods in heat transfer (eds., Chen J.L.S and Vafai K.), ASME-HTD, 62.

Zhang Z. and M.B. Pate. 1987. M.B., A semi-analytical formulation of heat transfer from structures with embedded tubes, Heat transfer in buildings and structures (eds.Kuehn TH). ASME-HTD, 78:17-25.

APPENDIX 1

Finite difference model

The explicit finite difference method (Athienitis, 2002) is suitable for modeling of non-linear heat diffusion problems such as the present case of heat transfer through the floor heating system and its control. It easily accommodates non-linear heat transfer coefficients and temperature-dependant heat sources such as auxiliary heating. The general form of the explicit finite difference formulation corresponding to node i and time interval p is:

$$T_{i,p+1} = \frac{\Delta t}{C_i}\left(q_i + \sum \frac{T_{j,p} + T_{i,p}}{R_{i,j}}\right) + T_{i,p} \qquad (8.1)$$

C is the capacitance, j represents all nodes connected to node i, while qi represents a heat source as auxiliary heating or solar radiation. The critical time step Δt (for all nodes i) is selected based on the following conditions to insure numerical stability:

$$\Delta t \leq \min\left(C_i \sum_j \frac{1}{R_{i,j}}\right) \qquad (8.2)$$

Simulation

Validation of the frequency domain model is performed using an explicit finite difference model (Athienitis, 1994), appropriately modified in order to obtain the room transient temperature to a step input of radiative gain. Wall transient thermal response analysis with finite difference technique is proven to provide a

more accurate estimation of temperature and heat flow. This model was originally developed to study the performance of a passive solar building. It assumes all the unheated wall surfaces as one surface and consequently does not represent in detail infrared radiation between room interior surfaces and but is accurate enough to conduct comparison analysis

The finite difference thermal network model for the room (Figure 3.1a) is as shown by Figure 8.1. It consists of two capacitances for the floor thermal capacity, interconnecting thermal resistances and another capacitance for the rest of the room. Walls room surfaces (1, 2, 3, 4, 5, 6, 7) represented by node 6 and the Floor surface (node 2) are coupled by convection (R12 and R16) with room air (node 1) and together by radiation (R26). q_{aux} represents the auxiliary floor internal heat source and may be reconnected to node 3 to simulate another installation depth. Room parameters and overall heat transfer coefficients identical to those used with the frequency domain model are assumed.

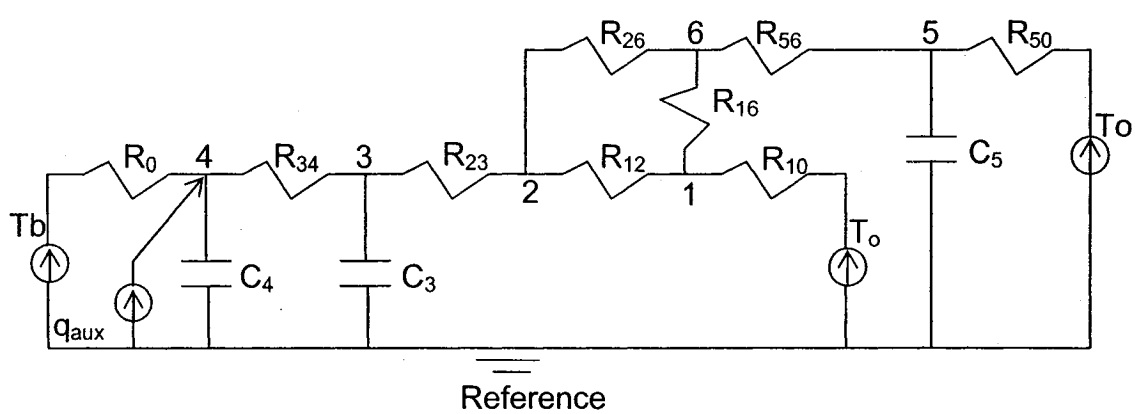

Figure 8.1: Thermal network of zone with floor heating system corresponding to room schematic Figure 3.1a.

Thermal capacitances and resistances are as follows:

Floor heating system:

$$C_{floor} = c_8 \rho_8 A_8 x_8 \qquad C_4 = \frac{C_{floor}}{2} \qquad C_3 = C_4$$

Interior layer of unheated surfaces (se=1, 2, 3, 4, 5, 6, 7).

$$C_5 = \sum_{se} A_{se} x_{se} c_{se} \rho_{se}$$

$$R_0 = \left(\frac{1}{u_8 A_8}\right) + \left(\frac{x_8}{4 k_8 A_8}\right) \qquad R_{34} = \frac{x_8}{2 k_8 A_8}$$

$$R_{23} = \frac{R_{34}}{2} \qquad R_{12} = \frac{1}{A_8 h_8}$$

$$R_{56} = \frac{1}{\sum_{se} 2 \frac{k_{se} A_{se}}{x_{se}}} \qquad R_{26} = \frac{1}{h_{8r} A_8}$$

$$R_{16} = \frac{1}{\sum_{se} A_{se} h_{se}} \qquad R_{5o} = \frac{1}{\sum_{se} \frac{A_{se}}{R_{se}}}$$

$$R_{1o} = \frac{1}{U_{inf} + \sum_{ii} \left(\frac{A_{wii}}{R_w} + \frac{A_{dii}}{R_d}\right)}$$

Radiation heat transfer coefficients between floor and unheated surfaces

$$h_{8r} = 3 W/m^2\,{}^\circ C$$

STABILTY TEST TO SELECT TIME STEP

The time step ΔT should be lower than the minimum of the three values in the vector TS.

$$TS = \left[\frac{C_3}{\left(\frac{1}{R_{23}} + \frac{1}{R_{34}}\right)}, \frac{C_4}{\left(\frac{1}{R_0} + \frac{1}{R_{34}}\right)}, \frac{C_5}{\left(\frac{1}{R_{56}} + \frac{1}{R_{50}}\right)} \right]$$

The time step is appropriately selected equal to Δt=50.26 seconds to insure concordance of conditions between the two methods. Simulation is performed at times T_p= p$\times\Delta t$ for a number of time steps p=0,1, 2....NT with NT=8000, for the same period of time used with the numerical inversion method to reach steady state.

Room air temperature is set to 20°C. All sources such as solar radiation (not shown in Figure 8.1), outside (To) and basement temperature (Tb) are set equal to zero in order to obtain the room transient response to a step input of a radiative gain, simulated with the auxiliary heating system q_{aux} set to 8400 watts. The initial temperature conditions are assumed as follows;

$$\begin{pmatrix} T_{1,0} \\ T_{2,0} \\ T_{3,0} \\ T_{4,0} \\ T_{5,0} \\ T_{6,0} \end{pmatrix} = \begin{pmatrix} 0 \\ 0 \\ 0 \\ 0 \\ 0 \\ 0 \end{pmatrix} {}^{\circ}C$$

An energy balance (8.3) is applied at each node at regular time intervals to obtain the temperature of the nodes as a function of time. These equations are then solved with the explicit method in which we march forward in time from the set of above initial conditions. T_1 represents the room air temperature. Simulations are performed with different floor internal heat source depth for concrete and carpeted floor as shown by Figures 5.22 a and b (chapter 5):

$$
\begin{pmatrix} qaux_{p+1} \\ T_{1,p+1} \\ T_{2,p+1} \\ T_{3,p+1} \\ T_{4,p+1} \\ T_{5,p+1} \\ T_{6,p+1} \end{pmatrix}
=
\begin{bmatrix}
qaux \\
\dfrac{\dfrac{T_{2,p}}{R_{12}} + \dfrac{T_{0,p}}{R_{10}} + \dfrac{T_{6,p}}{R_{16}}}{\left(\dfrac{1}{R_{12}} + \dfrac{1}{R_{10}} + \dfrac{1}{R_{16}}\right)} \\
\dfrac{\dfrac{T_{3,p}}{R_{23}} + \dfrac{T_{6,p}}{R_{26}} + \dfrac{T_{1,p}}{R_{12}}}{\left(\dfrac{1}{R_{23}} + \dfrac{1}{R_{26}} + \dfrac{1}{R_{12}}\right)} \\
\dfrac{\Delta t}{C_3}\left(\dfrac{T_{4,p} - T_{3,p}}{R_{34}} + \dfrac{T_{2,p} - T_{3,p}}{R_{23}} + qaux_p\right) + T_{3,p} \\
\dfrac{\Delta t}{C_4}\left(\dfrac{Tb_p - T_{4,p}}{R_0} + \dfrac{T_{3,p} - T_{4,p}}{R_{34}}\right) + T_{4,p} \\
\dfrac{\Delta t}{C_5}\left(\dfrac{T_{6,p} - T_{5,p}}{R_{56}} + \dfrac{T_{0,p} - T_{5,p}}{R_{50}}\right) + T_{5,p} \\
\dfrac{\dfrac{T_{2,p}}{R_{26}} + \dfrac{T_{5,p}}{R_{56}} + \dfrac{T_{1,p}}{R_{16}}}{\left(\dfrac{1}{R_{26}} + \dfrac{1}{R_{56}} + \dfrac{1}{R_{16}}\right)}
\end{bmatrix}
\tag{8.3}
$$

APPENDIX 2

Calculation of hourly and daily solar radiation

Using the average clearness index

Various methods can be used for estimating the total solar radiation on any surface. Real weather data may be employed which is cumbersome and time consuming or instead generate a weather data with the daily clearness index KT (Athienitis, 2002). This model, based on a correlation by Collares, Periera and Rabi, is intended for average days and can be used to approximate cloudy to clear days radiation with values of KT in the range 0.2 to 0.8.

<u>Solar geometry calculations (For room model under consideration Figure 3.1a)</u>

I=1,2...7 surfaces index representing the room exterior surfaces

n_d=day of the year ...n_d=15

L= 45° Latitude of the place (Montreal) under consideration

β= 90° Surface tilt angle of vertical walls (3, 7, 5, 6) and windows 1&2)

Room surfaces azimuth

Wall 3 and window 1	(South)	$\psi_3 = \psi_1 = (0-10)^\circ$
Wall 7 and window 2	(West)	$\psi_7 = \psi_2 = 90^\circ - \psi_1$
Wall 5	(East)	$\psi_5 = \psi_1 - 90^\circ$
Wall 6	(North)	$\psi_6 = \psi_1 - 180^\circ$

ρ_g=0.2 diffuse reflectance of total solar radiation

Equation of time

$$ET(n_d) = \left[9.87\left(4\pi\frac{n_d - 81}{364}\right) - 7.53\cos\left(2\pi\frac{n_d - 81}{364}\right) - 1.5\sin\left(2\pi\frac{n_d - 81}{364}\right)\right]$$

Apparent solar time Time array for one day t=0, 1...23

$$AST(t) = thr + ET + \frac{(STM - LNG)hr}{15deg}$$

Solar declination angle

$$\delta = 23.45\sin\left[\frac{360(284 + n_d)}{365}\right]^{\circ}$$

Hour angle

$$ha(t) = (AST(t) - 12hr)15\frac{degree}{hr}$$ (0 at solar noon)

Solar altitude

$$\alpha(t) = \sin^{-1}(\cos(L)\cos(\delta)\cos(ha(t)) + \sin(L)\sin(\delta))$$ For $\alpha(t)>0$, otherwise $\alpha(t)=0$

Solar azimuth

$$\phi(t) = \cos^{-1}\left(\frac{\sin(\alpha)\sin(L) - \sin(\delta)}{\cos(\alpha(t))\cos(L)}\right)\frac{ha(t)}{|ha(t)|}$$ Positive in the afternoon

Angle of incidence

$$\theta(t) = \cos^{-1}(\cos(\alpha(t))\cos(|\phi(t) - \psi|)\sin(\beta) + \sin(\alpha(t))\cos(\beta))$$

(Φ-ψ) is the surface azimuth for the room under consideration, East is negative

Sunset hour angle

$$ha_s = (\cos^{-1}(-\tan(L)\tan(\delta)))$$

For an inclined surface, the equation is modified to take in account the sunset and sunrise hour angle for the surface, which may be different from the daily sunset and sunrise hour angles.

$$H_s = \min\{(\cos^{-1}(-\tan(L)\tan(\delta))), \cos^{-1}(-\tan(L-\beta)\tan(\delta))\}$$

Calculation of hourly total k_t, beam k_b and diffuse k_d clearness indices

An estimation of a half-sinusoidal variation (day time hours only) of the hourly clearness indices is performed using the daily clearness index K_T which represents the ratio of daily total solar radiation incident on a horizontal surface to the extraterrestrial horizontal radiation for that day. The numerical simulations for cloudy and clear day radiation are performed respectively with K_T values of 0.3 and 0.7.

Total hourly clearness index

$$a_1 = 0.409 + 0.5016\sin(ha_s - 1.047) \qquad a_0 = 0.6609 + 0.4767\sin(ha_s - 1.047)$$

$$k_t = (a_1 + a_0\cos(\omega(t - 12hr)))K_T \quad \text{for } k_t > 0, \quad \text{otherwise } k_t = 0$$

The hourly diffuse clearness index is found from the following Orgill-Hollands correlation:

For $0 < k_t < 0.35 \quad \rightarrow \quad k_d = (1 - 0.249k_t)k_t$

For $0.35 < k_t < 0.75 \quad \rightarrow \quad k_d = (1.557 - 1.84k_t)k_t$

For $k_t > 0.75 \quad \rightarrow \quad k_d = 0.177\,k_t$

The beam atmospheric transmittance is obtained from the subtraction of the hourly diffuse clearness index from the hourly clearness index.

$$k_b = k_t - k_d$$

Calculation of the solar radiation incident on exterior walls

The total solar radiation incident on any surface can be estimated using the hourly extraterrestrial solar radiation,

Extraterrestrial normal solar radiation:

$$I_{on} = 1353\left[+10.033\cos\left(\frac{360 n_d}{365^\circ}\right)\right]$$

Incident beam radiation

$$I_b(t) = I_{on}\, k_b \cos(\theta(t))$$

Incident sky diffuse radiation

$$I_{ds}(t) = I_{on} \sin(\alpha(t)) k_d \left(\frac{1+\cos(\beta)}{2}\right)$$

Ground reflected diffuse radiation

$$I_{dg}(t) = I_{on} \sin(\alpha(t)) k_t\, \rho_g \left(\frac{1-\cos(\beta)}{2}\right)$$

$\left(\frac{1+\cos(\beta)}{2}\right)$ and $\left(\frac{1-\cos(\beta)}{2}\right)$ represent the view factor from vertical surfaces respectively to sky and to ground.

Total instantaneous solar irradiation incident on exterior vertical surfaces

$$I_t(t) = I_b(t) + I_{ds}(t) + I_{dg}(t)$$

Total instantaneous solar irradiation incident on horizontal surface (roof)

$$I_h(t) = I_{on} \sin(\alpha(t))(0.271 - 0.2939 k_b + k_b)$$

<u>Solar radiation transmitted through windows</u>

Glazing properties:

KL=0.1 extinction coefficient x glazing thickness (for a clear glass)

N_g=1.53 refractive index

Angle of refraction (Snell's law) and components reflectivity:

$$\theta'(t) = \sin^{-1}\left(\frac{\sin(\theta)}{n_g}\right) \qquad r(t) = \frac{1}{2}\left[\left(\frac{\sin(\theta(t)-\theta'(t))}{\sin(\theta(t)+\theta'(t))}\right)^2 + \left(\frac{\tan(\theta(t)-\theta'(t))}{\tan(\theta(t)+\theta'(t))}\right)\right]$$

Beam transmittance, τ, reflectance, ρo, and absorptance, α, of glazing.

$$a(t) = \exp\left[\frac{KL}{\sqrt{1-\left(\frac{\sin(\theta(t))}{n_g}\right)^2}}\right] \qquad \tau(t) = \frac{(1-r(t))^2 a(t)}{1-(r(t))^2(a(t))^2}$$

$$\rho o(t) = r(t) + \frac{r(t)\,(1-r(t))^2 a(t)^2}{1-(r(t))^2(a(t))^2} \qquad \alpha_s(t) = 1-\rho o(t)-\tau(t)$$

<u>For double glazed windows</u>: $$\tau_e(t) = \frac{(\tau(t))^2}{1-(\rho o(t))^2}$$

$$\alpha_i(t) = \alpha_s \frac{\tau(t)}{1-(\rho o(t))^2} \qquad \alpha_{oi}(t) = \alpha_s(t) + \alpha_s(t)\frac{\tau(t)\rho o(t)}{1-(\rho o(t))^2}$$

Transmitted beam solar radiation.

$$G_b(t) = I_b(t)\,\tau_e$$

Approximate value for diffuse transmittance

$$\tau_{ed} = \tau_e(11)$$ (Equal for all windows)

Instantaneous diffuse irradiation

$$G_d(t) = (I_{ds}(t) + I_{dg}(t))\,\tau_{ed}$$

Total instantaneous solar irradiation transmitted in room

$$G(t) = G_b(t) + G_d(t):$$

Solar radiation absorbed in glazing

$$G_{ao}(t) = \alpha_o(t) I_b(t) + \alpha_o(t)\left(I_s(t) + I_g(t)\right)$$ Outer glazing

$$G_{ai}(t) = \alpha_i(t) I_b(t) + \alpha_i(t)\left(I_s(t) + I_g(t)\right)$$ Inner glazing

Sources modeling

The different sources are then modeled with Fourier series over the range of frequency. Time origin from solar noon is reversed back to midnight to carry out calculation.

Solar components of sol-air temperature for exterior surfaces:

$$Ts_w(t) = I_t(t)\frac{\alpha s}{h_w}$$ Vertical walls

$$Ts_r(t) = I_h(t)\frac{\alpha s}{h_r}$$ Roof

αs, h_w and h_r represent wall absorptance (=0.9) and combined outside air film coefficient (assumed equal to 22 and 20 watt/m^2·°C respectively for vertical and horizontal surfaces).

Represented by a Fourier series: $Tsn = \sum_{it} Ts_{it} \frac{\exp(-j\omega t)}{24}$

Equivalent or sol-air temperature

$Teq = Ton + Tsn$ Where Ton is the Fourier representation of the outdoor air temperature and equal to: $Ton = \sum_{it} To_{it} \frac{\exp(-j\omega t)}{24}$

Total instantaneous solar radiation transmitted by windows:

$$Gt(t) = \sum G(t) \times Aw$$

Solar radiation absorbed by room surfaces may be modeled as in the present case as 70% absorbed by the floor surface and the remaining 30% by the interior walls proportionally to their surface as follows:

$S_8 = 0.7\ Gt$ Floor $\qquad$ $S_{ii} = 0.3\ Gt \dfrac{A_i}{\sum_i A_i}$ Interior wall

Represented by a Fourier series: $Sn = \sum_{it} S_{it} \dfrac{\exp(-j\omega t)}{24}$

<u>Solar radiation absorbed in glazing and released to room air is :</u>

$$Qg(t) = \sum \frac{A_w I_t(t)}{R_w}\left[\frac{\alpha}{h_o} + \left(R_w - \frac{1}{h_i}\right)\alpha_i\right]$$

Represented by a Fourier series: $Qgn = \sum_{it} Qg_{it} \dfrac{\exp(-j\omega t)}{24}$

APPENDIX 3

Selection of Poles z_j and Residues K_j' for M=10 and N=8

$z_1 = 11.83009373916819 + j\,1.593753005885813$

$z_2 = 11.22085377939519 + j\,4.792964167565670$

$z_3 = 9.933383722175002 + j\,8.033106334266296$

$z_4 = 7.781146264464616 + j\,11.36889164904993$

$z_5 = 4.234522494797000 + j\,14.95704378128156$

$k_1' = 16286.62368050479 - j\,139074.7115516051$

$k_2' = -28178.11171305163 + j\,74357.58237274176$

$k_3' = 14629.74025233142 - j\,19181.80818501836$

$k_4' = -2870.418161032078 + j\,1674.109484084304$

$k_5' = 132.1659412474876 + j\,17.47674798877164$